

Review

Metalliferous Coals of Cretaceous Age: A Review

Shifeng Dai ^{1,*} , Sergey I. Arbutov ^{2,3} , Igor Yu. Chekryzhov ³ , David French ⁴ , Ian Feole ⁵ , Bruce C. Folkedahl ⁵ , Ian T. Graham ⁵ , James C. Hower ^{6,7} , Victor P. Nechaev ³ , Nicola J. Wagner ⁸ , and Robert B. Finkelman ⁹ 

- ¹ College of Geoscience and Survey Engineering, China University of Mining and Technology (Beijing), Beijing 100083, China
 - ² School of Earth Sciences & Engineering, Tomsk Polytechnic University, 634050 Tomsk, Russia
 - ³ Far East Geological Institute, FEB of RAS, 690022 Vladivostok, Russia
 - ⁴ Earth and Sustainability Sciences Research Centre, School of Biological, Earth and Environmental Sciences, University of New South Wales, Sydney, NSW 2052, Australia
 - ⁵ Environmental Research Center, University of North Dakota Energy, 15 N 23rd St., Grand Forks, ND 58201, USA
 - ⁶ Center for Applied Energy Research, University of Kentucky, 2540 Research Park Drive, Lexington, KY 40511, USA
 - ⁷ Department of Earth & Environmental Sciences, University of Kentucky, Lexington, KY 40506, USA
 - ⁸ DSI-NRF CIMERA, Department of Geology, University of Johannesburg, Johannesburg 2006, South Africa
 - ⁹ Geosciences Department, University of Texas at Dallas, Richardson, TX 75080, USA
- * Correspondence: daishifeng@gmail.com

Abstract: Critical elements in coal and coal-bearing sequences (e.g., Li, Sc, V, Ga, Ge, Se, Y and rare earth elements, Zr, Nb, Au, Ag, platinum group elements, Re, and U) have attracted great attention because their concentrations in some cases may be comparable to those of conventional ore deposits. The enrichment of critical elements in coals, particularly those of Carboniferous-Permian and Cenozoic ages, have generally been attributed to within-plate (plume-related) volcanism and associated hydrothermal activity. However, Cretaceous coals are not commonly rich in critical elements, with the exception of some (e.g., Ge and U) in localised areas. This paper globally reviewed metalliferous coals from Siberia, the Russian Far East, Mongolia, South America, the United States and Mexico, Canada (Alberta and British Columbia), China, Africa, and Australasia (Victoria, Queensland, New South Wales, South Australia, Northern Territory, New Zealand, Nelson, West Coast, Canterbury, Otago, and Southland). The world-class Ge-U or Ge deposits in North China, Mongolia, and Siberia are the only commercially significant representatives of the Cretaceous metalliferous coals, which are related to bio-chemical reduction of oxidized meteoric, hydrothermal, or sea waters by organic matter of the peat bogs. The common Cretaceous coals worldwide are generally not rich in critical elements because intensive igneous activity led to extensive acidification of terrestrial and marine waters, which are responsible for the low coal metallogensis during the Cretaceous period, especially the Early Cretaceous time.

Keywords: critical metals; cretaceous coal; mineralization; global review; igneous activity



Citation: Dai, S.; Arbutov, S.I.; Chekryzhov, I.Y.; French, D.; Feole, I.; Folkedahl, B.C.; Graham, I.T.; Hower, J.C.; Nechaev, V.P.; Wagner, N.J.; et al. Metalliferous Coals of Cretaceous Age: A Review. *Minerals* **2022**, *12*, 1154. <https://doi.org/10.3390/min12091154>

Academic Editor: Frederick Lin Sutherland

Received: 26 August 2022

Accepted: 7 September 2022

Published: 13 September 2022

Publisher's Note: MDPI stays neutral with regard to jurisdictional claims in published maps and institutional affiliations.



Copyright: © 2022 by the authors. Licensee MDPI, Basel, Switzerland. This article is an open access article distributed under the terms and conditions of the Creative Commons Attribution (CC BY) license (<https://creativecommons.org/licenses/by/4.0/>).

1. Introduction

Critical elements in coal and coal-bearing sequences, such as Li, Sc, V, Ga, Ge, Se, and Y and rare earth elements (REY, or REE+Y) Zr, Nb, Au, and Ag, and platinum group elements, Re, and U, have attracted great attention in recent years [1–8], as these elements in some coals and coal-bearing sequences may have relatively high concentrations, comparable to those of conventional ore deposits [9,10]. Nowadays, world economies largely depend on high technologies in which critical elements play a vital role because they are driving some of the biggest advancements in technology and energy efficiency in the world [3,11]. The demand for these critical elements has grown rapidly due to their wide applications, but there are potential supply-related risks because (1) the resources of conventional ores of

these elements are becoming smaller and even exhausted; and (2) supplies of these critical elements are controlled by a limited number of countries/areas; for example, as of 2019, China produced ~85% of the world's rare earth oxides and ~90% of rare earth metals, alloys, and permanent magnets (<https://chinapower.csis.org/china-rare-earths/>, accessed on 6 September 2022). These reasons have prompted global exploration for new sources of these critical elements. One promising source of many of these critical elements is coal and coal-bearing sequences [3,9–20].

Previous investigations have shown that the enrichment of critical metals in coal is attributed to a number of geological and geochemical factors, including volcanism, sediment source regions, sedimentary environments, groundwater, and various syngenetic and post-diagenetic fluids [8,21]. Elevated concentrations of critical elements in coals, particularly those of Carboniferous-Permian and Cenozoic ages, were generally attributed to within-plate (plume-related) volcanism and associated hydrothermal activity [22,23]. Critical elements that were mineralized in these coals include Li, Be, Sc, Ti, V, Ga, Ge, Nb, Ta, Zr, Hf, REY, Ag, Au, and platinum group elements Th and U, among others [9,24,25]. However, compared with Carboniferous-Permian coals, Cretaceous coals, particularly those of Early Cretaceous age, which are globally associated with a peak of volcanic and metallogenic activities [8,26,27] and the formation of Large Igneous Provinces (LIPs; Figure 1) [28], are not commonly rich in the abovementioned critical elements, with the exception of some critical elements as mentioned below in localised areas.

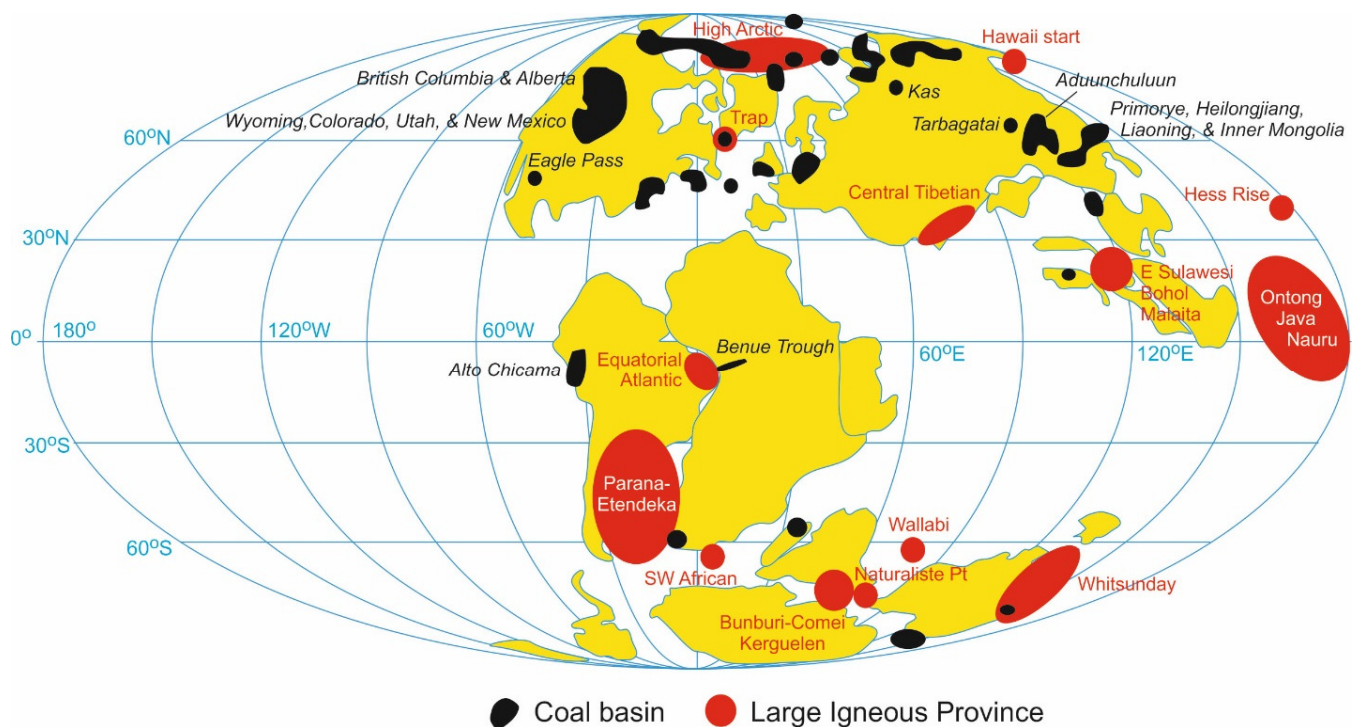


Figure 1. Global distribution of coal basins and LIPs in the Early Cretaceous. Coal basins and LIPs are shown after Ziegler et al. [29] and Ernst et al. [28], respectively. The names in black indicate locations of mineralized coals discussed below. The Benue Trough is shown after Akiniemy et al. [30]. The names in red and white indicate LIPs.

This paper globally reviews Cretaceous metalliferous coals from Siberia, the Russian Far East, Mongolia, South America, the United States and Mexico, Alberta and British Columbia, Canada, China, Africa, and Australasia (Victoria, Queensland, New South Wales, South Australia, Northern Territory, New Zealand, Nelson, West Coast, Canterbury, Otago, and Southland), and relevant data have been collected as much as possible. However, relevant data from other areas, such as Europe, South Asia, and Southeast Asia, were not

available for inclusion in this review paper due to various reasons mainly of absence of publications and/or occurrence of the Cretaceous coals.

The aim of this paper is to (1) discuss the available geological and geochemical data on some Cretaceous coals with elevated concentrations of critical elements; (2) summarize the reasons why the Cretaceous coals were globally unmineralized and subsequently to explore more information of global igneous activity and its influences on terrestrial and marine waters; and (3) provide more guidance on exploration and exploitation of metalliferous coals.

2. Metalliferous Coals in Siberia, the Russian Far East, and Mongolia

This section discusses the main geological and geochemical characteristics of the largest deposits of critical elements in Cretaceous age coals in Siberia, the Russian Far East, and Mongolia. The section does not provide information about multiple occurrences of U and associated diverse mineralization in areas of post-depositional hypergenic oxidation of the Cretaceous coal seams developed in different climatic zones. The information on REE mineralization in the coal of the Zhiganskoye deposit in the Lena Basin, reported by Kashyrtsev et al. [31], is also not given due to insufficient information.

2.1. Tarbagatai Ge Deposit in the Transbaikal Region

The Tarbagatai germanium deposit was discovered within a coal deposit of the same name. This sub-bituminous C coal deposit is located in the intermontane area of the same name, represented by a graben syncline. The deposit is 21 km long and 4–9 km wide with an area of about 150 km² (Figure 2) [32].

The Tarbagatai graben syncline is filled with freshwater-continental coal-bearing sediments of Lower Cretaceous age deposited within a structural unconformity on crystalline rocks of the Precambrian basement [32]. The coal-bearing deposits consist of the Doroninskaya and the Tigninskaya Formations. Located at the floor of the cross section, the Doroninskaya Formation is represented by a homogeneous layer of siltstone and argillite with thin interlayers of sandstone, which is common in the lowermost parts of the section. Conglomerate, fanglomerate (bajada breccia), gravelstone, and sandstone, occasionally with coal beds, are found at the floor of the cross section in the near-border parts of the depression. The thickness of the formation is 400–500 m. The Tigninskaya Formation sediments are conformably bedded. The Tigninskaya Formation is notable for its varied composition in terms of both facies and lithology. Sandstone, siltstone, and gravelstone are predominant, while pebble conglomerates, argillite, carbonaceous argillite, and coal are less common. From the floor to the top, the proportion of channel facies decreases, and the proportion of alluvial, meander, and marsh facies increases. The rocks become less coarse, and the thickness of the coal seams increases. The main coal-bearing formation is associated with the middle part of the formation (middle subformation). It is represented by sandstone, siltstone, and argillite with thick coal seams of a complex structure. In total, more than 20 coal seams and interlayers are recognized here of which the Tigninsky, Sputnik, Moshchny, and Pachka Promezhutochnaya have a working thickness [32].

The coal-bearing sediments are crumpled into gentle folds. The dip angles on the wings of the folds do not exceed 40°, usually varying from 5 to 20°.

The basement and the nearest flank of the depression are composed of biotite, biotite-amphibole, and amphibole-plagioclase crystalline schist and Proterozoic gneiss, Early Paleozoic granite-gneiss, and gneiss-like granite cut by the Paleozoic granitoid. Granitoids, including leucocratic rare-metal granite with tungsten, tin, bismuth, beryllium, and fluorite mineralization are predominant in the basement of the depression. Dispersion halos of Th, REE, Be, Ta, Nb, and Bi are very common. There is a Sn–Be ore occurrence near the northern flank of the depression. Some 18 km to the northeast, there is the greisen-hosted Bohm–Gorkhon tungsten deposit [33].

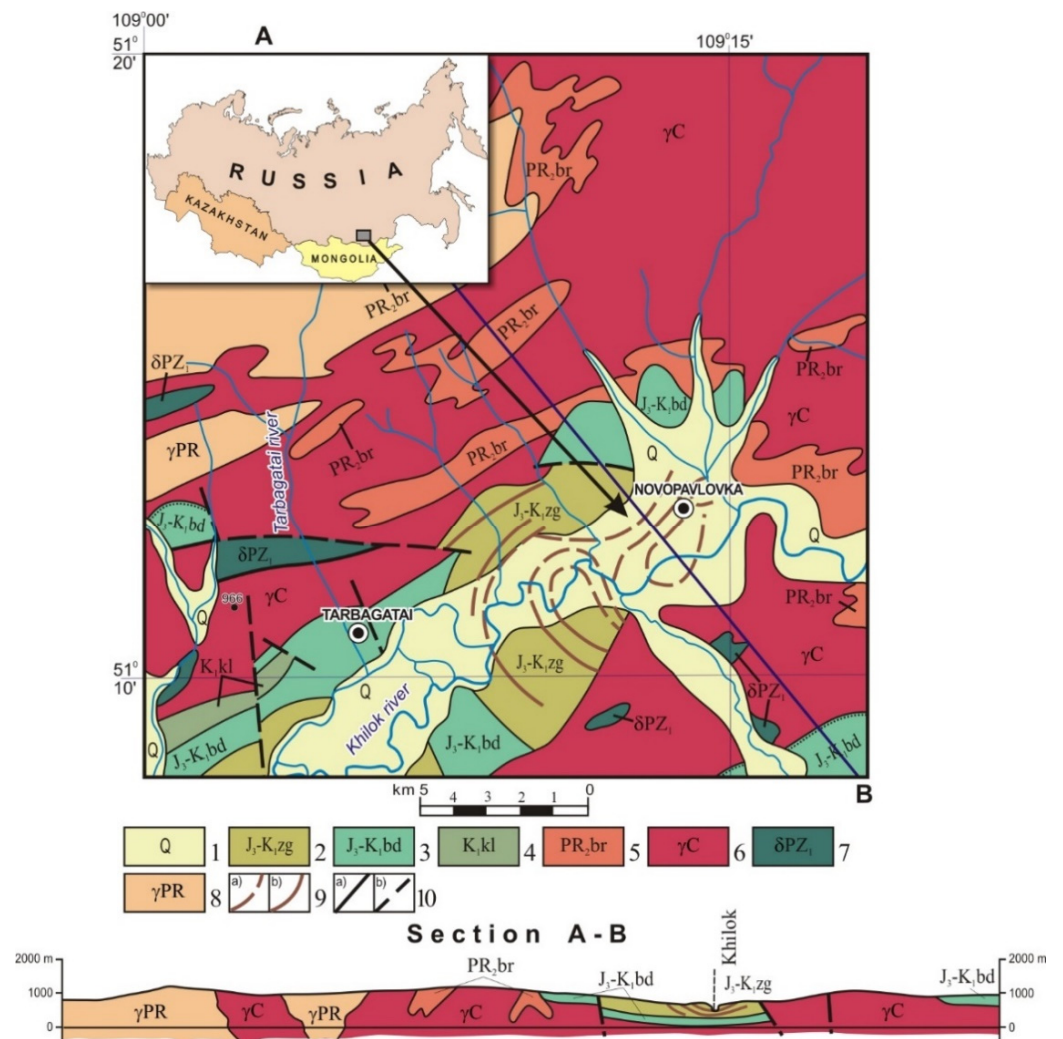


Figure 2. Geological map of the Tarbagatai deposit area [33]. Note: 1—Quaternary system., alluvial sand, gravel, and loam.; 2—Upper Jurassic—Lower Cretaceous, Zugmar Formation, sandstone, siltstone, mudstone, conglomerates, and coal; 3—Upper Jurassic—Lower Cretaceous, Badin Formation, sandstone, siltstone, conglomerates, and basaltic-trachyandesite; 4—Cretaceous system, Kulevskaya Formation, siltstone, mudstone, sandstone, and coal; 5—Proterozoic, Berezovaya Formation, biotite, biotite-amphibole crystalline schist and gneiss; 6—Carboniferous system, fine-grained, leucocratic granites; 7—Lower Paleozoic, diorite; 8—Proterozoic, granite, gneissic granite; 9—Coal seams: (a) hidden under alluvial quaternary deposits, (b) traced on the surface; 10—Fractures: (a) found, (b) assumed.

The sub-bituminous C coal in the deposit is mostly of medium ash, medium total sulfur ($S_t^d = 2.0\%–2.2\%$), and low phosphorous (0.011%–0.016%) type. Anomalous concentrations of W, Mo, Be, Ge, and REE were found at some sites in the Tigninsky, Sputnik, and Moshchny coal seams [32,34,35]. The existence of Ge-bearing coal in this deposit has been known since the middle of the 20th century. From 1964 to 1994, the coal in the northeastern part of the deposit with a Ge content of 120–130 ppm (whole-coal basis) was mined with industrial concentrates obtained from the fly ash.

The commercial Ge content is confined to the northeastern part of the deposit. Three sites with commercial Ge content were identified there [34]. One site (Tigninsky) is depleted, while the other two (Novy and Zugmarsky) are promising for development. The total Ge resources here exceed 710 t, of which the explored reserves of commercial categories amount to 380 t [34].

Within the Novy site, the Ge-bearing coal is confined to the Tigninsky, Sputnik, and Promezhutochny seams. Here, the Ge content varies from 15.8 to 497.8 ppm (90 ppm on average; on a whole-coal basis) in the Tigninsky seam, from 33.5 to 181.4 ppm (74.9 ppm on average) in the Promezhutochny seam, and from 22.5 to 249.0 ppm (59.7 ppm on average) in the Sputnik seam. The main Ge reserves are concentrated in the Tigninsky (about 67%) and Sputnik seams [34].

The Tigninsky seam is composed of semi-dull and dull massive, as well as lenticular-banded and striated-banded coal. Bands and inclusions are represented by unstructured carbonized wood. There are bands of vitrain and, less frequently, fusain.

The Sputnik seam is represented by semi-dull lenticular-banded coal with inclusions of semi-bright coal. Striated finely banded coal is also observed here. The coal is compact and mechanically strong.

The producing horizon is enriched in iron in the form of nodular and lenticular pyrite and siderite. Pyritization developed along fractures and bedding planes is typical here, and framboidal pyrite is abundant [36].

The distribution of Ge in the coal is extremely uneven. The highest concentrations and the main part of reserves are confined to the eastern part of the deposit. Some coals are characterized by very high concentrations, while others are close to the Clarke concentrations. The highest Ge content is associated with structural vitrain [34]. Vitrain occurs in the form of small lenses up to 3-cm thick and up to 30-cm long. A correlation was found between the structural features of the coal and its Ge content. In the area with high Ge content, the coal is represented by a homogeneous gelified substance. The coal is massive with rare small lenses of vitrain and vitrainized fragments of woody debris.

A highly significant correlation was found between Ge concentration and ash yields in the coal of the Tarbagatai deposit [34]. High concentrations of Ge in coal coincide with the areas of high ash yield, and the highest Ge content is confined to the coal with 15%–25% ash yield. No correlation was found between the thickness of the coal seams in the deposit and their Ge content.

The Ge-bearing coal is also enriched in Be, Ga [37], and Pb and in some areas in W, Mo, and REE [32,35]. Micro-grains of native Au were also detected in this coal [36]. In addition to the aforementioned elements, the coal ash contains anomalous amounts of U (up to 212 ppm), Au (up to 0.21 ppm), As (up to 351 ppm), Sb (up to 160 ppm), Cs (up to 102 ppm), and Zn (up to 616 ppm) (Table 1). Coal-related elements from the deposit have complex mineral associations, but insufficient knowledge prevents a reliable assessment of their complex processing prospects.

Table 1. The content of some associated elements in the Ge-bearing coal ash of the Tarbagatai deposit (ppm, ash basis; analyzed by instrumental neutron activation analysis).

Element	Average Content	Min	Max
Zn	166	53.1	616
As	88.3	8.6	351
Sb	6.2	0.9	160
Cs	30.2	1.3	102
Au	0.017	0.001	0.21
U	60.2	11.5	212

The critical element geochemistry of the coal reflects the geochemical characteristics of the rocks surrounding the coal-bearing depression and the metallogeny of the area. Together with the structural position of the mineralization in the coal basin and the absence of traces of synchronous or subsequent hydrothermal activity, they suggest a hypergenic model for the formation of the complex Be-W-Mo-Ge mineralization. Sources of the mineralization

are suggested to be the weathered metamorphic-granite complex. The mineralization age has not been determined.

2.2. Ge-Rich Lignite of the Kas Area

High-Ge-bearing lignite was identified in eastern Siberia on the eastern margin of the West Siberian Plate at the border with the Yenisey Ridge within the Kas depression. The lignite in the middle reaches of the Yenisey River, localized within the Meso-Cenozoic deposits of the Kas depression (Figure 3), is considered as a new promising source of Ge raw material in Russia [38,39].

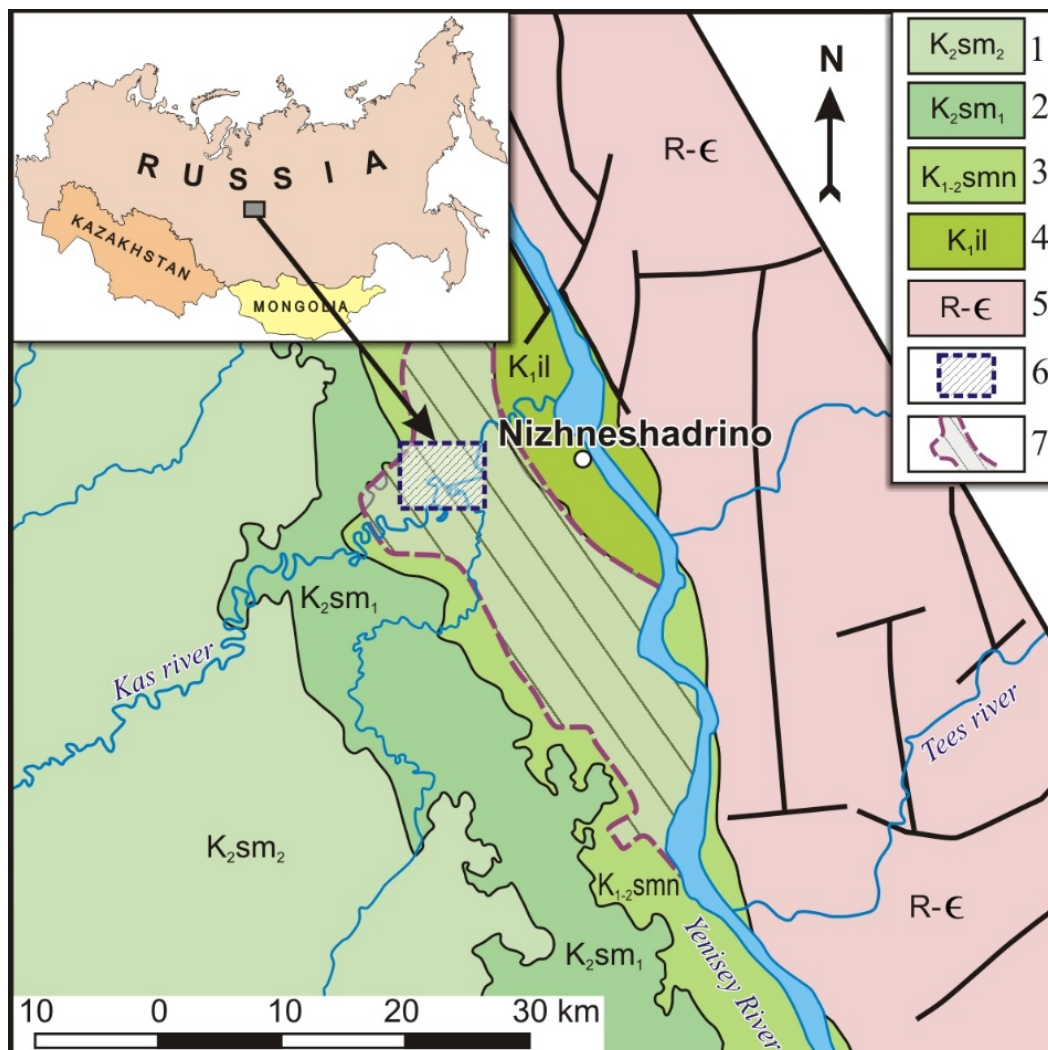


Figure 3. Geological map showing the location of the Nizhne-Kas germaniferous lignite area [38]. Note: 1—Upper Cretaceous system, Campanian–Maastrichtian stages, Symkaya Formation, upper subformation, Vari-grained quartz sand kaolinized with interlayers of kaolin clay and lignite; 2—Upper Cretaceous system, Cognac–Santonian stages.; Symkaya Formation, lower subformation., Vari-grained quartz sand with interlayers of kaolin clay; 3—Lower-Upper Cretaceous system, Albian–Cenomanian–Turonian stages, Simonovskaya Formation, Lake-alluvial deposits, Quartz sand with interlayers of clay and poorly lithified sandstone, germaniferous lignite; 4—Lower Cretaceous system, Valanginian–Barremian stages, Ilel Formation, Variegated clay and clayey sand with interlayers of siltstone, mudstone, sandstone, and inclusions of plant residue; 5—Riphean–Cambrian crystalline basement., Metasedimentary rock including granitoid, gabbroid, and ultrabasic bodies metamorphosed to amphibolite and greenschist facies; 6—The Serchanskoe Ge deposit; 7—Outlines of the Nizhne-Kas lignite deposit.

Anomalous Ge-bearing lignite in the basin of the Kas and Sym rivers (left tributaries of the Yenisey River) was first discovered by Yu.I. Gorky in the 1960s [40]. The highest concentrations of Ge (up to 380 ppm, ash basis) were detected in the horizons sampled in the coastal outcrops of the rivers. Later, detailed prospecting and exploration were carried out resulting in the identification of the 563 km² Ge-bearing Nizhne-Kas area with Ge resources exceeding 11,000 tons [41]. Within this area, there is the Serchanskoe deposit with an estimated resource of over 1112 t Ge [39,42]. According to these researchers, the content of Ge in the lignite in the Nizhne-Kas area varies from 35 to 543 ppm (whole-coal basis) with the ash yields in the lignite and mineralized lignite of 3.2%–84.8% [38,41,43,44]. In the lignite ash, the Ge content is 560–3600 ppm. The Ge-bearing potential of the Nizhne-Kas area is very high. In the future, it is expected to become one of the largest Ge deposits in the world.

The strata of the area include Jurassic, Cretaceous, and Neogene–Quaternary sedimentary sequences (Figures 3 and 4). The Jurassic coal-bearing sediments are represented by alternating gray sandstone, siltstone, and clay shale with brown coal seams and inclusions of charred plant residue. The coal of the Jurassic coal-bearing formation has an increased content of Ge, but no commercial Ge concentrations have been found [38,44]. Cretaceous continental deposits are represented by sand, poorly lithified sandstone, variegated clay, and clayey sand with siltstone and argillite interbeds including charred plant remnants (Figure 4). The Cretaceous deposits have a monoclinical, almost subhorizontal (1°40′–3°50′) bedding, dipping northwestward [42]. Lignite-bearing horizons are common in these deposits, and they are anomalously enriched in Ge in some areas.

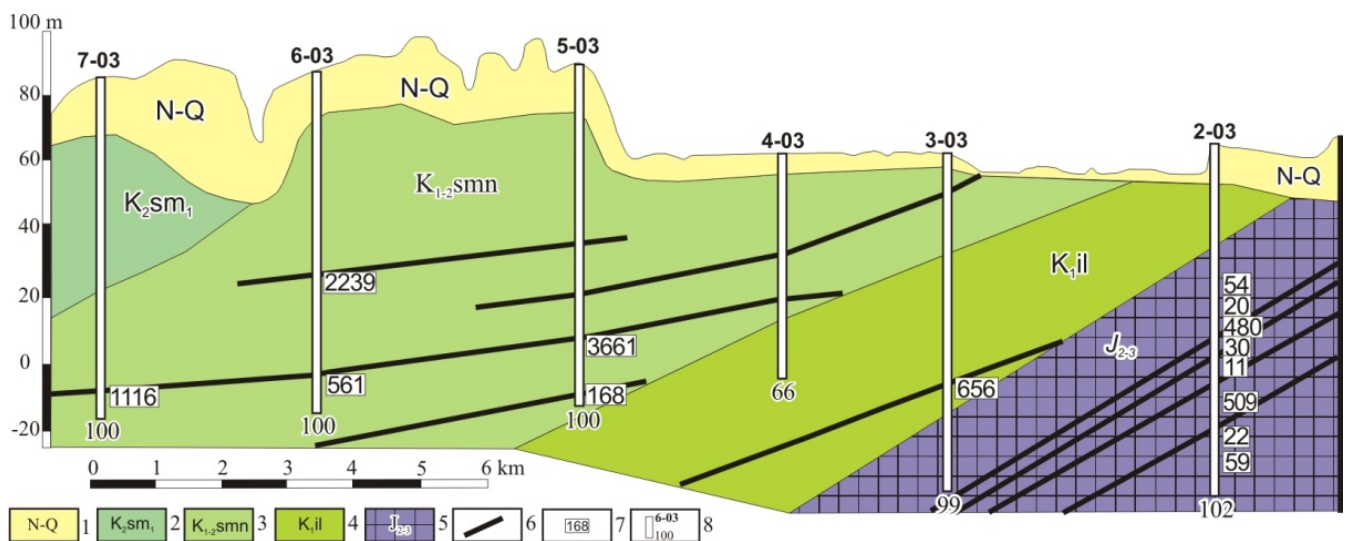


Figure 4. Schematic geological section of the lignite-bearing deposits along the Kas River [41]. Note: 1—Neogene–Quaternary undifferentiated systems, Sand, gravel-pebble, and loam with pebble; 2—Upper Cretaceous system, Symkaya Formation, Lake-alluvial deposits, Quartz sand with bands of clay and poorly lithified sandstone, lignite; 3—Lower–Upper Cretaceous system, Albian–Cenomanian–Turonian stages, Simonovskaya Formation, Gray sand with bands of clay, siltstone, and mudstone, lignite; 4—Lower Cretaceous system, Valanginian–Barremian stages, Ilel Formation, Variegated clay and clayey sand with bands of siltstone, mudstone, sandstone, and inclusions of charred plant residue; 5—Jurassic system, middle–upper divisions, Interbedded gray sandstone, siltstone, clay with lignite seams, and inclusions of charred plant remains; 6—lignite-bearing horizons; 7—Ge content in ppm of ash; 8—exploration well: its number above, depth in meters below.

The most Ge-rich lignite-bearing horizons are confined to the Aptian and Albian stages of the Lower Cretaceous (Figure 4). The lignite-bearing horizons are beds of loose and friable sandstone filled with lignite debris, i.e., carbonaceous woody remnants. The sandstone is predominantly composed of quartz and feldspar. It is characterized by a

significant content of clay minerals (kaolinite and montmorillonite). Among the heavy minerals, pseudorutile, monazite, ilmenite, zircon, and garnet are common. As a rule, these minerals are poorly rounded or semi-angular. Pseudorutile is predominant in the heavy fraction (up to 70%). Sandstone is light gray, fine- to medium-grained, and cross-bedded. The lignite horizon thickness varies from 0.3 to 2.6 m (0.8 m on average). Along strike, ore bodies in the Serchanskoe deposit were found by boreholes for more than 170 m. The distance between these in the cross section reaches 16 m on average, varying from 2 to 33 m [42].

According to the quality indicators (Table 2), the coal in the deposit is lignite A. Therefore, it can be burnt to obtain an ash with a 0.6% Ge concentrate [41]. The humic acids yield ranges from 5% to 78.6%, suggesting the presence of oxidized varieties in the lignite. The average specific weight of the lignite is about 1 t/m³ with porosity varying from 5.05% to 6%. The anhydrous resin yield is 2.2% to 10.1%, and the low-temperature coke yield is 55.6% to 81.5%.

Table 2. Quality indicators of lignite in the Nizhne-Kas area [41].

Indicator	Average Value
Calorific value (Q^{daf}), kcal/kg	6265
Total moisture (W^{T}), %	33.9
Ash content (A^{d}), %	17.2
Volatile matter (V^{daf}), %	50.7
Anhydrous tar (T^{d}), %	5.5
Humic acids (HA^{daf}), %	27.4

The nature of Ge is unclear, and its source remains unknown, but some authors [39] suggested that elevated Ge concentrations in the Kas Depression lignite were associated with the weathering products of several polymetallic deposits in the Yenisey Ridge, where increased Ge content was observed.

Later data on the composition of the lignite indicated that in addition to Ge, it is enriched in a large group of siderophile, lithophile, and chalcophile elements (Table 3).

This fact indicates the presumably hybrid source of Ge in the lignite. One of the sources may be equally represented by the Precambrian granitoids of the Yenisey Ridge, as indicated by the anomalously high content of U, Th, Y, lanthanides, Zr, Nb, Be, and Sn in the lignite ash. The possible influence of polymetallic sulfides is supported by the anomalous accumulation of As, Sb, Mo, Pb, Tl, Zn, Cd, Se, Ag, and Cu in lignite. High concentrations of siderophile elements (Cr, V, Ti, Sc, Co, Ni, and Fe) indicate a connection with numerous Precambrian basic to ultrabasic intrusions of the Surhnikhinsky Complex, common in the nearest flank of the Yenisey Ridge [45]. The ultrabasics contain accessory chromite and magnetite. Sulfides are represented by millerite, pentlandite, and pyrrhotite.

Sulfides, such as pyrite and galena, sulfates, and native elements, were found in the lignite. Pyrite occurs as framboids localized as single grains or their aggregates at the borders of cellular fibers and in desiccation cracks [42]. Such framboidal forms of pyrite aggregates indicate the role of micro-organisms in its formation [46]. Among the sulfates, barite is the most abundant. Both Cu–Zn (an intermetallic alloy) and As are found in the native form. The presence of the native form of elements indicates an ultra restorative environment. Native metals and intermetallic alloys have been found in coal, and such modes of occurrence rather than in sulfide forms are an insufficient amount of sulfur for sulfide formation in the coals [47–51].

Table 3. The content of elements in lignite and lignite ash * from the Nizhne-Kas area (ppm, analyzed by ICP-MS).

Element	Concentration		Element	Concentration		Element	Concentration	
	Lignite	Ash		Lignite	Ash		Lignite	Ash
Li	0.6	6.7	Nb	6.1	67.2	Dy	6.8	73.9
Be	1.1	12.1	Mo	22.6	248	Ho	1.3	13.8
Sc	10.7	117	Ag	0.26	2.8	Er	4.0	44.2
V	186	2034	Cd	0.34	3.8	Tm	0.59	6.5
Cr	235	2576	Sn	1.1	11.7	Yb	4.6	50.0
Co	14.9	163	Sb	4.8	54.8	Lu	0.60	6.6
Ni	36.3	398	Te	0.003	0.036	Hf	1.26	13.8
Cu	17.4	191	Cs	0.24	2.6	Ta	0.17	1.9
Zn	34.8	381	Ba	70.2	768	W	0.24	2.6
Ga	3.2	35.2	La	27.5	301	Au	<0.002	<0.02
Ge	180.0	1969	Ce	72.5	793	Hg	0.063	0.69
As	60.3	660	Pr	9.1	99.7	Tl	2.3	25.0
Se	2.2	24.6	Nd	43.6	477	Pb	13.9	152
Rb	4.5	49.7	Sm	10.0	110	Bi	0.026	0.3
Sr	7.8	85.4	Eu	2.3	24.7	Th	5.3	57.6
Y	28.7	314	Gd	8.6	94.2	U	7.2	79.2
Zr	113.1	1237	Tb	1.1	12.5	∑REE	192.5	2106

*—Calculated from lignite to ash.

No traces of hydrothermal activity in the Late Mesozoic (including the Cretaceous period) and Cenozoic were found in the area. The latest tectonic–magmatic activation in the region only occurs to the south in the Alate-Sayan folded area dated to the Jurassic [52,53].

Thus, the formation of Ge mineralization in lignite was most likely associated with hypergenic aqueous solutions enriched in a complex mixture of chalcophile, siderophile, and lithophile basic and rare metals that were absorbed by the organic matter in the lignite. The hydrogenous origin of the mineralization is supported by the distribution pattern of Ge and some other elements in clasts and trunks of the lignitized wood [39,42]. The normalized plots of REE distribution also indicate the acidic aqueous mode of REE input to the lignitized wood (Figure 5) [54,55]. The M-H type of REE distribution, common for the hydrogenous nature of lanthanide accumulation in coal, is typical in these samples [21].

The mode of formation of this type of mineralization in lignite is well studied and described [56]. Coals of this type have been found in different regions of the world, where they are characterized by a similar range of trace elements anomalously accumulated in lignite (e.g., Seredin and Magazina [57] in the Far East region, Vassilev et al. [58] in Bulgaria, and Hallam and Payne [59] in England).

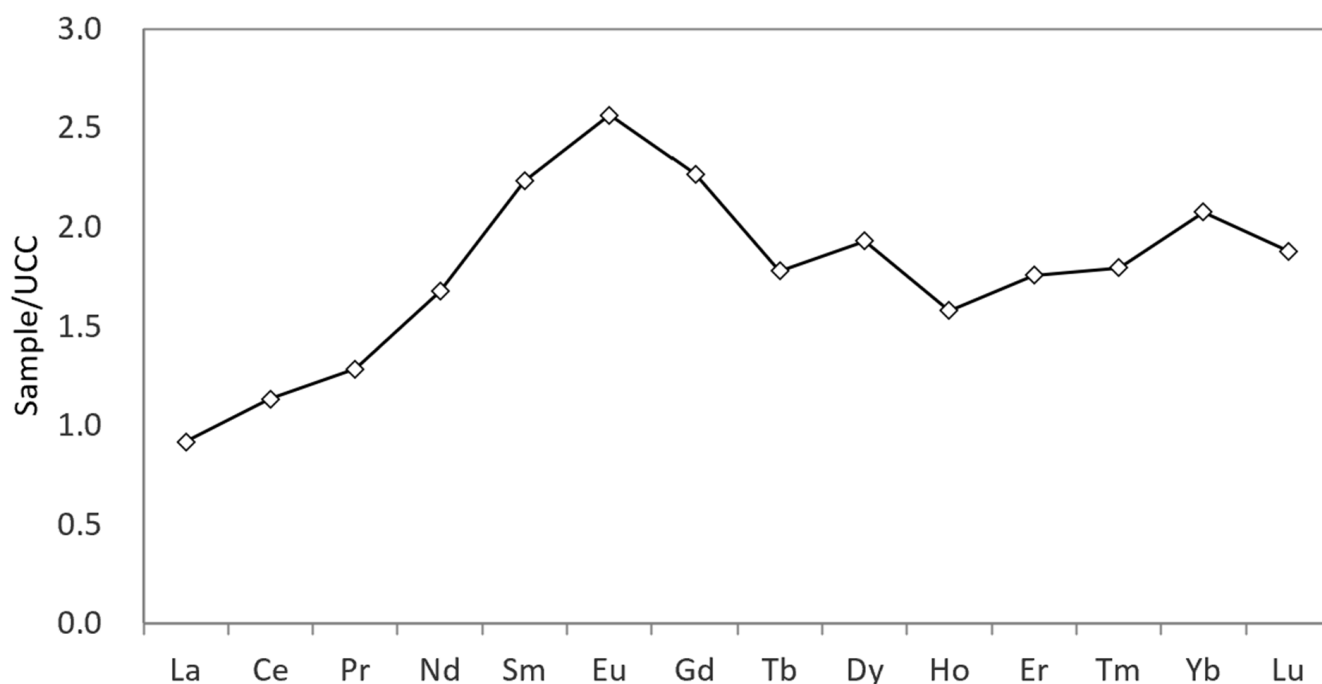


Figure 5. The Upper Continental Crust (UCC)-normalized REE distribution in lignite of the Nizhne-Kas area.

2.3. Au-REE-U-Rich Oxidized Coal of the Aduunchuluun Deposit

In Central and Northern Asia, so-called “sooty” coal is very common. It is widespread in the outcrops of coal seams under recent sediments or the erosion zones of coal seams. Sooty coal is the product of changes to coal in the oxidation zone. Oxidized coal is found in basins of different age, but it is most clearly manifested in the strata of young Mesozoic and Cenozoic coals. With the presence of U-enriched water in the coal oxidation process, radioactive anomalies and, occasionally, U deposits are formed in coal seams. This is especially typical for conditions within an arid or semi-arid climate [60].

The landscape and climate conditions in Mongolia along with the specific features of the coal seam occurrence, and the geochemical speciation of rocks flanking the coal-bearing depressions led to the formation of numerous radioactive anomalies in the oxidation zone of the coal seams. These anomalies were found in the currently developed Baganuur, Aduunchuluun, and Vumbat deposits [61]. Using oxidized coals for energy purposes may lead to the accumulation of significant amounts of hazardous radioactive waste in ash dumps and, ultimately, radioactive contamination of the environment, as happened in the Northern Great Plains of the U.S [62]. To ensure the environmental safety of the population, special measures are required for the disposal of oxidized coal and its processing waste. Studies have shown that in some cases these coals can be considered as independent complex ores. For instance, it was found that the oxidized coal of the Aduunchuluun deposit is a promising complex U–Au–rare–metal raw material [63].

The Aduunchuluun coal deposit is located in the Dornod aimak region of eastern Mongolia (Figure 6). It was discovered in 1951 and has been in production since the late 1950s. Proven coal reserves are 29 Mt and the resources –8 Mt [64]. At present, the coal is mined by open-pit methods. The annual production at the mine does not exceed 200 kt. The main consumer of coal is a local thermal power plant in Choibalsan city. A significant increase in production is possible due to very favorable mining conditions and large coal reserves.

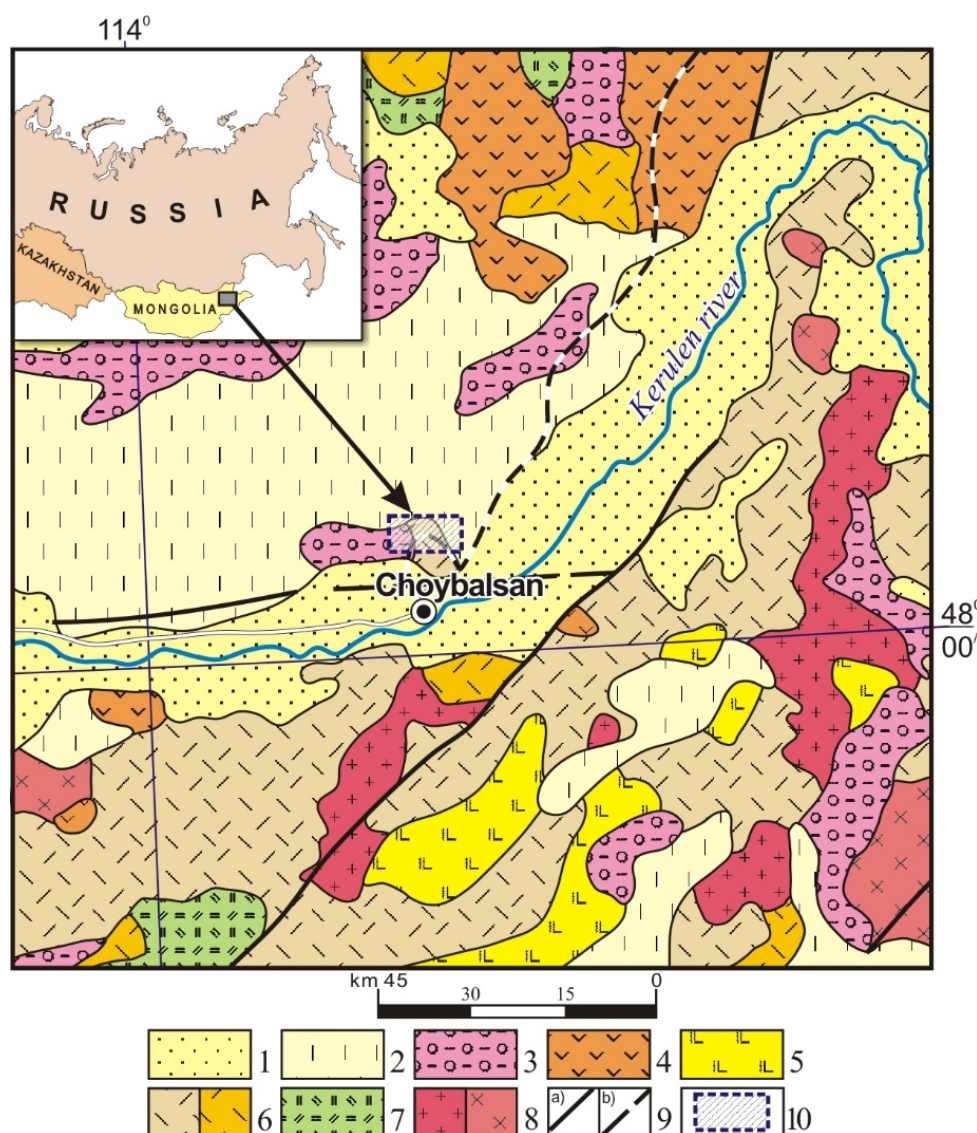


Figure 6. The location and geological map of the study area [65]. Note: 1—Quaternary gray-colored sandy rubble deposits; 2—Paleogene–Neogene gray-colored terrigenous (clayey siltstone, occasionally clayey sand) deposits; 3—Lower Cretaceous coal-bearing molasse; 4—Upper Jurassic–Lower Cretaceous basalt, basaltic andesite, and andesite; 5—Upper Jurassic–Lower Cretaceous basalt–trachybasalt, trachyandesite; 6—Middle–Upper Permian rhyodacite, rhyolite; 7—Upper Permian rhyolite, trachyrhyolite; 8—Triassic–Lower Jurassic granite, leucogranite; 9—Tectonic dislocations: (a) found, (b) assumed; 10—The developed area with the coal mine.

The Aduunchuluun coal deposit is located within a trough in the southern part of the Choibalsan depression in Eastern Mongolia. The coal-bearing deposits of Cretaceous age lie subhorizontally at an angle of 5–10° forming a 6 × 7-km brachysyncline of northwestward extension.

The deposit has a single thick coal seam lying in the coal-bearing strata of the upper sub-formation of the Dzunbainskaya Formation. The coal-bearing formation is represented by alternating dark gray and gray argillite, sand, and loosely cemented sandstone. A significant part of the formation is occupied by coal. Within the mined area, there is one seam up to 40-m thick, 34-m thick on average (Figure 7). In other areas, there are 2–3 seams from 1 to 10-m thick. The coal in the deposit is of the sub-bituminous C type. The average ash yield (A^d) is 16.7%, yield of volatiles is 48.1%, total sulfur (TS) is from 0.68 to 2.0% (1.1% on average), and the vitrinite reflectance (R_{max}) is 0.32% [66].



Figure 7. The sampling scheme in the Aduunchuluun coal mine (photo by Sergey Arbuzov).

The underlying rocks are terrigenous–volcanogenic strata of both pre-Cretaceous and Lower Cretaceous age. Acidic effusives are widespread in their composition. There are also intrusions of early Mesozoic leucocratic granites in the deposit area (Figure 6).

The features of the geological structure and metallogeny of Eastern Mongolia suggests the presence of rare-metal coals, including Ge-bearing coals. The deposit is located in an area of Mesozoic leucocratic granites, the zone of influence of the Bolshekhangin volcanic belt [67], and the Mongol-Priargun U province near the Dornotsky U district [68,69] at the border of W-Mo and Sn-W ore belts of Eastern Mongolia. In this area, the pre-Carboniferous intrusive-volcanogenic complexes of acidic composition (Figure 6) and numerous deposits and manifestations of polymetallic mineralization of hydrothermal and volcanogenic–sedimentary genesis are well-developed. The studies conducted during the exploration of the deposits showed the presence of localised weak anomalies of Ge. The Ge content of up to 176 ppm (whole-coal basis) was confirmed in the coal of the Aduunchuluun deposit during its exploration. Additional detailed studies were carried out to assess the U content. It was found that the upper part of the layer to a depth of 1.8 m is enriched with U up to commercially viable concentrations (0.02%–0.03% on whole-coal basis). A characteristic feature of the deposit is the presence of a well-defined oxidation zone. The coal seam in the area uncovered by the open pit mine is overlain by conglomerates, gritstones, and coarse-grained sandstone with a kaolinite binding mass. The upper part of the main industrial seam is often eroded to a depth of several meters. According to Mongolian researchers, the oxidation zone depth varies from 0.5 to 10 m [61]. The coal in the uppermost part of the seam is highly oxidized, often in the form of soot.

The average content of trace elements in the coal of the deposit, in general, is close to the coal Clarke (Table 4). Concentrations above the Clarke are common for U, Au, As, Ba, Sr, Co, Ge, and Br. The U and Au concentrations are elevated most notably by more than an order of magnitude. Arsenic, cobalt, and Ge concentrations are 3–5 times higher than the Clarke.

Table 4. The average content of selected trace elements in coal, coal ash, and coal-bearing rocks of the Aduunchuluun deposit (ppm; analyzed by INAA and ICP-MS, from Arbuzov and Mashenkin [63]).

Element	Aduunchuluun Deposit			Choibalsan City TPP	Clarke *	
	Coal	Conglomerate	Coal Ash	Bottom Ash	Coal	Coal Ash
Be	1.0	3.0	8.7	4.5	1.2	6.7
B	30	40	271	55	56	410
Sc	0.8	2.4	6.3	4.0	4.1	22
Ti	267	1500	2413	900	700	4000
Cr	6.8	39.6	62	35.5	15	82
Mn	64	200	578	600	100	550
Co	23.9	0.56	231	32.8	4.2	26
Ni	1.8	30	16.4	30	9.0	52
Cu	0.6	15	5.7	30	15	74
Ge	7.9	<2	71	<2	2.0	11
As	24.5	59	221	82	7.6	48
Rb	3.6	113	32.7	98	10	48
Sr	381	325	3437	501	120	750
Y	1.3	40	12.0	24	8.6	46
Zr	<30	80	nd	107	36	190
Sb	0.13	<0.2	1.2	<0.2	0.84	5.0
Cs	0.1	2.5	0.97	2.8	0.98	5.2
Ba	574	1083	4439	3453	150	900
La	8.6	55	63.8	39.3	10	62
Ce	10.3	112	76.0	27.8	22	120
Sm	0.67	8	12.7	2.3	1.9	11
Eu	0.28	9.7	2.8	0.8	0.5	2.3
Tb	0.18	1.1	1.6	0.37	0.32	2.0
Yb	0.71	2.7	6.2	2.7	1.0	5.5
Lu	0.061	0.35	0.40	<0.01	0.19	1.1
Hf	0.37	3.0	3.3	2.2	1.3	7.5
Ta	0.1	1.33	0.91	<0.05	0.26	1.4
Au	0.043	0.039	0.39	0.089	0.003	0.020
Th	1.0	5.1	9.4	4.5	3.3	19
U	32.8	0.36	296	196	2.9	16

*—Ketris and Yudovich [70]; nd, no data.

In the coal ash, the average U content is 296 ppm, suggesting that it can be considered as a run-of-the-mine U ore. The average amount of Au in the coal ash is also close to the minimum commercial content. The analysis of the vertical distribution of trace elements in the coal seam is linked to the anomalous concentrations of U, Au, As, Ba, Sr, and lanthanides with the subsequent epigenetic processes. This is confirmed by a sharp enrichment of the

near-roof zone of the seam in trace elements (Table 5). Here, the coal is strongly oxidized and distinguished by abnormally high, for coal ash, concentrations of U (0.11%–0.33%), Au (0.36–2.13 g/t), As (0.03%–0.06%), Ba (up to 2.6%), Co (up to 350 ppm), Y (up to 0.3%), and lanthanides (Σ REE up to 1.37%). The epigenetic nature of the identified anomalies is also supported by the non-equilibrium U-radium ratio characterized by an excess of U. Our data on the U-radium ratio are in good agreement with the results of the study of radioactive isotopes by Norov et al. [61]. An approximate calculation suggests that the age of U accumulation is no older than 1 million years.

Table 5. The content of trace elements in oxidized coal ash of the Aduunchuluun deposit (ppm, ash basis, analyzed by INAA and ICP-MS).

Elements	Element Content (ppm)			
	Sample ACh-4	Sample ACh-5	Sample ACh-6	World *
Be	1.1	743	275	6.7 ± 0.5
B	212	531	45.8	410 ± 30
Sc	5.3	9.4	18.8	23 ± 1
Ti	1972	4264	2855	4000 ± 200
V	7.4	40.3	52.2	140 ± 10
Cr	21.2	53.1	64.1	82 ± 5
Co	6.2	350	278	26 ± 1
Ni	13.8	457	279	52 ± 5
Cu	237	718	1063	74 ± 4
Zn	55.2	276	132	110 ± 10
Ga	7.4	10.6	8.2	29 ± 1
Ge	2.0	31.8	45.8	11 ± 1
As	126	212	790	48 ± 7
Br	77.3	144	194	32 ± 5
Rb	8.5	20.2	25.6	48 ± 5
Sr	1288	3551	2891	740 ± 70
Y	12.2	426	3063	44 ± 3
Zr	99.7	189	208	190 ± 10
Nb	10.6	29.7	9.2	18 ± 1
Mo	31.8	441	6.4	15 ± 1
Ag	0.16	2.1	0.9	0.59 ± 0.09
Cd	0.53	22.5	6.3	1.10 ± 0.17
Sn	2.5	10.6	6.4	4.7 ± 0.4
Sb	0.9	4.1	1.3	5.0 ± 0.4
Cs	1.6	0.3	0.5	5.2 ± 0.5
Ba	783	1640	1606	900 ± 70
La	22.4	222	1586	61 ± 3
Ce	42.4	300	3392	120 ± 10
Pr	5.2	33.7	447	13 ± 2
Nd	20.2	168.9	2197	58 ± 5
Sm	3.07	28.2	498	11 ± 1
Eu	0.56	7.05	123	2.3 ± 0.2

Table 5. Cont.

Elements	Element Content (ppm)			
	Sample ACh-4	Sample ACh-5	Sample ACh-6	World *
Gd	3.41	56.2	740	16 ± 1
Tb	0.52	6.61	106	2.0 ± 0.1
Dy	3.02	38.5	619	12 ± 1
Ho	0.56	10.2	131	3.1 ± 0.3
Er	1.63	32.9	381	4.6 ± 0.2
Tm	0.28	4.46	51.4	1.8 ± 0.3
Yb	2.45	29.1	337	5.5 ± 0.2
Lu	0.44	5.96	52.8	1.1 ± 0.1
Hf	2.9	3.1	5.0	7.5 ± 0.4
Ta	0.4	0.7	0.8	1.4 ± 0.1
W	7.0	15.4	5.4	6.0 ± 1.7
Au	<0.01	0.36	2.13	0.020 ± 0.005
Pb	15.9	58.4	33.0	38 ± 2
Th	8.3	8.7	13.9	19 ± 1
U	31	3272	1112	16 ± 2
∑REE	118	1370	13,723	
Ad, % **	11.4	17.5	40.9	

*—World coals according to Ketris and Yudovich [70]; ACh-4—weakly oxidized coal; ACh-5—oxidized coal; ACh-6—sooty coal at the contact with overlapping conglomerates; **—ash content of dry matter.

The hydrogenic accumulation model is supported by the character of the normalized graphs of REE (Figure 8). The M-H type of REE distribution is specific for the hydrogenic nature of lanthanide accumulation in coals [21]. The connection of lanthanide anomalies with the hypergene water is also confirmed by the presence of a weakly manifested cerium anomaly in the coal. This anomaly indicates the connection of aqueous solutions with the formation of the weathering crust.

The data obtained reveal pronounced geochemical zoning. With low mobility in hypergenic conditions, lanthanides (REE), Cr, Au, and As form anomalies directly at the border of the coal seam (Table 5, sample ACh-6). More mobile U, Ba, and Co form contrasting anomalies at a distance from the contact area (Table 5, sample ACh-5).

The study of the coal combustion residue samples (a mixture of fly ash, bottom ash, and slag; but the ratio between them is unavailable) from the Choibalsan city thermal power plant (TPP) showed a lower content of trace elements compared to the laboratory coal ash from the deposit. This may be due to various reasons, including heterogeneous distribution of trace elements in the coal seam, loss of the more volatile elements with emissions during coal combustion, their leaching by water from ash and slag, and redistribution in the ash dump. As only the near-surface part of the ash ponds has been studied, it is necessary to investigate the whole cross section.

Thus, studies have shown that the oxidized coal of the Aduunchuluun deposit and bottom ash from the ash pond of the Choibalsan city TPP can be considered as a promising source for the extraction of U, Au, and other associated trace elements.

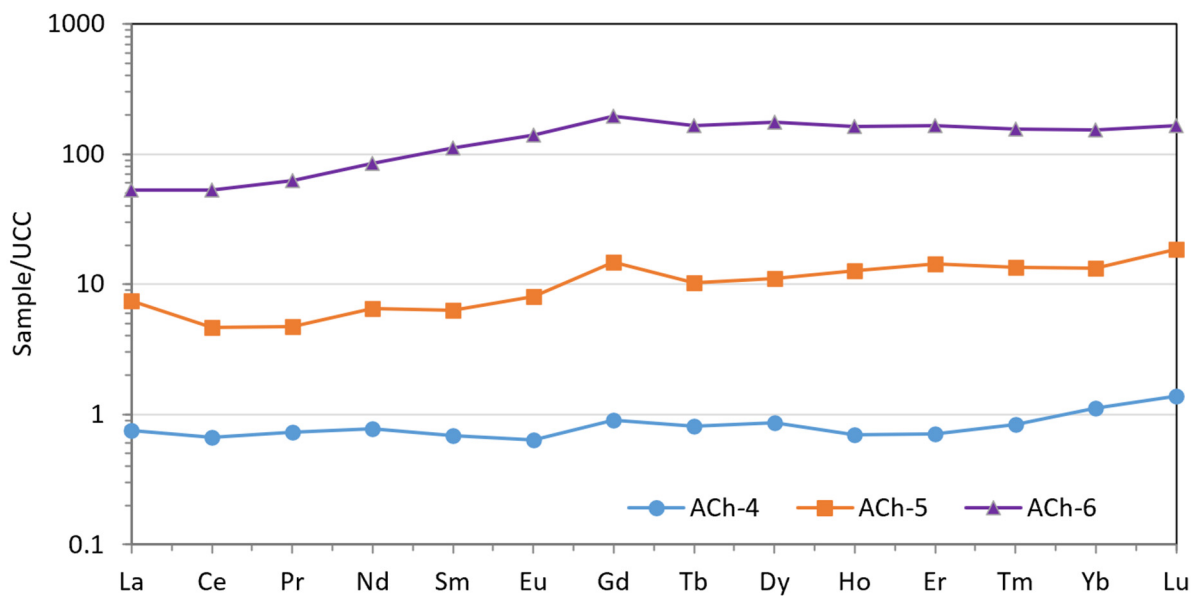


Figure 8. REE distribution patterns of weakly oxidized coal (ACh-4), oxidized coal (ACh-5), and sooty coal at the contact with the roof conglomerates (ACh-6); normalized for UCC according to Taylor and McLennan [71].

At present, the upper interval of the oxidation zone of the coal seam with a thickness of about 1.5 m goes to a dump. This part of the coal seam is the richest in U, Au, and lanthanides. A 10 km² plot of such coal contains about 12,000 tons of U, 1.8 tons of Au, and 12,000 tons of the sum of lanthanides and yttrium. According to a rough estimate, the U resources in the ash pond of the Choibalsan city TPP amount to about 50 tons and Au resources to more than 20 kg.

High levels of U in the coal and bottom ash also pose a radioecological hazard to public health. It is necessary to conduct specialized research on the disposal of radionuclide-enriched bottom ash and the possible safe use of highly radioactive oxidized coal.

2.4. Metalliferous Coals of Primorsky Krai

The Primorsky Krai region of the Russian Far East is known for its abundant metalliferous coals. Basins of the Primorsky Krai contain a significant part of the world's proven reserves of Ge (four deposits and several occurrences), as well as numerous occurrences of noble and rare-metal mineralization in the coals and coal-bearing rocks [21,22,24,72–76]. All of these coals and associated mineralization are of Cenozoic age, while no metalliferous coals of Cretaceous age have been discovered so far. However, thematic works by the Institute of Mineralogy, Geochemistry, and Crystal Chemistry of Rare Elements (Moscow, Russia), which were conducted at the end of the last century, revealed increased concentrations of some trace elements in the Cretaceous coals of the Primorsky Krai region (in parentheses, the concentration factor relative to the Clarke in coals): Ti (5.2), Nb (4.8), Rb (4.0), Zr (3.5), Cs (3.0), Ga (2.9), and La (2.5). Based on these studies, it was concluded that the Cretaceous coals with a similar geochemistry to the Cenozoic lignites are enriched in Nb, Zn, Pb, Ga, and Zr and depleted in P, Ba, Ag, Mn, Sc, and F.

It was also observed that the coal of the Partizansky Basin and Podgorodnensky deposit could be considered as potential sources for the extraction of Zn, Ga, B, and Pt, while the Lower Cretaceous coal of the Lipovetsky deposit could be a potential source of Ga. Commercial concentrations of Ag can be found in the Partizansky Basin coal. The geochemistry and critical element content of the Cretaceous age coals have been recently examined by some of the authors of this study, using published, archival, and recent unpublished data from six deposits (Podgorodnenskoye, Lipovetskoye, Ilyichevskoye, Konstantinovskoye, Partizanskoye, and Surazhevskoye).

Combined ICP-MS and INAA analyses of coal samples from these six Cretaceous age deposits showed that most of the trace elements are present in the coal in near-Clarke concentrations or slightly above them, and, therefore, they are not metalliferous. However, the Partizansky Basin coal (the Kalancha site and Severnaya mine) where the total REE content exceeds 100 g/t may be of interest. In general, the studied Cretaceous coals in the Razdolnensky and Partizansky Basins of the Primorsky Krai region are not metalliferous and not interesting as a source of rare metals. Possibly, the specificity of its composition is associated with the absence in the flank and in the basement of deposits of rare-metal granites, which are the main sources of rare elements in the known metalliferous lignites of the superimposed Cenozoic depressions (Pavlovskaya, Rakovskaya, Shkotovskaya, Nizhnebikinskaya, etc.). Another supposition is that the Early Cretaceous waters were oversaturated with organic acids that exerted a negative impact on the mineralization system [77].

3. Metalliferous Coals from South America

3.1. Peru

The intensely folded and faulted Alto Chicama field is located along the western slope of the Western Cordillera of the Peruvian Andes (Figure 9). The No. 5 seam, from which coal balls (“Bollas”) were extracted, occurs in the 930-m-thick Lower Cretaceous (Neocomian) Chimu Formation, the basal unit of the Goyllarisquiza Group [78]. The No. 5 seam averages 1.6-m thick and dips between 70 to 85 degrees. The reported anthracite quality for this seam is 4.7 moisture, 4.9 ash, 2.3% volatile matter, and 88.1% fixed carbon. The R_{\max} of the coal exceeds 6% [79,80].



Figure 9. Map of South America with the approximate locations of the coalfields mentioned in the text shown.

The U.S. Geological Survey's World Coal Quality Inventory (WoCQI) (https://www.usgs.gov/centers/gemsc/science/world-coal-quality-inventory-data?qt-science_center_objects=0#qt-science_center_objects, accessed on 6 September 2022) investigated 16 anthracites from Peru (Table S1), but the lanthanides were not analyzed. Peru sample BP2900 has 125-ppm Sc, 95-ppm Y, 124-ppm Co, 645-ppm Cu, 106-ppm Ga, 473-ppm Li, 53-ppm Nb, and 1094-ppm V (ash basis), the highest concentrations among the 16 samples in the Peru collection. The sample also has 71-ppm Th and 18-ppm U (ash basis). BP0108 has 1169-ppm Pb and 1128-ppm Zn and BP0104 has 8817-ppm Zn (ash basis). A total of 10 of the samples have more than 100-ppm Li (ash basis). Commercial prospects and the origin of these local enrichments have not been studied yet.

3.2. Other South American Countries

High through low volatile bituminous coals occur in the Maastrichtian portion of the Guaduas Formation in the Eastern Cordillera of the Andes of Colombia (Figure 9). The WoCQI sampling from Colombia was strictly from the Paleogene coals in Guajira state, so we do not have modern analyses of the Cretaceous coals.

Argentina has Neocomian coals in western Santa Cruz Province, Senonian coals in the Comodora Rivadavia region, and Danian coals in Chubut Province, all of these flanking the Andes in Patagonia (Figure 9) [81]. As with the Colombian coals, modern analyses are not readily available.

4. Metalliferous Coals from the United States and Mexico

Numerous studies on the stratigraphy of the Cretaceous of the western United States have been made over the course of the last century, and more recently, for example, Flores and Cross [82] described the Cretaceous and Cenozoic coals in the region. The prospects for coal mineralization and the resulting emplacement of critical elements have not drawn much attention even though the ongoing tectonic activity in the region [83] would appear to have offered ample opportunities for the emplacement of tonsteins (see discussion of Crowley et al. [84], below) and hydrothermal metamorphism accompanying igneous intrusions and thrust faulting.

Data for the western U.S. coals are presented in Tables S3 and S4. As analytical caveats, for the U.S. Geological Survey samples [85] (Table S3), only the W- and WA-prefix analyses were used in the discussion. Data reliability issues, including missing and some falsified analyses precluded the use of D-prefix analyses from that database. For the Penn State samples, the analytical methods employed at the time of the analyses (Direct Current (DC) Arc Emission Spectrography (installed in 1951; Harold Lovell personal communication to Hower, 1976) were not as precise as the methods employed at the time of this writing; details of the technique are in Grimes and Marranzino [86], so the REE, aside from La and Ce, were not detected.

4.1. Eagle Pass Coal, Maverick County, Texas, and Piedras Negras, Coahuila, Mexico

The Upper Cretaceous (Maastrichtian) Olmos Formation coal occurs northeast of Eagle Pass, Maverick County, Texas [87,88] and in the Sabinas Basin, Coahuila, Mexico (Figure 10) [89–93]. The coal is separated into three different mined beds, the C2, C1, and B. The C2 is the uppermost minable coal with an overburden range of 4.57 to 57.9 m, with an average of 20.4 m. The average thicknesses of the C2, C1, and B beds are 0.82, 0.49, and 0.55 m, respectively (Benson Chow, personal communication, 8 February 2019). The coal rank is high volatile C bituminous/sub-bituminous (0.52% R_{max} based on determination by Hower on the Zygarlicke et al. [94] samples; 0.46%–0.50% R_{max} based on the Penn State (PCOC) database.

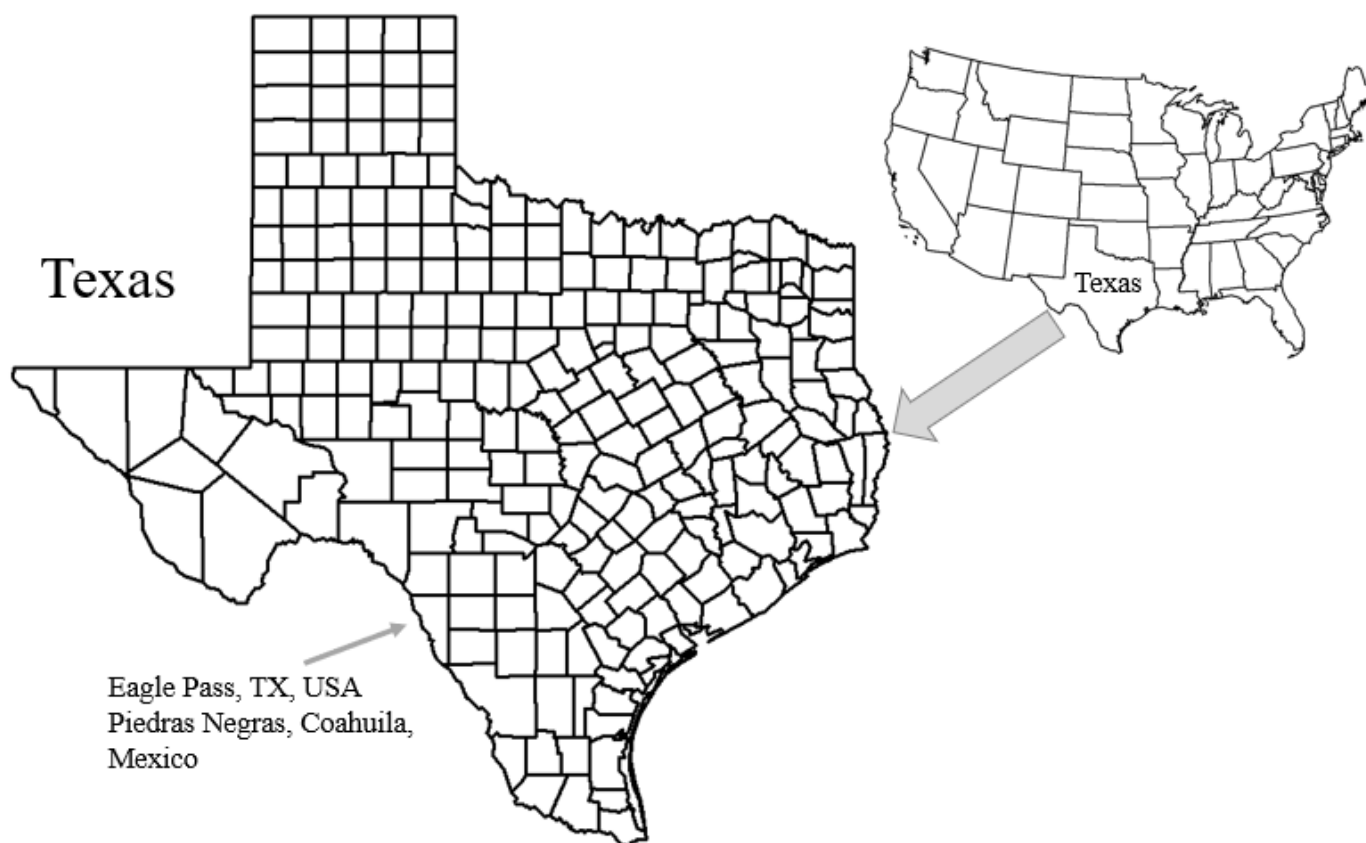


Figure 10. Location of Eagle Pass, Maverick Co., Texas, USA, and Piedras Negras, Coahuila, Mexico.

Analyses by Zygarlicke et al. [94] demonstrated that portions of the coal are enriched in REYSc (REE+Y+Sc) (Table S2). The coals (samples 124915, 124916, 124918, 124926, 124929, and 124930) all exceed 300-ppm REYSc (dry basis), with samples 124929 and 124930, the B Upper and B Lower splits, respectively, approaching and exceeding 1000-ppm REYSc. Sample 124919 (split C1U), identified as clay in the sampling, has a relatively high REYSc and, based on the ash yield, should be a coal. Based on the Upper Continental Crust normalized REE values (Figure 11) B lower (sample 124930), B upper (sample 124929), and C1L lower (sample 124826) have notable negative Eu anomalies. All the coals have H-type distributions ($Lu > La$), although C1L lower is only marginally H-type distribution (after Seredin and Dai [21]). Among the clays (Figure 11), 1B lower (sample 124927) and 1B upper (sample 124928) have notable negative Eu anomalies. The lowermost two coals and two clays are the only samples with notable negative Eu anomalies. C1U (sample 124919) has a light REE normalized pattern similar to the clays but is among the high REE coals with respect to its heavy REE pattern. C1U underlies coal C2L (sample 129418), a high REE sample. C1U clay and C2L coal have similar REE distributions.

The H-type distribution of REE in the mineralized coals from the Eagle Pass location indicates influence of alkaline waters [54].

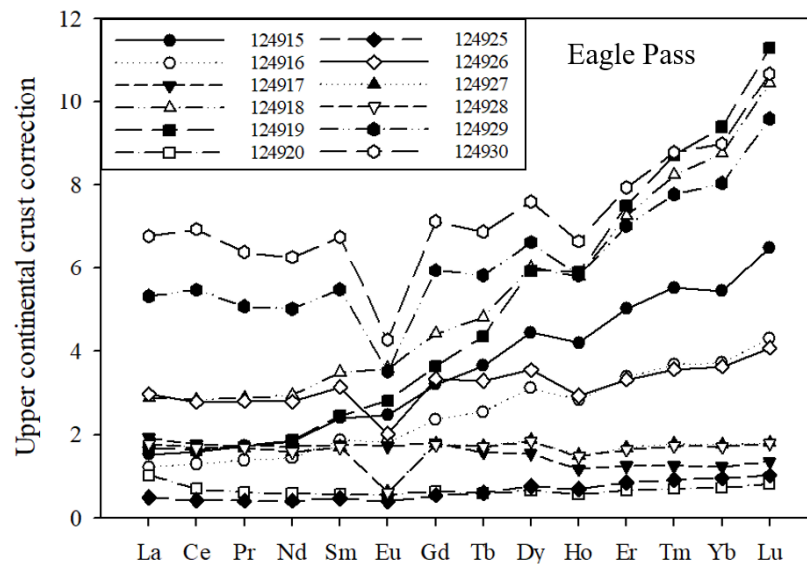


Figure 11. Upper Continental Crust normalized REE spider plots (after Taylor and McLennan [71]) for the Eagle Pass coal and clay lithologies.

4.2. Anthracite: Gunnison County, Colorado, and New Mexico Locations

The Late Cretaceous Mesaverde Formation coal from Gunnison County, Colorado, was metamorphosed to semianthracite, anthracite, and natural coke by a laccolith of Oligocene age (Figure 12) [95,96]. An anthracite (PSOC-158; (Table S4) has 5400-ppm Sn and 370-ppm Ce + La and a semi-anthracite (PSOC-161) has 1800-ppm Sn. As a caveat, note that the samples were reported to be grab samples, so they are not representative of the whole coal. Based on REE and Ce + La analyses (300 ppm < REE < 750 ppm) by Bragg et al. [85], the total REE for PSOC-158 is estimated to be in the 500- to 600-ppm (ash basis) range (Table S4, graph at row 5/column BO). While the Sn concentration is intriguing and could be indicative of further mineralization and the estimated REE content is high enough to provoke interest, we note that the coal is in a rugged terrain at a relatively high altitude and renewed mining might be uneconomical.

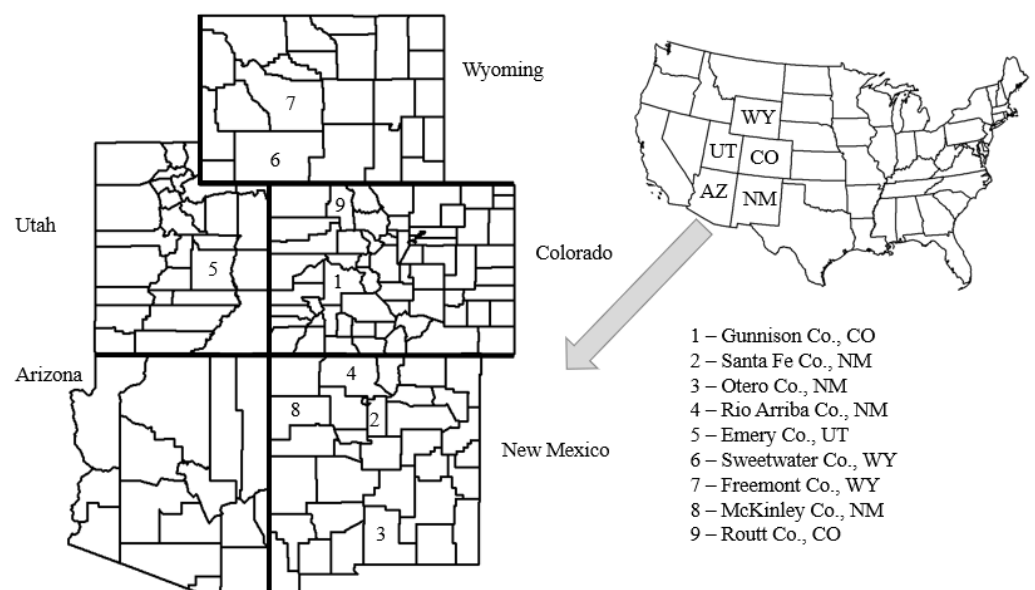


Figure 12. Western USA states with Cretaceous coals mentioned in this section (Alaska is on a separate figure). The counties with coal deposits are numbered on the key).

The Late Cretaceous (Campanian) Menefee Formation anthracite occurs in the Cerrillos coalfield, Santa Fe County, New Mexico [97–100]. None of the latter publications provide any details of the major oxide or minor/trace element chemistry. Bragg et al. [85] listed an anthracite in Otero County, New Mexico; aside from having 480-ppm REE and 573-ppm REYSc, the chemical analyses do not stand out from the other western US K coals.

The mineralization of Upper Cretaceous anthracites from Colorado and New Mexico were probably related to the post-Cretaceous igneous activity.

4.3. C Coal Bed, Emery Coalfield, Utah

Crowley et al. [84], building upon examinations of the ash fall deposits [101,102], examined the chemistry (after Crowley et al. [93]) of the C coal bed (Upper Cretaceous (Turonian) Ferron Sandstone Member of the Mancos Shale) with respect to the included tonsteins (persistent bands of altered volcanic ashes typically occurring within coal seams). The coal bed includes four tonstein partings, ranging from 3- to 40-cm thick, each including minerals diagnostic of a volcanic origin, including β -quartz, splinter-shaped quartz, euhedral zircon, and euhedral magnetite. The coal immediately adjacent to the tonsteins was found to have an enrichment in REE, Y, and Sc (Y analyzed by Optical emission spectroscopy; Ce, Lu, Sc, Sm, Yb, and Eu by Instrumental neutron activation analysis). This enrichment was attributed to a combination of “(1) leaching of volcanic ash by groundwater and subsequent uptake of ions by organic matter, (2) leaching of volcanic ash by groundwater and incorporation of ions into authigenic minerals, or (3) incorporation of volcanic minerals in peat.” [103].

As with the Gunnison County, Colorado, coals noted above, the Penn State data (Table S4) is hindered by the techniques in use at the time of the analyses. Although the C coal bed was not analyzed, there are a few, interesting analyses, including PSOC-438 (B coal bed) with 620-ppm Ce and 350-ppm La. PSOC-500 (Hiawatha coal bed) has 240-ppm Ce and 130-ppm La. Among the samples examined by Bragg et al. [75], one Emery County, Utah, coal has 1687-ppm REYSc (ash basis), and several others from the same county exceed 500-ppm REYSc. Several other high-REYSc coals, up to 1682-ppm REYSc in a coal from Wasatch County, are found among the K coals in the state.

4.4. North Slope, Alaska

Hypothetical coal reserves of the Cretaceous Albion–Cenomanian Nanushuk Group on the North (Arctic) slope of Alaska in the 650-km stretch from Corwin Bluff to Prudhoe Bay and north of the Brooks Range total 3.64 Tt, exceeding the 3.37 Tt hypothetical reserves in the conterminous (lower 48 states) United States (Figure 13) [104]. Coal rank increases from sub-bituminous to high volatile A/medium volatile bituminous (up to 1.11% Rmax) [105]. The latter report, though, does not report any chemistry beyond the proximate and ultimate analyses and the limited data in Bragg et al. [85] (Supplemental files “USGS Bragg et al.”) and in the Penn State data base (Supplemental files “Penn State K coal data”) does not show any anomalously high critical element data.

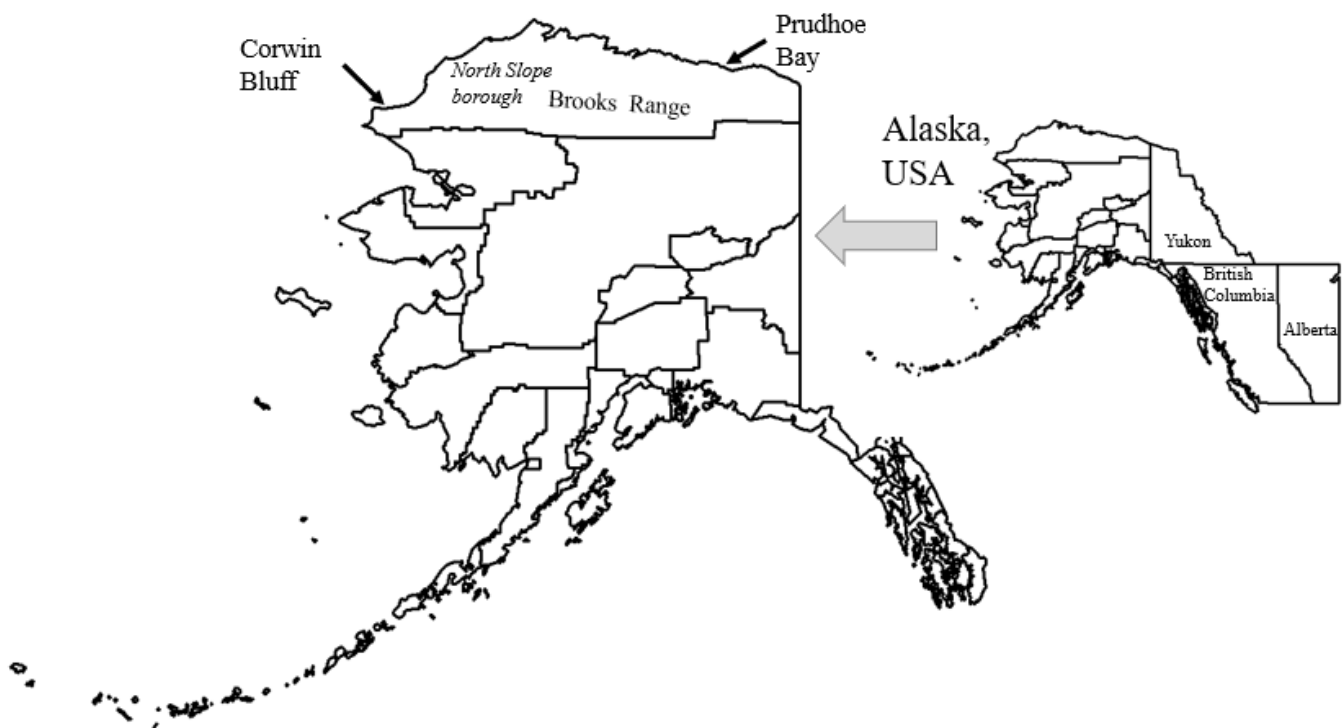


Figure 13. Location of Alaska with respect to the Canadian provinces of Alberta and British Columbia (coalfields discussed below) and Yukon Territory. The North Slope coal deposits are outlined by Corwin Bluff, the Brooks Range, Prudhoe Bay, and the Arctic Ocean (to the north).

4.5. Other Occurrences of Interest

Some of the Menefee Formation coals in the Monero coalfield (described by Hoffman [106]), Apache Mesa 7 1/2' quadrangle, Rio Arriba County, New Mexico, have high REYSc concentrations (Figure 12). Samples W223560, W223562, W223565, and W223564 have 6261-, 1538-, 1283-, and 980-ppm REYSc (ash basis), respectively [85]. Sample W223560 has 429-, 1857-, and 3000-ppm Sc, La, and Ce (ash basis), respectively, among the REYSc elements; 137-ppm Sb (the only sample with >54 ppm); and 14286-ppm F and 10,000-ppm Cl (ash basis). Sample W223566 has 914-ppm Ge (ash basis), one of only eight coals of 180 Cretaceous coals in this set with more than 100-ppm Ge (Table S3). Germanium enrichment in coal can be related to leaching of Ge from roof and floor rocks [107,108] from adjacent Ge-rich rocks, such as igneous intrusions, the source of the enrichment in the coal-based Spetsugli deposit, Russian Far East [75,109,110], or from hydrothermal fluids [111,112]. W223560 has 786-ppm Th and 371-ppm U (ash basis). The coal rank is high volatile B to high volatile A bituminous rank [106]. Reiter and Clarkson [113] and Clarkson and Reiter [114] suggested that heat advection from the San Juan volcanic complex of Paleogene age influenced the coal rank and was probably responsible for the coal mineralization.

The Upper Cretaceous Lance Formation coals in the Green River Basin, Sweetwater County, Wyoming, have elevated Ge contents, with samples W218937, W318939, W218940, and W218970 having 267-, 237-, 194-, and 421-ppm Ge (ash basis), respectively (Table S3). Sample W218939 has 543-ppm REYSc, the highest concentration among the coals in the Wyoming portion of the basin. W227750, Moffat County, Colorado, has 1307-ppm REYSc and 123-ppm Th, one of two samples with >100-ppm Th.

Samples W210031 (Wind River Basin, Fremont County, Wyoming), sample W235624 (San Juan Basin, McKinley County, New Mexico), and an averaged analysis from the Green River Basin (Routt County, Colorado; adjacent to Sweetwater County, Wyoming) are the other coals with more than 100-ppm Ge (ash basis) with 124-, 105-, and 237-ppm Ge, respectively (Table S3).

5. Metalliferous Coals from Alberta and British Columbia, Canada

The most important Cretaceous coals in Canada are found in British Columbia (BC) and Alberta (AB) (Figure 14). From west to east, coals are found in the Insular (Graham and Vancouver islands BC); the Klappen and Groundhog coalfields and the Telkwa coalfield in the Intermontane Belt (BC); the Flathead, Crowsnest, and Elk Valley coalfields (collectively, the East Kootenay coalfields in southeast BC), the Peace River coalfield (northeast BC), and numerous small basins in Alberta, collectively the Rocky Mountain Belt; and the Plains coalfields in Alberta. Coal rank varies from sub-bituminous in the Plains coalfields to anthracite on Graham Island, in the Sustut Basin, and in the Klappen and Groundhog coalfields (all in BC) [115–117]. The geologic structure in the Intermontane and Rocky Mountain areas was formed during the Laramide Orogeny of Late Cretaceous–Paleogene age [115–117], and the Insular region was impacted by the accretion of the Wrangellia microplate to North America in the Late Cretaceous [118,119].

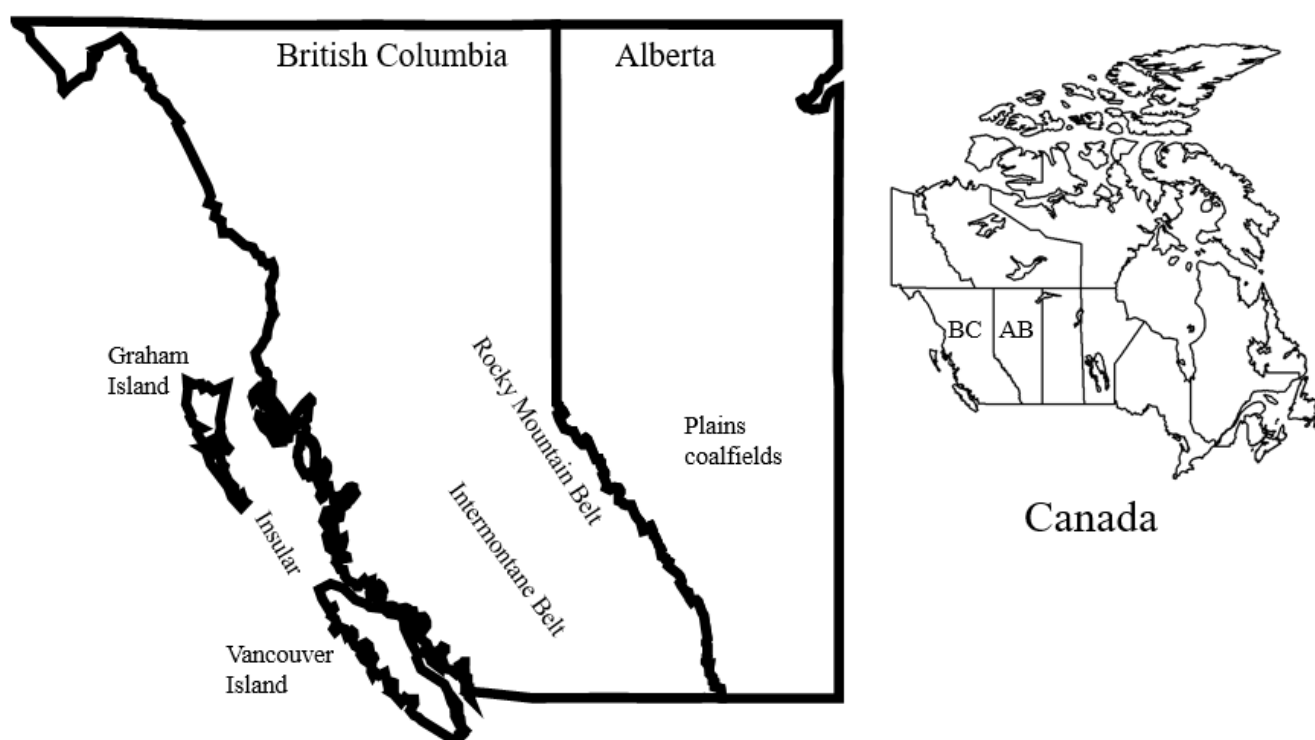


Figure 14. General locations of Cretaceous coalfields in British Columbia and Alberta.

Van der Flier-Keller and Goodarzi [120] investigated high volatile bituminous coals on Vancouver Island. Among the elements of interest, Nb and Y were analyzed by XRF; Au, Sc, W, and the REE were analyzed by instrumental neutron activation analysis (INAA); and Ag, Ni, Ge, and Zn were analyzed by direct current plasma emission spectroscopy. On the ash basis, the Suquash coals are enriched in Sb and depleted in Nb compared with the Nanaimo and Comox coals. REE were highest in the Comox coals. The dominant source rocks for Cretaceous sediments were a calc-alkaline suite and ferrotholeiitic basalt volcanic rocks and granodiorites. A granodiorite in the northwest Comox Basin contributed to a north-to-south decrease in Cr, Ni, Rb, and Ta in the coals accompanied by an increase in the concentrations of Au, Sb, Zr, and HREE. LREE, Ga, and Mo are high in the Comox coals owing to the influence of the adjacent granodiorites. Van der Flier-Keller and Goodarzi [121] further compared the Comox and Nanaimo coal chemistry, albeit with a more restricted list of elements (REE were not included) to Intermontane and Rocky Mountain coals.

Van der Flier-Keller [122] investigated the REE content in five Cretaceous and two Eocene basins in British Columbia. As above, she used INAA to analyze the REE. The REE values for the coals were normalized against the Average North American Shale (ANAS)

(also known as the North American shale composite (NASC)) values after Haskin et al. [123]. Except for the Insular Suquash Basin coals, the Cretaceous coals show a slight enrichment in HREE versus LREE (Supplemental files “van der Flier-Keller 1993”); the Suquash coals show a more pronounced HREE enrichment (Figure 15). The Insular Nanaimo and Comox coals show positive Eu anomalies while the northeast Rocky Mountain Quintette Basin coals show a negative Eu anomaly. All of the coals have an H-type distribution (Upper continental crust (UCC)-normalized Lu>La) probably indicating some alkaline water influence [54]. The shale-normalized (after Van der Flier-Keller [122]) and UCC-normalized distributions for the Suquash coals resemble those of tholeiitic basalt (after Piper [124]). Seeing no relationship between REE and the age of the coals and their rank, Van der Flier-Keller [122] attributed the REE variations to the source of detrital minerals and the geochemical conditions responsible for diagenetic transformations of REE-bearing minerals. While the REE distributions, particularly for the Suquash coals, are interesting, the overall concentrations of the REE are not particularly high (Table S5). Similarly, Goodarzi et al.’s [117] limited analyses of the Elk Valley coals (only La and Ce were analyzed by INAA) do not suggest that the ash-basis total REE values would be more than a few hundred ppm (Table S6).

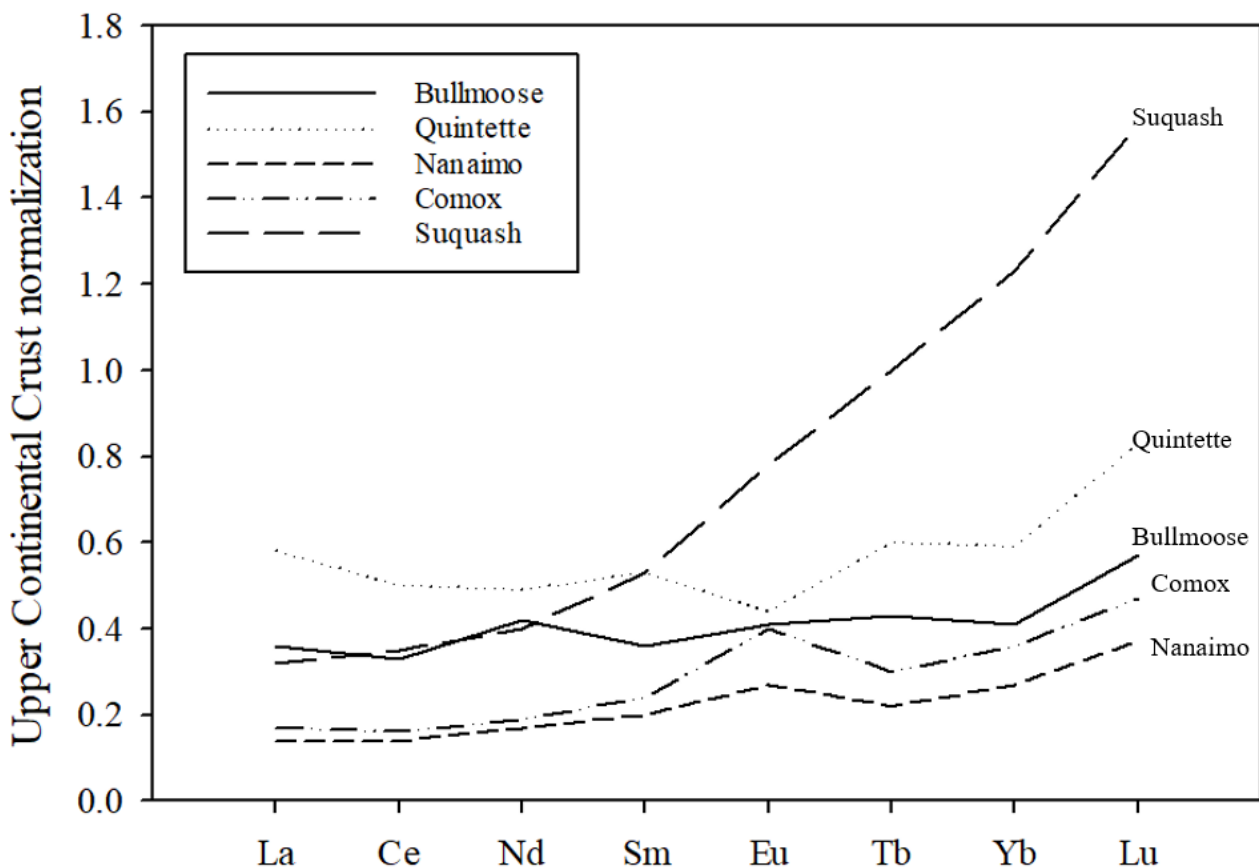


Figure 15. Upper Continental Crust normalization (after Taylor and McLennan [71]) for basin averages of Cretaceous coals from British Columbia [122].

6. Metalliferous Coals from China

There are six major coal-forming periods in China: Late Carboniferous and Early Permian (C₂–P₁), Late Permian (P₂), Late Triassic (T₃), Early and Middle Jurassic (J_{1–2}), Late Jurassic and Early Cretaceous (J₃–K₁), and Paleogene and Neogene (E–N) [125]. Note that the Late Jurassic and Early Cretaceous age are usually combined because the coals of the two ages generally spatially co-exist. The recoverable coal reserves of the six coal-forming periods are 38.1% (C₂–P₁), 7.5% (P₂), 0.4% (T₃), 39.6% (J_{1–2}), 12.1% (J₃–K₁), and 2.3% (E–N) [126].

Table 6 lists concentrations of some selected elements in coals from different coal-forming periods in China [125]. The concentrations of V (CC = 1.23), Mn (CC = 1.45), Ge (CC = 1.32), As (CC = 1.59), and Sb (CC = 1.63) in the J₃–K₁ coals are slightly higher than those of common Chinese coals; the average concentrations of other elements in the J₃–K₁ coals are close to or lower than those in the common Chinese coals. Overall, the elements in the J₃–K₁ coals are not distinctly enriched compared with other coals from other coal-forming periods.

Table 6. The average concentration of elements in coals from different coal-forming periods in China (ppm, on a whole-coal basis).

Elements	C-P ₁	P ₂	T ₃	J ₁₋₂	J ₃ –K ₁	E-N	Average	Number of Samples	CC
Be	1.92	2.42	2.67	2.41	1.88	0.93	2.13	1198	0.88
V	39.59	94.69	74.89	14.37	43.08	62.85	34.97	1266	1.23
Cr	15.81	29.02	50.40	11.40	11.89	43.33	15.35	1592	0.77
Mn	56.8	166.2	77.1	171.1	180.6	42.7	124.9	1268	1.45
Co	4.24	10.24	7.72	8.59	8.09	11.75	7.07	1485	1.14
Ni	11.75	24.11	28.14	11.97	10.56	56.46	13.72	1335	0.77
Cu	21.97	40.51	34.21	10.55	13.57	45.18	18.40	1296	0.74
Zn	48.99	41.69	80.21	32.22	48.54	59.36	42.11	1394	1.15
Ga	9.88	8.27	9.48	2.77	7.48	4.77	6.64	1986	1.13
Ge	3.35	2.95	0.74	2.46	3.90	0.96	2.96	3189	1.32
As	2.57	6.37	10.01	3.23	6.04	12.16	3.79	3386	1.59
Mo	3.47	9.47	3.14	1.92	2.55	3.44	3.19	599	0.80
Cd	0.30	0.62	0.99	0.13	0.16	0.44	0.25	1303	0.64
Sb	0.68	1.80	3.62	0.61	1.37	1.03	0.84	527	1.63
La	19.5	18.8	20.6	4.95	17.0	24.6(17.9)	22.5	392	0.76
Ce	37.1	38.1	55.8	9.40	31.3	44.1(32.4)	46.7	392	0.67
Nd	17.2	17.3	16.2	5.17	14.0	20.9(16.3)	22.3	392	0.63
Sm	3.28	3.55	3.08	0.86	2.61	4.44(3.0)	4.07	392	0.64
Eu	0.57	0.68	0.60	0.18	0.43	1.04(0.66)	0.84	392	0.51
Tb	0.46	0.55	0.45	0.16	0.33	0.57(0.42)	0.62	392	0.53
Yb	1.32	1.54	1.48	0.50	0.90	1.42(1.07)	2.08	392	0.43
Lu	0.24	0.25	0.25	0.09	0.16	0.24(0.17)	0.38	392	0.42
REE	79.66	83.8	79.0	21.1	67.3	97.7(73.1)	97.7	392	0.69
Hg	0.22	0.42	0.45	0.11	0.19	0.06	0.19	1401	1.00
Tl	0.35	0.42	0.67	0.55	0.44	1.29	0.47	1018	0.94
Pb	20.34	26.95	20.38	8.76	12.29	26.21	15.41	1387	0.80
Th	8.71	8.20	9.07	3.01	4.91	3.72	5.84	934	0.84
U	2.60	4.29	3.90	1.24	1.72	3.93	2.41	1319	0.71

C-P, Carboniferous–Permian; P₂, Upper Permian; J₁₋₂, Lower-Middle Jurassic; J₃–K₁, Upper Jurassic–Lower Cretaceous; E-N, Eocene–Neogene. CC, the ratio of element concentrations in J₃–K₁ coals vs. common Chinese coals. The values out of and in the brackets are average concentrations of REE in the Eocene and Neogene coals, respectively. Data are from Ren et al. [125].

However, in terms of specific coals in China, some elements are slightly elevated in coals from northeastern China (Figure 16) [125]. Coals from other areas in China, however, are not rich in elements. For example, the coals from the Jixi Coalfield in Heilongjiang Province are slightly enriched in V (71.6 ppm), and Co (14.5 ppm); the J₃–K₁ coals from the Tiefa Coalfield in Liaoning Province are slightly enriched in V (73.6 ppm), Cr (29 ppm), Ni (23.99 ppm), Ga (15.3 ppm), and Zn (74.3 ppm); the J₃–K₁ coals from the Heihe Coalfield in Heilongjiang are slightly enriched in Cr (30 ppm). Elevated As in the J₃–K₁ coals are found in the Yimin (30.9 ppm) and Huolinhe (12.88 ppm) coalfields in Inner Mongolia, Shuangyashan (17.2 ppm) and Suibin (8.75 ppm) coalfields in Heilongjiang Province, and the Badaohao deposit (23.3 ppm) in Liaoning Province. Elevated Mo in the J₃–K₁ coals are found in the Yuanbaoshan deposit (5.78 ppm) in Inner Mongolia and Fuxin Coalfield (5.28 ppm) in Liaoning Province. Elevated Sb in the J₃–K₁ coals are found in the Huolinhe Coalfield (3.99 ppm) in Inner Mongolia. Elevated Th in the J₃–K₁ coals are found in the Heihe (10.63 ppm) and Shuangyashan (9.83 ppm) deposits in Heilongjiang Province [125].



Figure 16. Locations of some coalfields in China [127].

Although some local coals as presented above have elevated concentrations of elements, their concentration coefficients are lower than 10. However, Ge in two Cretaceous coal deposits from China is most significantly enriched, i.e., in the Wulantuga and Yimin deposits of Inner Mongolia, northern China. The former is now being mined for industrial Ge [127], and the latter has a huge potential as an economically viable Ge ore deposit [127].

6.1. Wulantuga Ge Ore Deposit

The Wulantuga Ge ore deposit is located in the southwestern Shengli Coalfield in Inner Mongolia, northern China (Figure 17). The coal-bearing strata where the Ge ore deposit is hosted are the Shengli Formation of Early Cretaceous age [128–130]. The Ge deposit is confined to a 2.2-km² area [131] relative to the 342-km² area covered by the Shengli Coalfield (Figure 17). The thickness of the coal seam hosting the Ge deposit, i.e., No. 6 coal, varies from 0.8 to 36.2 m and averages 16.1 m, thinner than the same coal seam outside of the Ge deposit in the Shengli Coalfield, up to 244.7 m in the center of the coalfield.

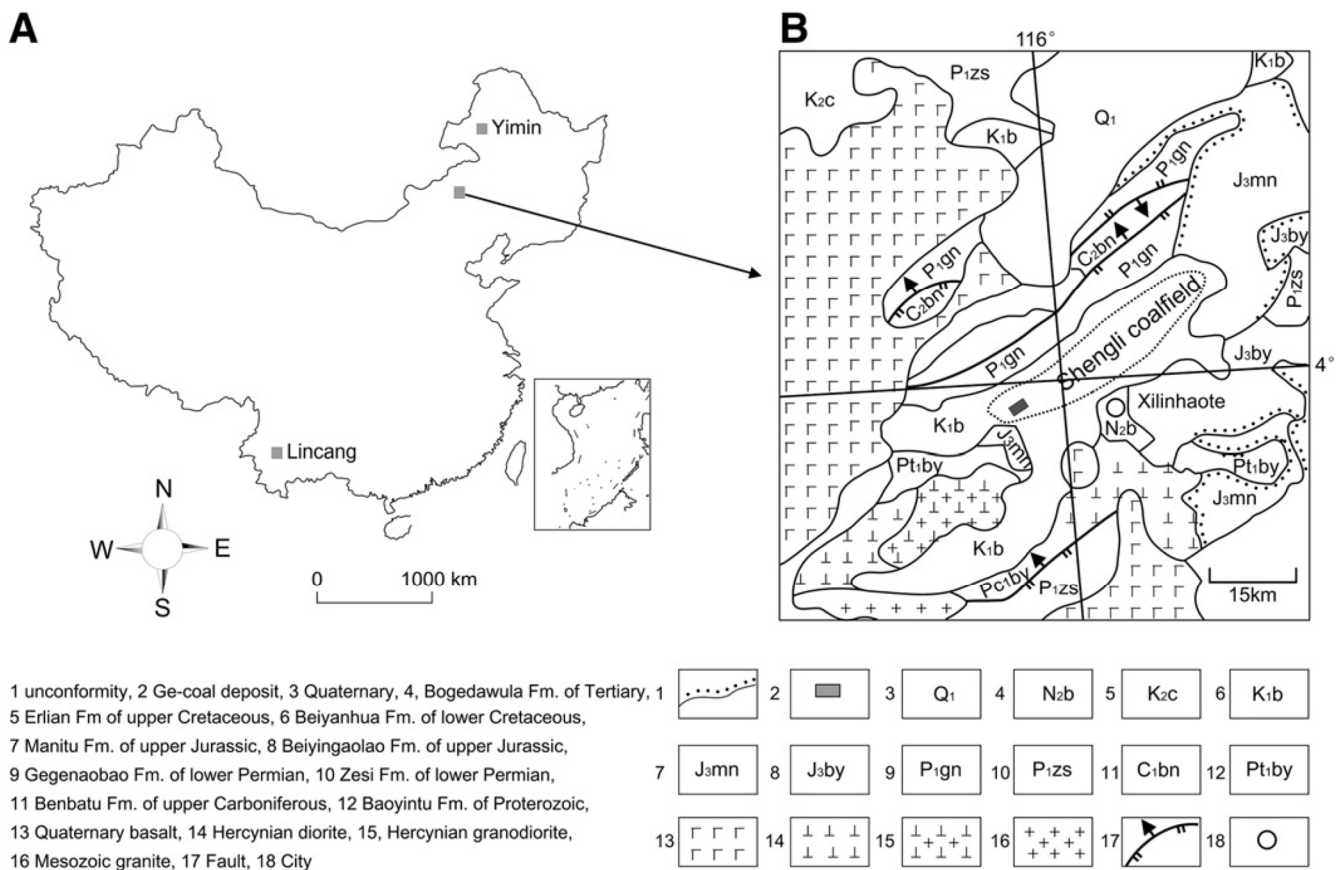


Figure 17. Location of the Shengli Coalfield and Wulantuga Ge ore deposit in Inner Mongolia, northern China. (A), location of the Shengli Coalfield; (B), geological background of the Shengli Coalfield.

It was estimated that Ge reserves in the Wulantuga deposit are 1700 t (coals with Ge concentration >100 ppm; whole-coal basis) [130]. The designed capacity for Ge extraction in the Ge extraction plant for the Wulantuga deposit is 100 t/y. The high-purity zone-refined Ge ingots (99.99999%) are produced from the extraction plant. A number of studies showed a wide range of Ge concentration in the No. 6 coal, e.g., 32–820 ppm with an average of 137 ppm (whole-coal basis) [130], 22 to 1894 ppm with an average of 427 ppm (whole-coal basis) [132], 23.3 to 1424 ppm with an average of 168 ppm (whole-coal basis) [133], and 45 to 1170 ppm with an average value of 273 ppm (whole-coal basis) [131].

The No. 6 Coal hosting the Ge deposit is characterized by a low rank with a maximum huminite reflectance of 0.45% and by a low ash yield averaging 8.77% [131]. Petrologically, the coal dominantly comprises textinite (43.9%), fusinite (33.0%), and to a lesser extent, semifusinite (12.5%). Fungus, as the maceral funginite, has also been identified in the coal [100]. Minerals in the coal mainly consist of quartz, and to a lesser extent, aluminosilicates (kaolinite, illite, illite/smectite), gypsum and pyrite. Traces of rutile and anatase have also been identified in the coal. Quartz in the coal is of both terrigenous and authigenic cell-filling origins [131,132]. Pyrite in the coal was derived from epithermal solutions during peat deposition [131].

The source of Ge in the deposit was derived from granitoids which are located to the southwest of the deposit [125–128]. The granitoids were subjected to hydrothermal fluid leaching and then the Ge-rich hydrothermal solutions laterally migrated from SW to NE into the peat and were consequently incorporated into the organic matter.

Geochemically, the Ge deposit has two element assemblages with elevated concentrations, i.e., Ge–W and As–Hg–Sb–Tl. It was reported that the concentration of W in the deposit is highly enriched but may vary greatly, e.g., on a whole-coal basis, 115 ppm reported by Dai et al. [131], 507 ppm reported by Zhuang et al. [132], and 35–627 ppm

reported by Du et al. [130]. The concentrations of As, Hg, Sb, and Tl are highly elevated, i.e., 499, 3.165, 240, and 3.15 ppm, respectively (whole-coal basis) [131]. The enrichment of this assemblage is attributed to epithermal (50–200 °C) solutions [9,131]. The water solutions were acidic as indicated by H-type distribution of REY in the UCC-normalized patterns of the Ge-richest coals from the Wulantuga deposit (Figure 18), such as those suggested for the Kas and Aduunchuluun Ge-coal deposits in Sections 2.2 and 2.3 (Figure 1).

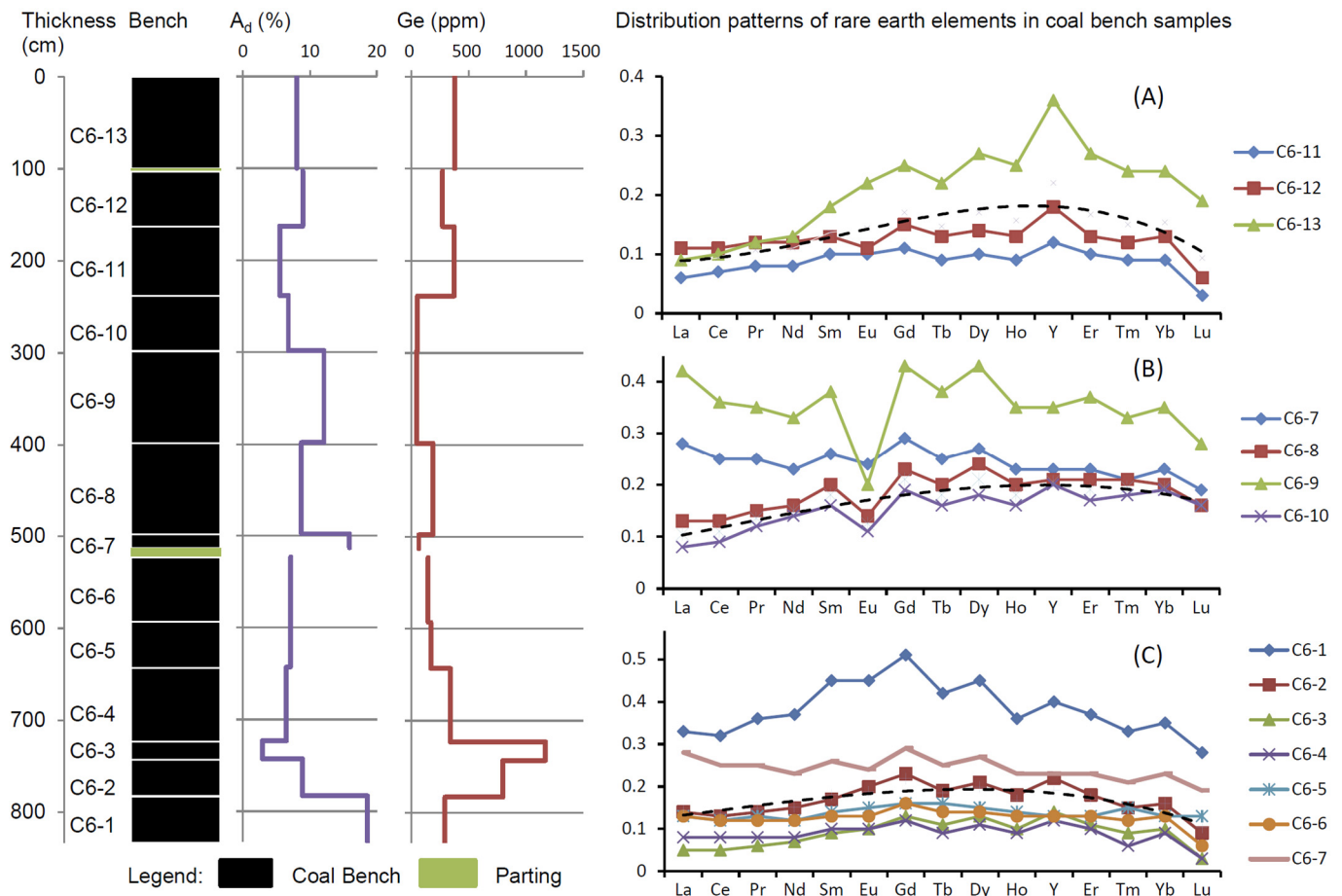


Figure 18. Ash yield, Ge concentration (whole-coal basis), and REY distribution pattern in the section of the No. 6 Coal. REE plots (after Dai et al. [131]) normalized to Upper Continental Crust (UCC) [71]. (A), REY distribution patterns of the upper section of the coal seam including benches C6-11, C6-12, and C6-13; (B), REY distribution patterns of the middle section of the coal seam including benches C6-7 to C6-10; (C), REY distribution patterns of the lower section of the coal seam including benches C6-1 to C6-7.

6.2. Yimin Ge Ore Deposit

The Yimin Ge deposit is located in the Yimin Coalfield of northeastern Inner Mongolia, northeastern China (Figure 16). The coal-bearing sequences where this Ge deposit occurs are of Early Cretaceous age and include the Damoguaihe Formation and the Yimin Formation. The Yimin Ge deposit was discovered in 1992, and subsequent work confirmed a resource of ~4000 t Ge [134]. Seven coal seams in the Damoguaihe Formation, and partings as well, are characterized by high concentration of Ge, i.e., >100 ppm (whole-coal basis). The Ge concentrations in the coal seams and partings significantly vary, from <1 to 470 ppm, but are generally in the range of 50–200 ppm (whole-coal basis) [135].

The spatial distribution of Ge and elemental assemblage in the Yimin Ge deposit [135] are similar to those in the Wulantuga Ge deposit [132,136]. For example, Ge is mainly enriched along the margins of the Yimin coal deposit and decreases towards the center of

the deposit; elements including As (155 ppm) and W (9.84 ppm) are also enriched in the Yimin coal (whole-coal basis) [135]. However, the coal seams in the Yimin deposit were subjected to shallow felsic intrusions, and this caused a relatively higher rank (low volatile bituminous) than the Wulantuga coals. The REY distribution patterns of coals from the Yimin deposit also show the M-type enrichment, suggesting a significant influence of acidic waters (Figure 19) [54]. The concentration of Ge in the rank-elevated coals in the Yimin deposit is not enriched but was enriched in the adjacent sub-bituminous coals [137].

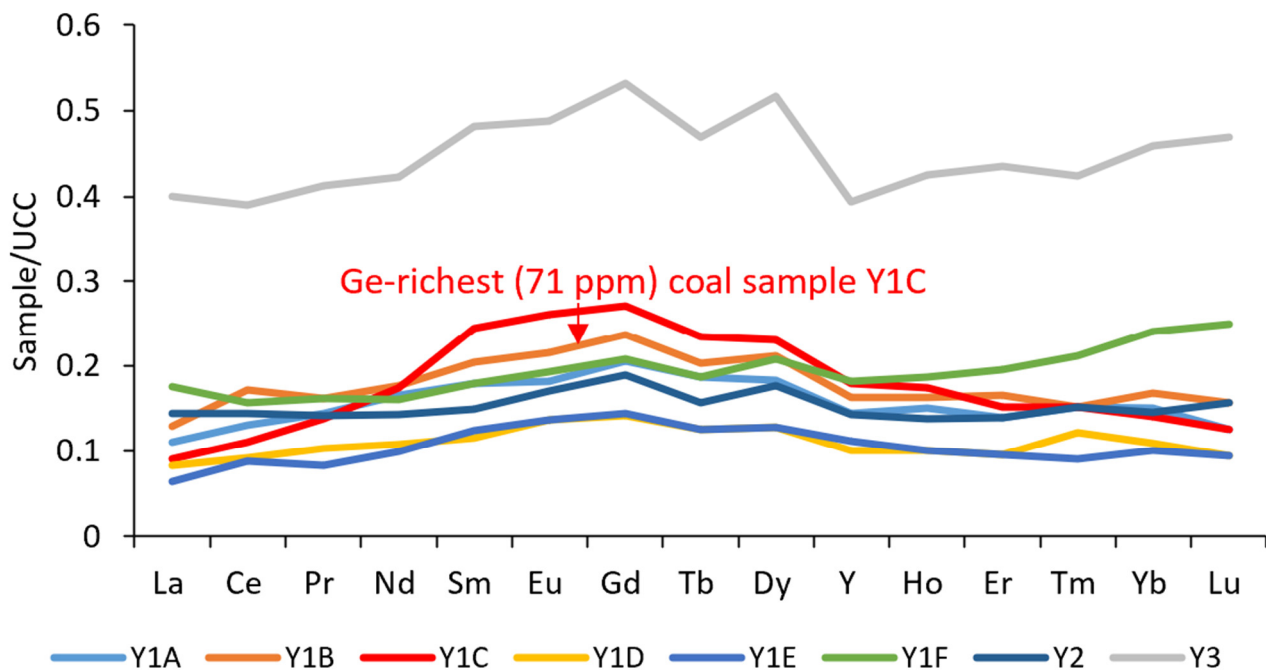


Figure 19. REY distribution patterns of Ge-rich coals from the Yimin deposit (based on the data from Li et al. [135]).

7. Metalliferous Coals from Africa

Africa hosts approximately 5% of the global proven recoverable coal reserves, of which 3% is documented for South Africa. Coal-bearing strata typically occur in Permian aged deposits in the southern half of Africa, and deposits of Triassic, Cretaceous, and Miocene age are documented in the northern half of the continent (Figure 20; refer to <https://pubs.er.usgs.gov/publication/ofr20081258> (accessed 6 September 2022) for the Google Earth map). Of the Cretaceous coal-bearing sedimentary successions, those from Nigeria are best documented, although deposits have also been reported from Algeria, Benin, Egypt, Libya, Mali, Mauritania, Niger, Senegal, and Sudan [138,139]. The Cretaceous coal-bearing facies of North Africa formed in a warm to humid climate and experienced major marine transgressions and regressions of the Tethys Sea, associated with the break-up of Gondwana and Laurasia, the initial opening of the Atlantic Ocean, and formation of the Equatorial Atlantic Magmatic Province [140,141]. The Lower Cretaceous coal facies formed along the Tethys shoreline in the northern parts of North Africa and appear absent in the southern North African basins, although local fluvial deposits may occur in these regions [138]. In the Late Cretaceous, as the Tethys Sea experienced a southward transgression and Atlantic waters moved northwards linking to the Tethys Sea, coal facies developed along the epicontinental seaways and coastal plains across North Africa [138].

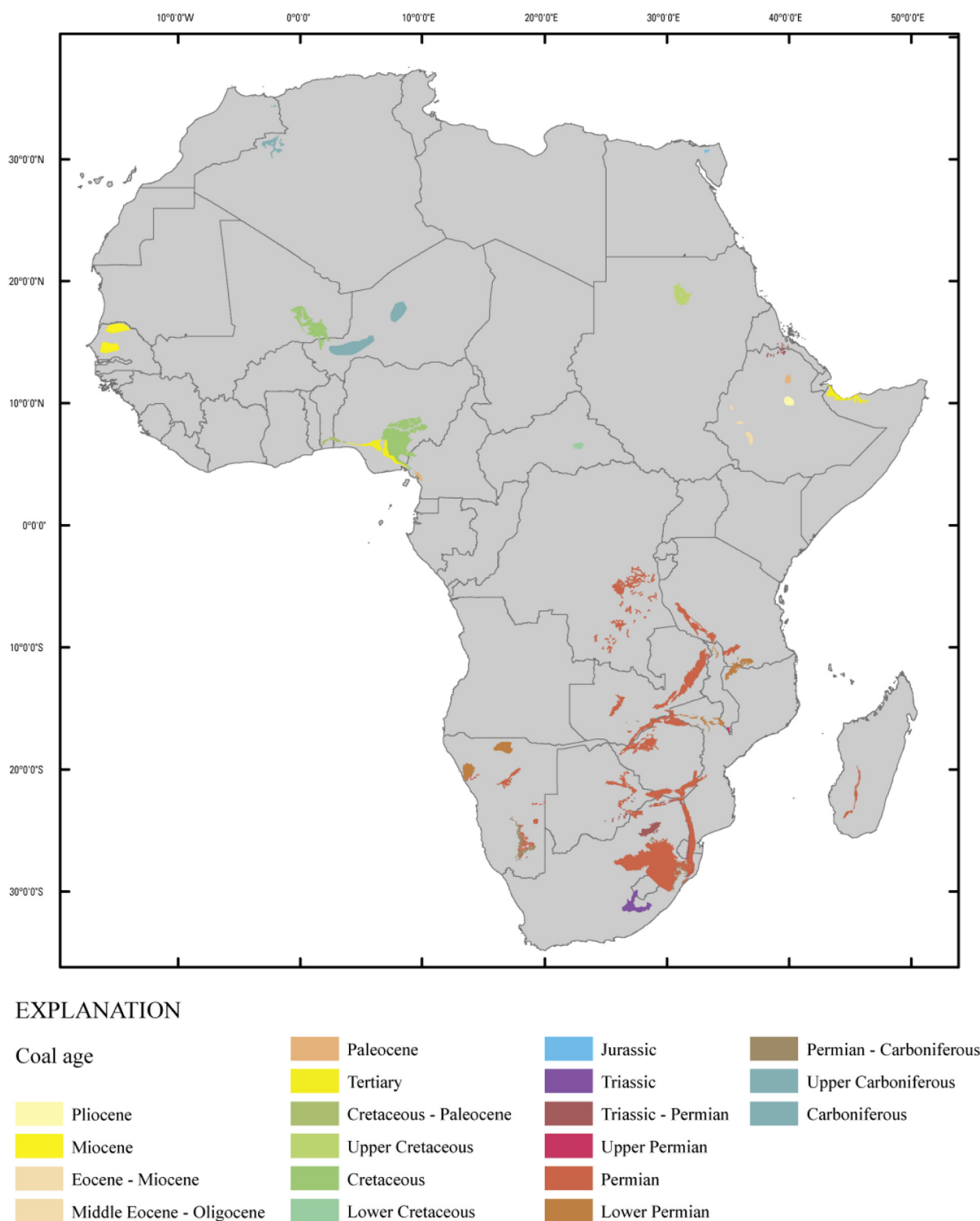


Figure 20. Distribution and ages of coal deposits in Africa [142].

The Nigerian Cretaceous-aged coal deposits are lignitic to sub-bituminous to bituminous in rank [143,144], and the coal seams are usually interbedded with bands of shales and mudstones, some of which are oil-bearing. Chukwa et al. [145] reported Nigerian coal deposits as 39% bituminous, 49% sub-bituminous, and 12% as lignite. The coal industry in Nigeria is under revival with government plans to enhance the coal-based power supply

due to energy supply shortages. Most of the coal deposits (>2 billion metric tons) are suitable for power generation due to their inherently low sulphur content. Some coal may be suitable for metallurgical applications due to the high vitrinite content, but the coal rank may be a limiting factor. There is limited information pertaining to the suitability of these coals for alternative uses.

Coals in Nigeria are predominately located in the Benue Trough (Figure 21) and in some outlying states, although limited information is currently available for the latter. The Benue Trough is a linear, intracratonic, and graben inland sedimentary basin infilled by Cretaceous–Tertiary marine, paralic, and continental sediments. Many episodes of tectonic events related to the Central West Africa Rift System have resulted in basin fragmentation, block faulting, subsidence, and rifting. The reader may consult Akinyemi et al. [146] and Obaje [147] and references therein for further geological information pertaining to the Benue Trough and Abubakar [148] for the stratigraphic succession thereof. The Benue Trough is geographically subdivided into the Upper Benue Trough (UBT), the Middle Benue Trough (MBT), and the Lower Benue Trough (LBT) (Figure 21). Mangs et al. [144] concluded that the geological history and variable depositional environments of the Benue Trough impacted the coal quality in the three sub-basins, with the MBT differing from the UBT and LBT. Liptinite appears to be absent in the vitrinite-rich MBT samples, and ash values, on average, are higher compared to the UBT and LBT samples [144]. Obaje et al. [149] undertook Rock Eval pyrolysis on samples across the Anambra Basin (LBT) and UBT Benue Trough and concluded that the coal deposits are Type III kerogens, thus capable of generating oil and gas in the deeper subsurface. The samples from Lafia-Obi in the MBT were clearly different, indicating low gas potential [149]. The total sulphur values for the LBT coals are generally low (below 1%), with higher values reported for MBT samples (Table 7).

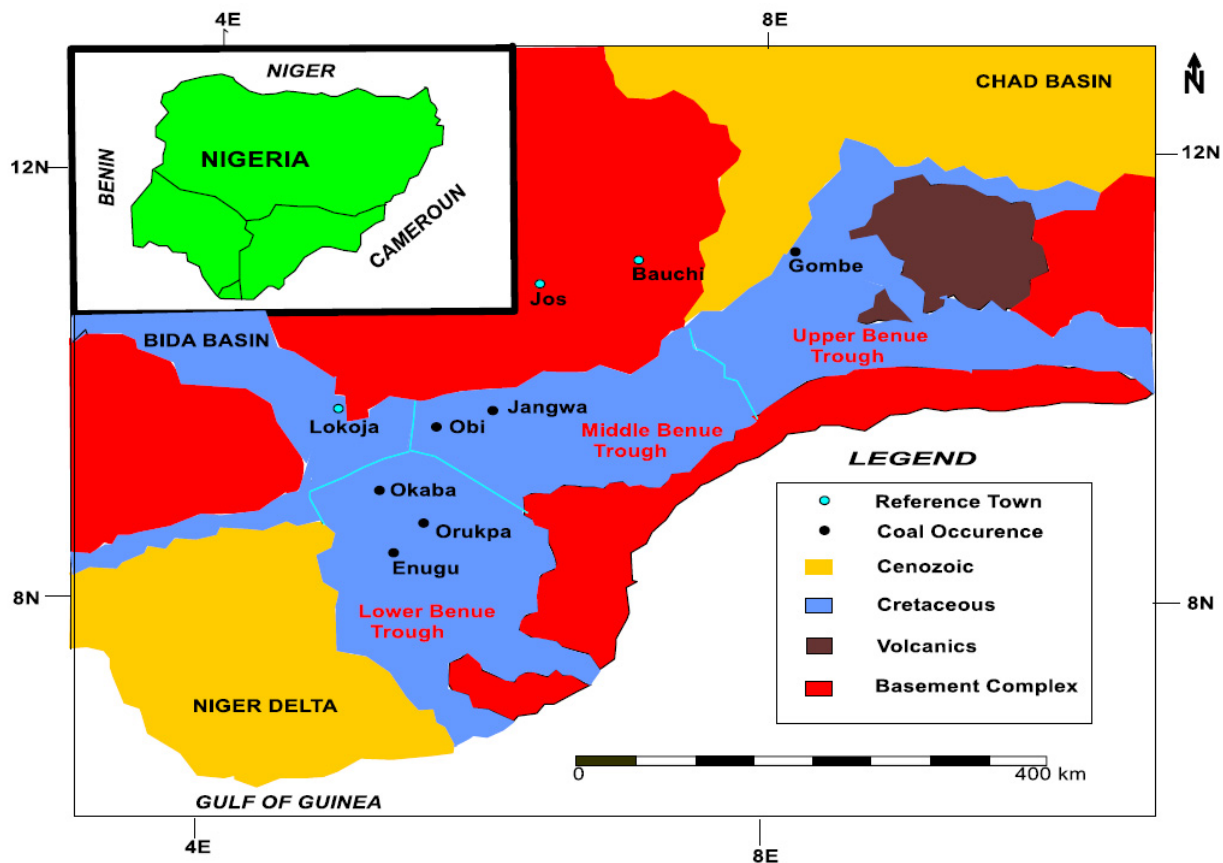


Figure 21. Geological map indicating the major coal occurrences in the Benue Trough of Nigeria (modified after Obaje et al. [150], extracted from Akinyemi et al. [146]).

Table 7. Proximate (as received basis, %) and ultimate (dry and ash-free basis, %) analyses, high heating values (GCV, MJ/kg), petrography, and SiO₂/Al₂O₃ ratios for coals from Nigeria.

Sub/Basin	Sources	Formation	Location	Proximate Analysis				GCV	Ultimate Analysis					Petrography		SiO ₂ /Al ₂ O ₃	
				VM	FC	Ash	M		TS	C	H	N	O	Rr	V/H		
UBT	Mangs et al., 2022 [144]	Lamja SST	Lamja/Chikila average	26.9	49.1	18.9	5.1	24.5	0.8	75.8	5.7	2.0	15.7	0.7	66.5	3.30	
		Gombe SST	Maiganga average	28.2	48.0	17.0	7.6	23.9	2.2	73.6	6.0	1.5	16.8	0.5	40.5	3.13	
	Akinyemi et al., 2020 [146] **	Lamja SST	Lamja/Chikila average	34.1	50.2	9.3	6.3	28.8	0.7	75.5	5.9	1.5	16.5	0.7	88.2		
		Gombe SST	Garin-Maiganga	39.1	45.4	4.1	11.35	29.47	0.39	65.78	5.31	0.80	27.72	0.35	43.8		
	Akinyemi et al., 2021 [30] §	Gombe	Maigaanga	39.1	45.4	4.1	11.35		0.37	63.07	5.09	0.77	26.58	0.39	43.7	1.25	
		Lamja	Chikila	35.3	53.8	7.9	3.07		0.67	74.04	5.48	1.50	10.45	0.71	90.1	0.00	
			Lamza	32.0	43.1	11.9	12.91		0.49	57.51	4.99	1.13	23.94	0.72	86.1	2.19	
	Ayinla et al., 2017 [151]	Gombe FM	Maiganga average						0.29	73.23	5.68	1.25	19.55	0.34	58.3	2.93	
	Yandoka et al., 2015 [152]	Lamja FM	Lamja						0.65							2.61	
	MBT	Mangs et al., 2022 [144]	Awgu FM	Shankodi average	23.0	46.1	22.1	8.8	19.9	0.9	70.4	5.1	2.0	21.8	0.8	85.9	3.73
Awgu FM			Kwagshir (Obi coal)	20.5	60.0	18.3	1.20	27.85	1.27	81.12	5.12	2.09	10.41	1.00	85.1	5.28	
Awgu FM			Akunza Migili	40.8	45.6	3.7	10.00	28.73	2.08	70.98	6.96	1.57	18.40	0.35	48.1	2.17	
Akinyemi et al., 2020 [146] **			Okaba	40.0	43.7	7.7	8.63	27.92 *	0.80	67.96	5.82	1.38	24.05	0.45	58.9		
			Lafia-Obi	46.0	35.2	7.2	11.59	26.24 *	1.83	66.60	6.65	0.98	23.89	0.35	66.4		
			Labi-Obi	46.0	35.2	7.2	11.59		1.74	61.80	6.17	0.91	22.17	0.39	64.4	4.04	
Akinyemi et al., 2021 [30] §			Duduguru	76.4	16.6	0.5	6.51		0.62	59.64	5.49	1.30	32.95			2.34	
		Awgu	Shankodi-Jangwa	40.7	39.2	15.0	5.16		2.03	71.46	6.40	1.37	18.76			2.94	
			Agwatashi	35.2	53.8	8.1	2.98		0.67	74.20	5.55	1.48	9.99			1.99	
			Mamu FM	Average	36.1	47.5	10.4	6.3	28.2	1.3	75.4	6.7	1.8	14.9	0.45	48.1	2.55
LBT	Mangs et al., 2022 [144]	Nsukka FM	Average	32.8	49.3	12.5	5.4	28.0	1.1	77.3	6.5	2.0	13.3	0.48	41.9	1.95	
		Odukpani FM	Average	34.3	46.1	6.6	13.1	29.2	0.7	73.6	7.5	1.8	16.5	0.40	59.6	2.21	
			Enugu	21.7	19.6	55.5	3.17	11.43 *	0.45	72.38	6.86	0.97	19.34	0.52	66.9		
	Akinyemi et al., 2020 [146] **		Imiegba	24.1	15.4	56.8	3.77	10.16 *	1.57	60.97	7.68	0.62	29.16	0.42	91.4		
			Mamu	Enugu	21.7	19.6	55.5	3.17		0.20	32.18	3.05	0.43	8.6	0.55	53.3	2.67
		Akinyemi et al., 2021 [30] §	Mamu	Okaba	40.0	43.7	7.7	8.63		0.74	62.73	5.37	1.27	22.2	0.49	58.6	3.24
				Imiegba	24.1	15.4	56.8	3.77		0.68	26.37	3.32	0.27	12.61	0.45	56.8	1.33

* Note: errors were determined in the publication; upon consultation with the authors in 2022, corrected data appears in this table; # GCV is HHV = higher heating value; § RoV max reported; O content is by difference; V/H, vitrinite or huminite; Rr, vitrinite random reflectance.

Ayinla et al. [151], Akinyemi et al. [30,143,146], Mangs et al. [144], and Yandoka et al. [152] provided recent geochemical, petrological, and mineralogical data for Cretaceous coals of Nigeria (Tables 7 and 8), while Ogala et al. [153] provided data for some elements from the Anambra Basin (LBT). It is difficult to draw accurate correlations between the published data in Tables 7 and 8 as there is some degree of inconsistency in the reporting of the sample location, formation and seam, analytical equipment, and even analytical reporting basis. Akinyemi [30,146] reported trace element and rare earth element data generated by LA-ICP-MS, stating that ICP-MS is a more accurate method. The samples were generally grab samples and hence may not be representative, impacting on the consistency of the data reported in the literature. However, the data provided is indicative of Cretaceous Nigerian coals from rank to ash content, maceral and mineral composition, and geochemistry within and between the three sub-basins.

The Gongola and Yola sub-basins occur in the UBT, and coal deposits are hosted in the Gombe and Lamja Formations (Maastrichtian), respectively. On average, the reported ash content for UBT coals is 10.5% (Table 7). The variable reflectance data within the UBT results in the classification of samples from the Lamja Formation as Medium Rank C bituminous coal, and those from Maiganga (Gombe Formation) as Low Rank B coals or lignite (mean vitrinite reflectance values below 0.4%). Ayinla et al. [151] determined that the Gombe Formation (Gongola Sub-Basin, UBT) formed in an upper deltaic plain, with sediments derived from a terrestrial source, deposited under sub-oxic to oxic conditions in a humid-warm climate. Yandoka et al. [152] determined that the Lamja Formation (Yola Sub-Basin, UBT) formed in a delta plain fresh water to marine environment under suboxic to relatively oxic conditions and a terrigenous sediment source. The average $\text{SiO}_2/\text{Al}_2\text{O}_3$ ratio (2.2) indicates dominance of kaolinite and quartz.

The Awgu (Coniacian) and Lafia (Maastrichtian) Formations host the coal seams in the MBT. On average, the reported ash content for MBT coals is 10% (Table 7). The average $\text{SiO}_2/\text{Al}_2\text{O}_3$ ratio (3.21) indicates a possible dominance of kaolinite over quartz.

The Anambra Basin and Abakalili Syncline in the LBT host several coal-bearing formations of Cretaceous age [149]. On average, the reported ash content for LBT coals is 9.8% [144], although the average in Table 7 is 32% with the inclusion of the high ash samples reported by Ayinkemi et al. [30,146]. The reflectance data reported by Mangs et al. [144] and Akinyemi et al. [30,146] is more consistent in the LBT samples than the UBT and MBT samples, with an average mean random reflectance value of 0.45%, thus classifying the coals as sub-bituminous. The average $\text{SiO}_2/\text{Al}_2\text{O}_3$ ratio (2.32) indicates dominance of kaolinite and quartz.

Akinyemi et al. [143] determined a detrital mineral source based on the dominance of quartz and clay minerals with some epigenetic carbonates and (rare) sulphides [30]. The various elemental ratios (such as Ni/Co versus V/Cr) indicate oxic depositional environments [143]. Ogala et al. [153] concluded that the trace element values are low and generally do not indicate health or technological concerns; later publications do not disagree with this finding. For example, As is below 4.5 ppm across all sample locations in all three sub-basins (Table 8).

The trace element and rare earth element data presented in Table 8 show a degree of variability between the authors and locations. The correlation coefficients (CC, being the ratio of elemental concentration versus the average hard coal value reported by Ketris and Yudovich (Figure 22) [70]) for most trace elements reported by various authors (Table 8) fall in the normal range ($0.5 < \text{CC} < 2$). Arsenic is highly depleted across all three sub-basins. There is slight enrichment of Mn in the UBT samples and slight enrichment of Eu, Mn, and Sm in the LBT samples; there is no enrichment in the MBT samples.

Table 8. Geochemical data: Select trace and rare earth elements for Nigeria Cretaceous coals (whole-coal basis; ppm).

Sub/Basin	Author	Formation	Location	As	Ba	Ce	Co	Cr	Cu	Eu	Hf	La	Mn	Nb	Ni
UBT	unpublished	Lamja S	Lamja/Chikila average	1.58	69.30	19.10	8.50	19.40	20.10	0.40	0.15	7.75	47.95	9.95	13.01
		Gombe	Maiganga (A & B ave)	2.83	213.03	36.33	13.88	16.55	12.80	0.60	2.85	15.7	353.6	14.95	14.08
	Akinyemi et al., 2021 [30]	Gombe	Maigaanga		207.35	5.48	0.64	1.55	3.41	0.10	0.18	5.57		2.90	1.61
		Lamja	Chikila		105.95	13.98	1.28	16.45	13.20	0.29	2.31	7.04		5.75	6.10
			Lamza		63.25	49.19	10.01	28.25	16.67	0.79	1.35	25.44		21.66	21.81
	Ayinla et al., 2017 [151]	Gombe	Maiganga (A & B ave)		174.7	8.9	4.3	24.4	7.6					4.0	8.3
	Yandoka et al., 2015 [152]	Lamja	Lamja		45.2		1.3	5.1	5.0						
MBT	unpublished	Awgu	Shankodi average	0.70	203.27	6.23	6.43	13.82	22.28	0.43	0.13	2.68	33.68	3.72	29.25
		Awgu	Kwagshir (Obi coal)	1.10	36.8	1.5	2.7	11.2	16.6	0.1	0.1	0.7	15.2	0.8	11.5
		Awgu	Akunza Migili	4.48	43.3	3.0	22.3	5.5	13.3	0.1	0.2	1.2	231.1	1.8	15.0
	Akinyemi et al., 2021 [30]		Labi-Obi		124.6	16.3	1.5	16.1	15.4	0.3	2.6	8.3		6.6	4.4
			Duduguru		111.0	45.8	11.3	48.0	20.2	0.9	3.7	24.5		20.7	20.0
		Awgu	Shankodi-Jangwa		43.5	4.0	8.3	5.7	6.9	0.1	0.4	1.9		2.2	7.7
			Agwatashi		422.5	91.2	12.0	102.4	24.0	1.8	5.2	51.8		41.7	33.5
LBT	unpublished	Mamu	various	0.93	70.58	11.52	7.27	14.63	13.83	0.37	0.52	4.88	87.75	6.87	15.58
		Nsukka	various	1.14	44.80	32.05	5.25	16.28	14.85	0.33	1.25	11.28	8.88	11.95	11.83
		Odukpani	various	0.92	127.23	8.33	16.10	9.60	104.10	0.30	0.20	4.10	847.7	5.50	28.77
	Akinyemi et al., 2021 [30]	Mamu	Enugu		48.70	3.90	6.08	7.15	10.79	0.10	0.38	1.76		1.97	6.65
		Mamu	Okaba		174.10	9.76	2.11	21.90	23.00	0.30	3.00	5.56		4.76	11.00
			Imiegba		374.20	194.25	9.70	68.35	10.81	8.19	4.51	92.45		101.65	22.85
World coal	Ketris and Yudovich, 2009 [70]			8.3	150.0	23.0	5.1	16.0	16.0	0.5	1.2	11.0	86.0	12.0	13.0
UCC	McLennan, 2001 [154]			1.5	550.0	64.0	17.0	83.0	25.0	0.9	5.8	30.0	600	12.0	44.0
SARM 19 measured	previously unpublished data			5.64	159.59	41.81	4.71	31.43	11.79	0.59	2.20	19.81	137.72	16.27	10.60
		R2 value	Al ₂ O ₃	−0.40	0.09	0.20	0.10	0.16	0.06	0.15	0.04	0.17	0.00	0.20	0.37
		R2 value	TiO ₂	−0.06	0.00	0.04	0.11	0.03	0.12	0.02	0.01	0.04	0.19	0.04	0.16
		R2 value	ash	−0.30	0.11	0.47	0.00	0.05	0.00	0.68	0.03	0.40	−0.10	0.54	0.05
Sub/Basin	Sources	Formation	Location	Pb	Rb	Sm	Sr	Th	U	V	Y	Zn	Zr	ΣLREE	
UBT	unpublished	Lamja S	Lamja/Chikila average	7.75	4.15	1.97	52.35	4.25	0.46	20.00		44.45	5.65	39.17	
		Gombe	Maiganga (A & B ave)	6.88	1.18	3.03	75.30	5.43	0.73	14.68		71.45	127.00	70.61	
	Akinyemi et al., 2021 [30]	Gombe	Maigaanga	1.99	0.21	0.60	228.35	0.45	0.09	1.94	2.27	2.00	6.39	14.65	
		Lamja	Chikila	22.85	0.52	1.13	28.75	2.92	0.09	23.70	9.82	5.65	83.50	28.19	
			Lamza	10.03	18.86	3.88	154.30	6.49	2.66	36.49	13.69	27.31	45.74	100.96	

Table 8. Cont.

Sub/Basin	Sources	Formation	Location	Pb	Rb	Sm	Sr	Th	U	V	Y	Zn	Zr	∑LREE	
	Ayinla et al., 2017 [151]	Gombe	Maiganga (A & B ave)	3.4	2.0		97.7	1.6		11.8				12.88	
	Yandoka et al., 2015 [152]	Lamja	Lamja		3.2		27.8			6.2					
MBT	unpublished	Awgu	Shankodi average	19.12	4.63	1.27	32.70	2.45	0.54	8.23		27.90	1.80	14.34	
		Awgu	Kwagshir (Obi coal)	4.0	3.6	0.2	27.7	1.1	0.36	11.5		19.7	1.2	3.31	
		Awgu	Akunza Migili	2.0	0.2	0.4	60.2	0.5	0.31	4.4		44.1	3.2	6.51	
	Akinyemi et al., 2021 [30]		Labi-Obi		5.5	0.8	1.3	23.6	3.5	0.88	17.9	11.80	5.3	98.2	32.78
			Duduguru		18.8	13.1	4.1	37.6	8.2	2.38	64.6	16.6	18.7	136.6	95.99
		Awgu	Shankodi-Jangwa		1.0	0.3	0.5	35.8	0.7	0.19	12.6	4.1	15.4	13.3	8.70
		Agwatashi		24.7	52.3	8.2	111.2	22.3	5.83	141.7	30.3	54.6	184.1	194.71	
LBT	unpublished	Mamu	various	6.00	0.62	1.50	34.25	2.13	0.89	18.98		26.47	17.55	25.13	
		Nsukka	various	6.18	0.95	2.30	27.05	3.35	1.01	20.28		26.10	56.25	57.90	
		Odukpani	various	3.63	0.37	1.14	40.10	1.10	0.52	9.73		35.97	5.60	19.37	
	Akinyemi et al., 2021 [30]	Mamu	Enugu		0.73	0.15	0.41	38.70	0.62	0.23	12.85	4.19	10.85	13.00	8.14
		Mamu	Okaba		1.92	0.83	1.07	29.10	3.73	1.02	27.80	14.62	8.50	120.20	21.45
			Imiegba	38.69	9.51	26.23	167.45	15.03	4.25	75.80	47.82	26.15	158.45	422.77	
World coal	Ketris and Yudovich, 2009 [70]			7.8	14.0	2.0	110.0	3.3	2.4	25.0	8.2	23.0	36.0	48.47	
UCC	McLennan, 2001 [154]			17.0	112.0	4.5	350.0	10.7	2.8	107.0	22.0	71.0	190.0	111.38	
SARM 19 measured	previously unpublished data			15.20	1.99		77.13	9.19	3.70	18.67		12.60	166.62		
		R2 value	Al ₂ O ₃	0.22	0.10	0.17	−0.01	0.21	0.18	0.14	0.85	0.37	0.04		
		R2 value	TiO ₂	0.01	0.07	0.04	−0.02	0.06	0.06	0.01	0.74	0.49	0.02		
		R2 value	ash	0.33	0.00	0.62	0.05	0.06	0.06	0.00	0.50	0.00	0.02		

UCC, upper continental crust.

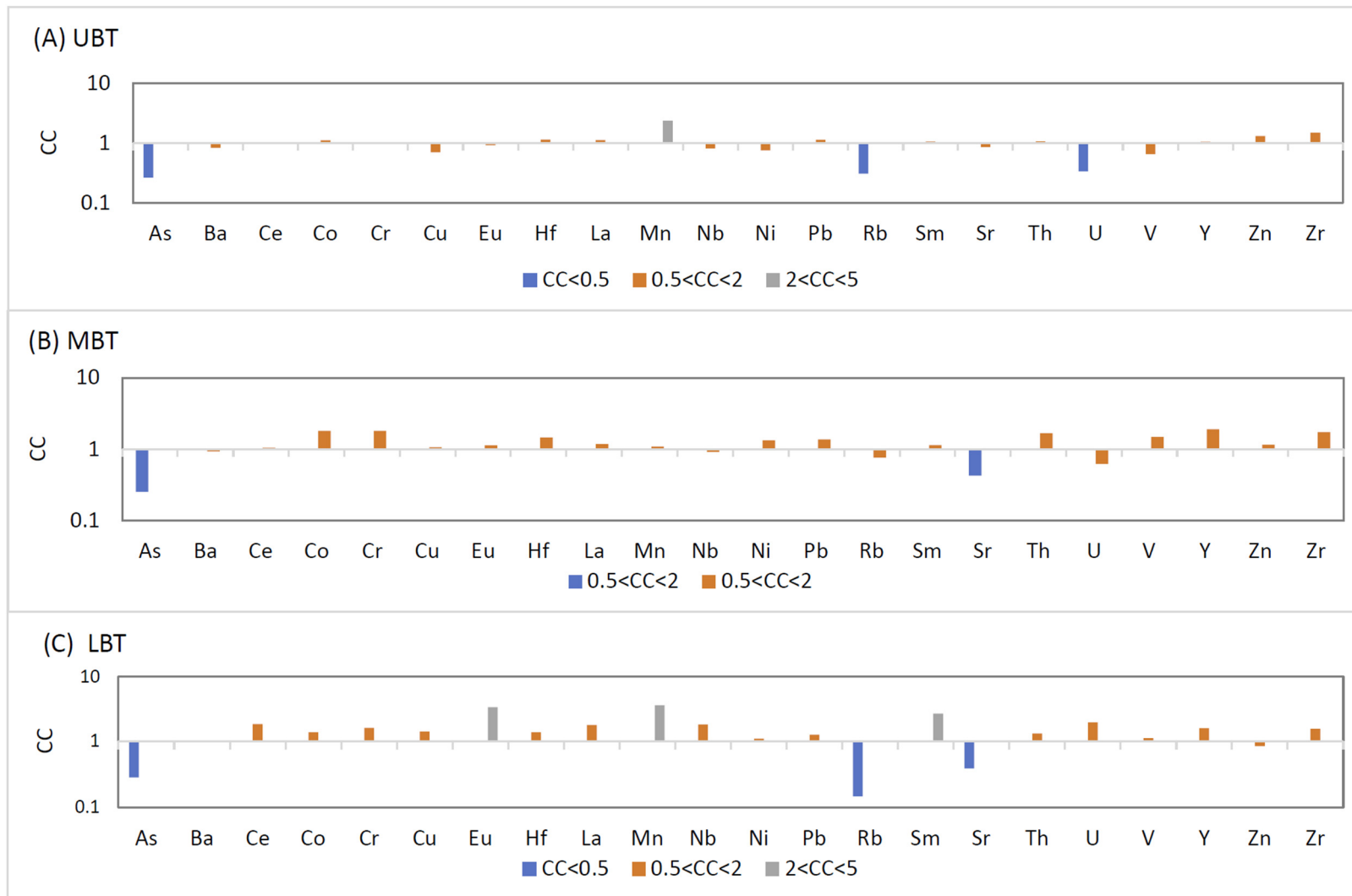


Figure 22. Concentration coefficients (CC) for trace elements in the Benue Trough coals (using data averaged from Table 8). Total hard coal data are from Ketris and Yudovich [70]; (A) UBT; (B) MBT; (C) LBT.

The average total LREE values for the UBT and MBT data reported in Table 8 compare to values derived from Ketris and Yudovich [70]: UBT = 44.41 ppm, MBT = 50.91 ppm. The average LBT data (92.46 ppm) includes the high values derived for the Imiegba coal [30]; the values reported for this sample are far higher than upper continental crust data presented by McLennan [154]. If the Imiegba sample is excluded, then the average total LREE value for the LBT is 26,40 ppm, lower than the Ketris and Yudovich [70] value of 45.63 ppm.

Neodymium is enriched relative to the upper continental crust values [154]. Zhao et al. [155] determined that Zr, Hf, and Nb occur as adsorbed ions in clay minerals, with a rough correlation noted between Nb and Zr and Al_2O_3 on a whole-coal basis. However, no correlations were determined for these samples. Alternatively, Zhao et al. [156] determined a better correlation of Zr and Nb with TiO_2 on a whole-coal basis, with anatase as the main carrier of these elements; but again, no correlations were determined for the Nigerian coals.

The data discussed herein is on a whole-coal basis; assessing ashed samples may provide better insight into the concentrations and modes of occurrence of trace and rare earth elements in Nigerian coals. The organic matter may act as a dilutant, especially where the element is primarily or exclusively associated with minerals. It is likely that the trace and rare earth elements in the coal deposits of the Benue Trough have a complex origin, with mixed clastics from a number of sources, influenced by the depositional environment and possibly including volcanic material. Each sub-basin appears slightly different in its mineralogy and geochemical characteristics.

8. Australasia

The summaries below are taken from state regional syntheses [155–162] and references therein.

8.1. Victoria

Cretaceous coals are found in the Gippsland Basin, a passive margin basin filled with Cretaceous and Cenozoic terrestrial and marine sediments. The coals occur within the lower Cretaceous (Aptian to Albian) Wonthaggi Formation, a unit dominantly consisting of epiclastic volcanic sandstone and mudstone. The Wonthaggi coal measures occur in the lower part of the Wonthaggi formation and comprise carbonaceous shales, mudstones, and thin coal seams. Coal was mined in several coalfields from the 1840s until the 1960s. The Wonthaggi coals are high volatile bituminous coals having 5%–10% air-dried moisture, 30%–35% volatile matter, and ash yields of 6%–12%. Random vitrinite reflectance varies between 0.50–0.67, although more deeply buried coal has reflectance values exceeding 0.9. Lower Cretaceous coals are also known from the Torquay and Otway Basins and are of sub-bituminous rank with a high ash yield. No publicly available trace element data could be located for these coals.

8.2. Queensland

The Jurassic–Cretaceous epeiric Eromanga Basin contains subhydrous lignite sub-bituminous black coal within the late Albian Winton Formation. However, the seams are generally thin and of poor quality so are considered to be uneconomic. Thin coal seams also occur within the Bungil Formation and Drildool Beds of the Surat Basin.

Thin coal seams have been recorded within the Albian Burrum Coal Measures of the Maryborough Basin. Coal was mined from 1866 until 1997. The coal is strongly coking but was used as a thermal coal. The early Cretaceous (Albian) Styx coal measures within the intracratonic Styx Basin were mined until 1963. The coal is a high volatile bituminous coal with an ash yield of 8.3%–15.5% and a random reflectance of 0.82% to 0.93%. The coal measures are likely correlatives of the Burrum Formation in the Maryborough Basin.

As in the case for Victoria, no trace element data has been published for these coals.

8.3. New South Wales

Thin coal lenses are known to occur within the Blythesdale Group within the Great Artesian Basin sequence, but little else is known about them.

8.4. South Australia

Coal seams are known to occur within the Winton Formation of the Eromanga Basin and are possibly broadly correlative with those known to occur in the Winton Formation in the Queensland portion of the same basin. Thin coal beds are present within the Eumerall Formation of the Otway Basin. Coal seams are also present in the Platypus Formation within the Cretaceous Duntroon Basin, and thin coal seams are present in the overlying Wigunda Formation. No analytical data are available for these coals.

8.5. Northern Territory

Thin coal seams have been recorded in the Winton Formation of the Eromanga Basin which are probably correlative with those recorded in the Queensland and South Australian segments of the same basin and have been described as being brown to black in colour and interbedded with carbonaceous mudstone.

8.6. New Zealand

Economically significant Cretaceous coals are confined to the South Island of New Zealand and were deposited in a transgressive environment on a pre-Cretaceous basement that was deformed during the Rangitata Orogeny (142 to 99 Ma). Five coal regions are recognized in the South Island viz. Canterbury, Nelson, Otago, Southland, and the West Coast (Figure 23).

8.7. Nelson

Minor coal occurs within the Pakawau Group which has been dated as Upper Senonian by plant microfossils. The formation consists of freshwater conglomerates, sandstones, mudstones, and seams of bituminous coal. Coal has been mined at Puponga and Mangarakau: coal at Puponga is high volatile bituminous with low sulphur contents and that at Mangarakau sub-bituminous.

8.8. West Coast

Bituminous coal occurs within the upper Cretaceous Paparoa Coal Measures that were deposited in fault-bounded basins in fluvial to fluvial-lacustrine intermontane environments with little or no marine influence. The peat swamps developed in narrow fault bounded basins adjacent to an axial meandering river system. The coal is mostly high volatile bituminous (although the rank can vary from lignite to sub-bituminous) and is characterised by having low ash yields (<10%), low sulphur (0.3% to 1.0%), and high vitrinite (~80%). Some coals have unusually high crucible swelling numbers. (>9). The coal seams are discontinuous and lensoidal and are folded and faulted.

West Coast coals exhibit significant variation when compared to Clarke values. Although most elements have lower values, the Strongman samples, particularly Strongman 2 [2A], show either comparable values or significant enrichment (Table 9). Strongman 2 2A shows enrichment in B, Cs, Li, Nb, Rb, and Sn; Strongman 2 [P532A] in Co, Cs Mn, and Ni; Strongman 2E in Be, Mn, and Ni and Strongman 2 [2B] in Co and Ni.



Figure 23. New Zealand Cretaceous coalfields (after New Zealand Petroleum and Minerals).

Crocoite ($PbCrO_4$) has been reported as occurring in the lower portion of the Main Seam in the Rewanui Coal Measures of the Paparoa Group, but its origin is uncertain [163].

Medium to high volatile high sulphur bituminous coal of possible upper Cretaceous age occur near Haast and may be equivalents of the Cretaceous–Eocene Paparoa and Brunner equivalents.

Table 9. Trace element concentrations in some New Zealand Cretaceous coals (after Soong and Berrow [164] and Moore et al. [165]).

Sample	Strongman 2 E Seam	Strongman 2 [P532A]	Strongman 2 [2A]	Strongman 2 [2B]	Strongman	Liverpool	Spring Creek	Ohai	Wairaki	Wairaki	Wangaloa	Clarke Values (All Coals)
Coal Region	West Coast	West Coast	West Coast	West Coast	Westcoast	Westcoast	West Coast	Southland	Southland	Southland	Otago	
Coalfield	Greymouth	Greymouth	Greymouth	Greymouth	Greymouth	Greymouth	Greymouth	Ohai	Ohai	Ohai	Kaitangata	
Formation	Paparoa	Paparoa	Paparoa	Paparoa	Paparoa	Paparoa	Paparoa	Morely	Morely	Morely	Taratu	
Rank	Bituminous	Bituminous	Bituminous	Bituminous	Bituminous	Bituminous	Bituminous	Sub-bituminous A	Sub-bituminous A	Sub-bituminous A	Sub-bituminous	
Ag	bld	bld	bld	bld	n.a.	n.a.	bld	n.a.	n.a.	bld	n.a.	0.095
As	0.40	0.45	0.94	0.82	n.a.	n.a.	0.38	n.a.	n.a.	bld	n.a.	8.3
Au	bld	bld	bld	bld	n.a.	n.a.	bld	n.a.	n.a.	bld	n.a.	0.0037
B	27.0	44.1	71.7	61.5	75.6	16.5	21.5	45.9	46.8	48.0	243	52
Ba	174	63.9	129	37.7	25.2	71.5	275	147	132	96.0	59.4	150
Be	3.11	1.62	2.03	1.56	2.52	0.83	0.62	0.15	Bld	0.00	bld	1.5
Bi	0.02	bld	bld	bld	n.a.	n.a.	0.01	n.a.	n.a.	bld	n.a.	0.97
Cd	0.01	bld	bld	0.04	n.a.	n.a.	0.01	n.a.	n.a.	bld	n.a.	0.22
Cl (%)	bld	bld	0.01	bld	n.a.	n.a.	bld	n.a.	n.a.	bld	n.a.	0.02
Co	4.86	7.11	5.93	8.61	4.20	4.18	1.91	0.87	0.35	1.16	3.73	5.1
Cr	7.18	9.90	15.6	3.98	3.15	20.9	5.10	2.30	1.17	1.16	0.54	16
Cs	0.74	2.43	10.9	1.23	n.a.	n.a.	0.08	n.a.	n.a.	0.04	n.a.	1.0
Cu	1.67	2.34	7.96	2.50	2.52	9.35	1.27	4.59	3.90	2.64	1.89	16
Ga	0.75	2.70	6.08	1.72	1.68	1.65	0.34	1.53	0.39	0.56	1.35	5.8
Ge	0.87	1.17	1.20	0.90	1.05	0.55	0.25	bld	Bld	0.08	bld	2.2
Hg	<0.02	0.06	0.09	0.06	n.a.	n.a.	<0.02	n.a.	n.a.	0.06	n.a.	0.1
Li	2.76	6.75	18.7	4.92	2.31	4.13	2.08	1.28	0.35	0.96	4.05	12
Mn	122	135	42.1	73.8	54.6	2.31	80.3	6.63	8.19	21.2	59.4	86
Mo	0.10	0.36	bld	0.16	0.25	0.06	0.10	0.10	0.12	0.21	0.16	2.2
Nb	0.45	3.60	6.71	1.23	n.a.	n.a.	0.49	n.a.	n.a.	1.20	n.a.	3.2
Ni	15.9	16.2	14.0	20.5	10.1	13.2	13.2	3.06	3.32	1.68	4.32	13
Pb	1.69	4.50	8.11	2.05	2.52	3.30	0.62	2.04	3.90	bld	5.40	7.8
Rb	3.12	13.5	39.0	4.02	4.07	1.10	0.35	0.26	0.08	0.24	0.16	14
Sb	0.03	0.18	bld	0.12	n.a.	n.a.	0.02	n.a.	n.a.	bld	n.a.	0.92
Sc	0.50	1.53	3.90	0.98	0.84	2.20	0.19	1.02	0.39	0.76	bld	3.9
Se	0.46	1.00	1.20	0.76	n.a.		0.80	n.a.	n.a.	0.40	n.a.	1.3

Table 9. Cont.

Sample	Strongman 2 E Seam	Strongman 2 [P532A]	Strongman 2 [2A]	Strongman 2 [2B]	Strongman	Liverpool	Spring Creek	Ohai	Wairaki	Wairaki	Wangaloa	Clarke Values (All Coals)
Sn	0.36	0.90	3.12	0.41	1.68	1.10	0.17	2.04	2.34	bld	5.40	1.1
Sr	5.46	23.4	31.2	14.3	27.7	51.7	3.56	300	265	264	124	11
Te	0.01	bld	bld	bld	n.a.	n.a.	0.01	n.a.	n.a.	bld	n.a.	
Th	0.46	bld	3.28	0.45	n.a.	n.a.	0.28	n.a.	n.a.	0.44	n.a.	3.3
Tl	0.05	bld	0.31	0.16	bld	bld	0.05	bld	bld	bld	bld	0.63
U	0.11	0.36	0.69	0.18	n.a.	n.a.	0.06	n.a.	n.a.	0.08	n.a.	2.4
V	0.52	9.90	26.5	4.92	3.36	8.25	bld	3.06	1.76	2.04	1.62	23
Y	0.37	0.99	2.03	0.78	1.68	1.65	0.23	0.77	0.59	0.36	0.54	8.4
Zn	6.58	10.8	6.24	3.28	4.20	14.8	4.32	4.18	8.97	1.16	27.5	23
Zr	11.3	bld	bld	bld	8.40	24.7	2.47	7.65	11.7	bld	1.08	36

8.9. Canterbury

Although the coal in the Canterbury region is mostly sub-bituminous with low ash (5%) and sulphur contents of 0.5% to 1%), the rank varies from lignite to anthracite, the latter due to thermal metamorphism of lignite. The coals were deposited in a transgressive environment on eroded Triassic–Jurassic Torlesse Group, changing north westward from a fluvial to coastal swamp environment and marginal marine environment, and the seams tend to be thin and lensoidal. The coals are upper Cretaceous, occurring in the Broken River coal measures and were mined in small quantities at Glentunnel, Avoca, Malvern Hills, and anthracite at Acheron.

8.10. Otago

Cretaceous coal varying in rank from sub-bituminous to bituminous has been mined sporadically at Shag Point and Papakaio since the 1860s. The coal measures were deposited in a fault angle depression and are interbedded with quartz conglomerates.

Coal is present in the upper Cretaceous Taratu Formation with sub-bituminous B and lignite coals occurring in the Kaitangata field with lignite been confined to the western part of the coalfield. The coals typically have an ash yield of 4%–11% and contain 1.5%–4.5% sulphur. They are unusual in having a high inertinite content (up to 30%) in comparison to other New Zealand Cretaceous coals which usually contain less than 5% inertinite. The coals were deposited in a fault angle depression in a fluviolacustrine environment with a minor marine influence in the upper section. Coal has been mined in the area since the 1860s. Some 17 coal bearing members are interbedded with conglomerate, sand, and clay.

When compared to Clarke values, only B and Sn show significant enrichment with most other elements occurring either in significantly lower concentrations or being approximately equivalent (Co, Pb, Sr, and Zn).

The Green Island coalfield near Dunedin also occurs within the Taratu Formation and has been mined sporadically since the 1860s.

8.11. Southland

Within the upper Cretaceous Ohai Group, coal occurs in the lower Wairo Coal Measures and the upper Morely Coal Measures. The sediments were deposited in a fluviolacustrine environment in a fault-controlled basin. The rank varies from sub-bituminous A to high volatile bituminous C with vitrinite + liptinite content >90%, a typical ash yield of 3%, and 0.2% sulphur content. The seams are lenticular and seam splitting, and washouts are common.

Three analyses of trace elements from the Ohai coalfield show most elements occur in significantly lower concentrations compared to the Clarke values, enrichment being shown only by Sr and, to a lesser extent, Sn.

9. Discussion

Elevated concentrations of critical elements in coals, particularly those of the Carboniferous–Permian and Cenozoic ages, have generally been attributed to within-plate (plume-related) volcanism and associated hydrothermal activity [22,23,166–179]. Critical elements that were mineralized in these coals are various, including Li, Be, Sc, Ti, V, Ga, Ge, Nb, Ta, Zr, Hf, REY, Ag, Au, and platinum group elements Th and U, among others [9,24,25]. However, compared with Carboniferous–Permian coals, the Cretaceous coals, particularly those of Early Cretaceous age, which are globally associated with a peak of volcanic and metallogenic activities [8,26,27,180] and the formation of Large Igneous Provinces (LIPs; Figure 1) [29], are commonly not enriched in the abovementioned critical elements, with the exception of some critical elements in localised areas as present above. This is especially enigmatic because several Early Cretaceous LIPs, including the abnormally extensive High Arctic and Parana–Etendeka LIPs each larger than Mkm² (Figure 1) [29], are closely associated with coal basins. The rare, but significant exceptions are the world-class Ge±U

coal deposits in North China, Mongolia, and Siberia, which are located, however, far away from the major volcanic provinces (Figure 1).

One possible explanation for the lack of volcanic-related mineralization in the Early Cretaceous coals is that peat deposition in Early Cretaceous times, particularly in the volcanic regions, suffered from intense emanations of CO₂ and other greenhouse gases in addition to acidic rains, which led to significant acidification of surficial and ground waters. These processes promote mobilization and transportation (dissemination) of relatively water-resistant elements (REY, Nb, Ta, Zr, Hf, Ga, precious metals, and others) but prevent their deposition and accumulation (concentration and enrichment) in the peat environments. This explanation has already been suggested by the isotopic–geochemical study of Early Cretaceous and Cenozoic coals from the Russian Far East, the latter of which are rich, while the former are poor in critical elements [77]. One solid line of evidence for strong acidic influence on the Early Cretaceous sedimentation is a strong silicification (high SiO₂/Al₂O₃ ratio) of the Early Cretaceous coals relative to the Cenozoic ones. This study also showed in several examples from Asia and Africa (Sections 2, 6 and 7) that more or less significant accumulations of the Cretaceous metalliferous coal originated under the influence of acidic waters. In contrast, the enrichment of REY and associated critical elements in the North American coals (Sections 4 and 5) was attributed to alkaline waters. It is unclear if this a consequence of difference in local or regional conditions due to the low level of geochemical knowledge on the American coals.

The Cretaceous coals are also depleted in lithium, which is currently in high global demand. As suggested by some recent studies [155,181,182], one of the most significant factors controlling lithium mineralization in coal is the mixture of acidic ground waters or hydrothermal solutions with alkaline seawater, which causes an Li extraction from clastic material and its deposition in and around coal seams. Acidification of the Cretaceous oceans associated with high volcanic activity and mantle degassing [183] may have negatively influenced this process.

10. Conclusions

A major conclusion of this study is that intensive igneous activity that led to extensive acidification of terrestrial and marine waters was responsible for the low coal metallogenesis during the Cretaceous period, especially the Early Cretaceous time.

The world-class Ge ± U deposits in North China, Mongolia, and Siberia are the only commercially significant representatives of the Cretaceous metalliferous coals. They are located, however, far away from the major volcanic provinces. We offer the following explanation for this phenomenon. The enrichment of redox-sensitive elements such as Ge, U, Mo, and V in coal are related to bio-chemical reduction of oxidized meteoric, hydrothermal, or sea waters by organic matter of the peat bogs [76,111,112,181,184,185]. This process might be partly suppressed by anomalously low oxygen content in the atmosphere during the mid-Cretaceous that was also associated with high volcanic activity and greenhouse emanations [186]. However, this negative effect was evidently not strong enough to completely suppress the mineralization of coals with redox-sensitive elements, as evidenced by the Cretaceous Ge- and U-rich coals found in China, Russia, and other countries. It should also be considered that the age of this mineralization is not well defined. It might be late or post-Cretaceous related to a global increase in atmospheric pO₂ in these times [186].

More future work should be conducted to verify the hypotheses above, including more case studies on individual Cretaceous coal deposits, igneous activity during the Cretaceous period and its influences on terrestrial and marine waters, and oxygen content in the atmosphere during and post-Cretaceous age.

Supplementary Materials: The following supporting information can be downloaded at: <https://www.mdpi.com/article/10.3390/min12091154/s1>. Table S1. Coal quality data from U.S. Geological Survey's World Coal Quality Inventory program U.S. Geological Survey's World Coal Quality Inventory (WoCQI) (https://www.usgs.gov/centers/gemsc/science/world-coal-quality-inventory-data?qt-science_center_objects=0#qt-science_center_objects, accessed on 24 January 2020). Table S2. Sc, Y, and REE for samples from Eagle Pass, Texas (after Zygarlicke et al., 2019 [94]). Table S3. Cretaceous coals of the western United States from U.S. Geological Survey database (Bragg et al. 1998 [85]). Table S4. Cretaceous coals from the western U.S. from the Pennsylvania State University (PSOC) database. Table S5. Data from van der Flier-Keller (1993) [122]. Table S6. Goodarzi et al.'s (2009) Table 6 [117]. Concentrations of elements in coals (mg/kg, coal-base) for the combined geological section of the Elk Valley coalfield.

Author Contributions: Note: Authors are in alphabetical order of surname, with the exceptions of the first and the last authors. S.I.A. and I.Y.C. contributed the data for Siberia, Russia Far East, and Mongolia; S.D. contributed the data for China; J.C.H., Finkelman R.B.F., I.F. and B.C.F. contributed the data for South America, United States, Mexico and Canada; N.J.W. and V.P.N. contributed the data for Africa; D.F. and I.T.G. contributed the data for the New Zealand; V.P.N. drafted the sections on Introduction and Discussion. All authors have read and agreed to the published version of the manuscript.

Funding: This research was financially supported by the National Natural Science Foundation of China (Nos. 91962220, 92162105), the Russian Science Foundation (Project no. 18-17-00004), and the Russian Foundation for Basic Research (No. 21-55-53013). Portions of the study were done in collaboration with U.S. Department of Energy contract DE-FE0029007 to the University of North Dakota Energy & Environmental Research Center, U.S. Department of Energy contract DE-FE0032053 to the Texas Bureau of Economic Geology, and Ruben Garibay and Fernando Lopez at Farming Hydrasource Mine (Eagle Pass, Texas). The support of the Department of Science and Innovation South Africa through its funding agency, the National Research Foundation, and the Centre of Excellence for Integrated Mineral and Energy Resource Analysis (DSI-NRF CIMERA, grant number 91487) towards this research is hereby acknowledged. Opinions expressed and conclusions arrived at, are those of the author(s) and are not necessarily to be attributed to the CoE, DSI or NRF. The unpublished data was generated during the PhD study of Mangs.

Conflicts of Interest: The authors declare no conflict of interest.

References

1. Lin, R.; Soong, Y.; Granite, E.J. Evaluation of trace elements in U.S. coals using the USGS COALQUAL database version 3.0. Part I: Rare earth elements and yttrium (REY). *Int. J. Coal Geol.* **2018**, *192*, 1–13. [[CrossRef](#)]
2. Lin, R.; Soong, Y.; Granite, E.J. Evaluation of trace elements in U.S. coals using the USGS COALQUAL database version 3.0. Part II: Non-REY critical elements. *Int. J. Coal Geol.* **2018**, *192*, 39–50. [[CrossRef](#)]
3. Hower, J.C.; Granite, E.; Mayfield, D.; Lewis, A.; Finkelman, R. Notes on contributions to the science of rare earth element enrichment in coal and coal combustion byproducts. *Minerals* **2016**, *6*, 32. [[CrossRef](#)]
4. Wei, Q.; Rimmer, S.M. Acid solubility and affinities of trace elements in the high-Ge coals from Wulantuga (Inner Mongolia) and Lincang (Yunnan Province), China. *Int. J. Coal Geol.* **2017**, *178*, 39–55. [[CrossRef](#)]
5. Blissett, R.S.; Smalley, N.; Rowson, N.A. An investigation into six coal fly ashes from the United Kingdom and Poland to evaluate rare earth element content. *Fuel* **2014**, *119*, 236–239. [[CrossRef](#)]
6. Bullock, L.A.; Parnell, J.; Perez, M.; Armstrong, J.G.; Feldmann, J.; Boyce, A.J. High selenium in the Carboniferous coal measures of Northumberland, North East England. *Int. J. Coal Geol.* **2018**, *195*, 61–74. [[CrossRef](#)]
7. Fiket, Ž.; Medunić, G.; Furdek Turk, M.; Kniewald, G. Rare earth elements in superhigh-organic-sulfur Raša coal ash (Croatia). *Int. J. Coal Geol.* **2018**, *194*, 1–10. [[CrossRef](#)]
8. Nechaev, V.P.; Dai, S.; Sutherland, F.L.; Graham, I.T.; Nechaeva, E.V. The Cretaceous turn of geological evolution: Key evidence from East Asia. *Acta Geol. Sin.* **2018**, *92*, 1991–2003. [[CrossRef](#)]
9. Seredin, V.; Finkelman, R.B. Metalliferous coals: A review of the main genetic and geochemical types. *Int. J. Coal Geol.* **2008**, *76*, 253–289. [[CrossRef](#)]
10. Dai, S.; Finkelman, R.B. Coal as a promising source of critical elements: Progress and future prospects. *Int. J. Coal Geol.* **2018**, *186*, 155–164. [[CrossRef](#)]
11. Massari, S.; Ruberti, M. Rare earth elements as critical raw materials: Focus on international markets and future strategies. *Res. Policy* **2013**, *38*, 36–43. [[CrossRef](#)]

12. Hedin, B.C.; Hedin, R.S.; Capo, R.C.; Stewart, B.W. Critical metal recovery potential of Appalachian acid mine drainage treatment solids. *Int. J. Coal Geol.* **2020**, *231*, 103610. [[CrossRef](#)]
13. Hower, J.C.; Qian, D.; Briot, N.J.; Hood, M.M.; Eble, C.F. Mineralogy of a rare earth element-rich Manchester coal lithotype, Clay County, Kentucky. *Int. J. Coal Geol.* **2020**, *220*, 103413. [[CrossRef](#)]
14. Karayigit, A.I.; Yerin, Ü.O.; Oskay, R.G.; Bulut, Y.; Córdoba, P. Enrichment and distribution of elements in the middle Miocene coal seams in the Orhaneli coalfield (NW Turkey). *Int. J. Coal Geol.* **2021**, *247*, 103854. [[CrossRef](#)]
15. Li, X.; Dai, S.; Nechaev, V.P.; Graham, I.T.; French, D.; Wang, X.; Zhao, L.; Zhao, J. Mineral Matter in the Late Permian C1 Coal from Yunnan Province, China, with Emphasis on Its Origins and Modes of Occurrence. *Minerals* **2021**, *11*, 19. [[CrossRef](#)]
16. Han, Q.; Liu, J.; Shang, N.; Zhao, S.; Jia, R. Optimization of Operating Parameters for Coal Low-Temperature Ashing: A Suitable and Efficient Treatment Method for Mineral Analysis in Coal. *Minerals* **2022**, *12*, 1119. [[CrossRef](#)]
17. Jia, R.; Liu, J.; Han, Q.; Zhao, S.; Shang, N.; Tang, P.; Zhang, Y. Mineral matter transition in lignite during ashing process: A case study of Early Cretaceous lignite from the Hailar Basin, Inner Mongolia, China. *Fuel* **2022**, *328*, 125252. [[CrossRef](#)]
18. Sutcu, E.C.; Şentürk, S.; Kapıcı, K.; Gökçe, N. Mineral and rare earth element distribution in the Tunçbilek coal seam, Kütahya, Turkey. *Int. J. Coal Geol.* **2021**, *245*, 103820. [[CrossRef](#)]
19. Liu, J.; Dai, S.; He, X.; Hower, J.C.; Sakulpitakphon, T. Size-Dependent Variations in Fly Ash Trace Element Chemistry: Examples from a Kentucky Power Plant and with Emphasis on Rare Earth Elements. *Energy Fuels* **2017**, *31*, 438–447. [[CrossRef](#)]
20. Widmer, J.; Nakano, J.; Nakano, A.; Bennett, J. Concentrating rare earth elements to phosphate in molten coal ash by a temperature gradient approach. *Int. J. Coal Geol.* **2021**, *235*, 103688. [[CrossRef](#)]
21. Seredin, V.V.; Dai, S. Coal deposits as potential alternative sources for lanthanides and yttrium. *Int. J. Coal Geol.* **2012**, *94*, 67–93. [[CrossRef](#)]
22. Dai, S.; Chekryzhov, I.Y.; Seredin, V.V.; Nechaev, V.P.; Wang, X.; Ward, C.R.; Hower, J.C.; Graham, I.T.; Ren, D. Metalliferous coal deposits in East Asia (Primorye of Russia and South China): A review of geodynamic controls and styles of mineralization. *Gondwana Res.* **2016**, *29*, 60–82. [[CrossRef](#)]
23. Arbuzov, S.I.; Spears, D.A.; Vergunov, A.V.; Ilenok, S.S.; Mezhibor, A.M.; Ivanov, V.P.; Zarubina, N.A. Geochemistry, mineralogy and genesis of rare metal (Nb-Ta-Zr-Hf-Y-REE-Ga) coals of the seam XI in the south of Kuznetsk Basin, Russia. *Ore Geol. Rev.* **2019**, *113*, 103073. [[CrossRef](#)]
24. Seredin, V.V.; Tomson, I.N. The West Primorye noble-rare metal zone: A new Cenozoic Metallogenic Taxon in the Russian Far East. *Dokl. Earth Sci.* **2008**, *421*, 745–750. [[CrossRef](#)]
25. Dai, S.; Seredin, V.V.; Ward, C.R.; Hower, J.C.; Xing, Y.; Zhang, W.; Song, W.; Wang, P. Enrichment of U–Se–Mo–Re–V in coals preserved within marine carbonate successions: Geochemical and mineralogical data from the Late Permian Guiding Coalfield, Guizhou, China. *Miner. Depos.* **2015**, *50*, 159–186. [[CrossRef](#)]
26. Ronov, A.B. *Stratisphere, or Sedimentary Cover of the Earth (Quantitative Research)*; Nauka: Moscow, Russia, 1993; Volume 144. (In Russian)
27. Nechaev, V.P.; Sutherland, F.L.; Nechaeva, E.V. Metallogenic evolution of Northeast Asia related to the Cretaceous turn of geological evolution. *Minerals* **2022**, *12*, 400. [[CrossRef](#)]
28. Ernst, R.E.; Bond, D.P.G.; Zhang, S.-H.; Buchan, K.L.; Grasby, S.E.; Youbi, N.; El Bilali, H.; Bekker, A.; Doucet, L.S. Large igneous province record through time and implications for secular environmental changes and geological time-scale boundaries. In *Large Igneous Provinces: A Driver of Global Environmental and Biotic Changes*, 1st ed.; Ernst, R.E., Dickson, A.J., Bekker, A., Eds.; Wiley: Hoboken, NJ, USA, 2021; Volume 255, pp. 3–26.
29. Ziegler, A.; Eshel, G.; Rees, P.M.; Rothfus, T.; Rowley, D.; Sunderlin, D. Tracing the tropics across land and sea: Permian to present. *Lethaia* **2003**, *36*, 227–254. [[CrossRef](#)]
30. Akinyemi, S.A.; Nyakuma, B.B.; Jauro, A.; Olanipekun, T.A.; Mudzielwana, R.; Gitari, M.W.; Saikia, B.K.; Dotto, G.L.; Hower, J.C.; Silva, L.F.O. Rare earth elements study of Cretaceous coals from Benue Trough basin, Nigeria: Modes of occurrence for greater sustainability of mining. *Fuel* **2021**, *304*, 121468. [[CrossRef](#)]
31. Kashyrtsev, V.A.; Zueva, I.N.; Suknev, V.S.; Mitronov, D.V.; Syundyukov, S.H.A.; Andreyeva, G.V.; Kapysheva, G.I.; Livshits SKh Popov, V.I. Paragenetic associations of rare earth elements in Mesozoic coals of the northern part of the Lena Basin. *Otechestvennaya Geol.* **1999**, *4*, 65. (In Russian)
32. Chaban, N.N.; Fedorov, V.P.; Nikitina, N.K.; Kuklina, G.L. *Tarbagatai Deposit. Coal Base of Russia. Coal Basins and Deposits of Eastern Siberia (Tunguska and Taimyr Basins, Deposits of Transbaikalia)*; Geoinformmark: Moscow, Russia, 2001; Volume 4, pp. 394–402. (In Russian)
33. Syzikh, V.I.; Skalkin, V.I.; Egorov, O.N. *Geological Map. Sheet M-49-VIII. Scale 1:200000*, 1st ed. 1961. Available online: http://geolkart.ru/list_200.php?idlist=M-49-VIII&idlist_d=P&gen=1&g (accessed on 6 September 2022).
34. Avdeev, P.B.; Kuzhikov, A.A.; Kuklina, G.L. Prospects of Germanium–Coal Tarbagatajsky Coal Deposit in Transbaikalia. *Min. Inf. Anal. Bull.* **2015**, *4*, 26–31, (In Russian with English Abstract).
35. Admakin, L.A.; Parada, S.G. Statistical allocation of the parageneses of minor elements from the associations in fossil coals. *Dokl. Earth Sci.* **2019**, *485*, 260–263. [[CrossRef](#)]
36. Dulzon, O.A. Mineral inclusions in coals of Transbaikalia. *Bull. Tomsk. Polytech. Inst.* **1976**, *264*, 16–17. (In Russian)
37. Sidorova, G.P.; Yakimov, A.A.; Ovcharenko, N.V.; Gushchina, T.O. Rare trace elements in coals of Transbaikalia. *Transbaikal State Univ. J.* **2019**, *25*, 26–33. (In Russian) [[CrossRef](#)]

38. Ozersky, A.Y.; Ekhanin, A.G. Prospects for study and development of germanium resources in the Lower Cretaceous lignite of the Kas area. *Bull. Tomsk. Polytech. Univ.* **2009**, *314*, 41–43. (In Russian)
39. Makarov, V.A.; Podkopaev, O.I.; Koz'min, D.G.; Naidko, V.I.; Shimanskiy, A.F.; Kopytkova, S.A. Lignite from Central Watershed of the Yenisey River and Prospects. *J. Sib. Fed. Univ. Eng. Technol.* **2014**, *7*, 862–871. (In Russian with English Abstract)
40. Gorky, Y.K. To the classification of coals according to their germaniferousness. In *Geology and Geochemistry of Minerals of the Krasnoyarsk Region*; Krasnoyarsk Publishing House: Krasnoyarsk, Russia, 1964; pp. 75–85. (In Russian)
41. Evdokimov, A.P.; Ozersky, A.Y.; Ekhanin, A.G. Germanium-bearing lignite of the southeast margin of the West Siberian plate. *Explor. Prot. Miner. Resour.* **2004**, *6*, 26–29. (In Russian)
42. Naidko, V.I.; Makarov, V.A.; Koz'min, D.G.; Shimanskiy, A.F.; Fertikov, A.I. Geologic and Geochemical Features of Cretaceous Ge-Bearing Lignites in the Yenisey Middle Reaches. *Russ. Geol. Geophys.* **2019**, *60*, 86–96. [[CrossRef](#)]
43. Evdokimov, A.P.; Ekhanin, A.G.; Kuzmin, V.I.; Ozersky, A.Y. New data on germaniferous Mesozoic lignite in the Kas River basin (Krasnoyarsk Territory). In *Geology of Coal Deposits: Interuniversity Scientific Thematic Collection*; Publishing House of the Ural Mining and Geological Academy: Yekaterinburg, Russia, 2002; Volume 12, pp. 181–187. (In Russian)
44. Ozersky, A.Y.; Ekhanin, A.G. Germanium resources in Lower Cretaceous lignite of the Kas area and tasks for their study and development. *Geo-Siberia* **2006**, *5*, 48–53. (In Russian)
45. State Geological Map of the Russian Federation. *Scale 1:1 000 000 (Third Generation). Angara-Yenisey Series. Sheet O-46-Krasnoyarsk. Explanatory Note*; Cartographic Factory VSEGEI: St. Petersburg, Russia, 2009; pp. 1–500. (In Russian)
46. Kizil'shtein, L.Y. Morphology and origin of some syngenetic pyrite occurrences in coal seams of the Donetsk basin. *Lithol. Miner. Resour.* **1967**, *2*, 122–124. (In Russian)
47. Seredin, V.V. Elemental metals in metalliferous coal-bearing strata. In *Proceedings of the ICCS'97, Essen, Germany, 7–12 September 1997*; Volume 1, pp. 405–408.
48. Dai, S.; Liu, J.; Ward, C.R.; Hower, J.C.; French, D.; Jia, S.; Hood, M.M.; Garrison, T.M. Mineralogical and geochemical compositions of Late Permian coals and host rocks from the Guxu Coalfield, Sichuan Province, China, with emphasis on enrichment of rare metals. *Int. J. Coal Geol.* **2016**, *166*, 71–95. [[CrossRef](#)]
49. Ilyenok, S.S. Native elements in coals and ashes of coals of Azeysky deposit of Irkutsk coal basin. *Bull. Tomsk. Polytech. Univ.* **2013**, *323*, 65–71. (In Russian)
50. Ilyenok, S.S.; Arbuzov, S.I. Metalliferous coals of Azeyskoe deposit of Irkutsk coal basin/Bulletin of the Tomsk Polytechnic University. *Geo Assets Eng.* **2018**, *329*, 132–144. (In Russian)
51. Lavrik, N.A.; Komarova, V.S.; Konovalova, N.S.; Litvinova, N.M. Native iron and other micromineral phases in the coals and ash of the Ushumunskoe lignite deposit and the Sutarskoe manifestation (Maly Khingan). In *Proceedings of the V International Scientific Conference "Contemporary Problems of the Regional Development"*, Vigo, Spain, 14–16 May 2018; Institute for Complex Analysis of Regional Problems FEBRAS: Birobidzhan, Russia, 2014; pp. 179–180.
52. Globa, V.A.; Gordienko, I.V.; Shmakov, A.P. On hydrothermal occurrences in Jurassic deposits of the Eastern Sayan. *Geol. Geophys.* **1964**, *12*, 127–134. (In Russian)
53. Hain, V.E. Regional Geotectonics. In *Trans-Alpine Asia and Australia*; Nedra: Moscow, Russia, 1979; p. 356. (In Russian)
54. Johannesson, K.H.; Zhou, X. Geochemistry of the rare earth element in natural terrestrial waters: A review of what is currently known. *Chin. J. Geochem.* **1997**, *16*, 20–42. [[CrossRef](#)]
55. Shand, P.; Johannesson, K.H.; Chudaev, O.; Chudaeva, V.; Edmunds, W.M. Rare earth element contents of high pCO₂ groundwaters of Primorye, Russia: Mineral stability and complexation controls. *Water Sci. Technol. Lib.* **2005**, *51*, 161–186.
56. Yudovich, Y.E. Notes on the marginal enrichment of Germanium in coal beds. *Int. J. Coal Geol.* **2003**, *56*, 223–232. [[CrossRef](#)]
57. Seredin, V.V.; Magazina, L.O. Mineralogy and geochemistry of the fossil wood, Pavlovsk coal deposit. *Lithol. Polezn. Iskop.* **1999**, *2*, 158–173.
58. Vassilev, S.V.; Eskenazy, G.M.; Tarassov, M.P.; Dimov, V.I. Mineralogy and geochemistry of a vitrain lens with unique trace element content from the Vulche Pole coal deposit, Bulgaria. *Geol. Balc.* **1995**, *25*, 111–124.
59. Hallam, A.; Payne, K.W. Germanium enrichment in lignites from Lower Lias of Dorset. *Nature* **1958**, *181*, 1008–1009. [[CrossRef](#)]
60. Kislyakov, Ya.M.; Shchetochkin, V.N. The role of Mesozoic exogenetic-epigenetic processes in the formation of uranium-coal deposits. *Geol. Ore Depos.* **1994**, *36*, 148–168.
61. Norov, N.; Davaa, S.; Enkhbat, N. Study on natural activity of Mongolian coal using gamma spectrometry. Radioactivity and Radioactive Elements in the Environment. In *Materials of the 2nd International Conference*; Tandem-Art: Tomsk, Russia, 2004; pp. 749–751.
62. Stetler, L.D.; Stone, J.J.; Schwalm, A. Off-site impacts from abandoned uranium mines in the North Cave Hills, Harding County, South Dakota. *Proc. South Dak. Acad. Sci.* **2007**, *86*, 159–167.
63. Arbuzov, S.I.; Mashenkin, V.S. Oxidation zone of coal deposits—A promising source of noble and rare metals (on the example of deposits in Central Asia). Problems and prospects of development of the mineral resource base and enterprises of the energy sector in Siberia. In *Materials of the Inter-Regional Scientific Conference*; Publishing house of TPU: Tomsk, Russia, 2007; pp. 26–31. (In Russian)
64. Zheleznova, N.G.; Kuznetsov, U.Y.; Matveev, A.K.; Cherepovsky, V.F. *Reserves of Coal of the World Countries*; Nedra: Moscow, Russia, 1983; p. 167. (In Russian)

65. Yanshin, A.L. (Ed.) *Map of Geological Formations of the Mongolian People's Republic. Scale 1:1500000*; GUGK: Moscow, Russia, 1989. (In Russian)
66. Erdenetsogt, B.-O.; Lee, I.; Bat-Erdene, D.; Jargal, L. Mongolian coal-bearing basins: Geological setting, coal characteristics, distribution, and resources. *Int. J. Coal Geol.* **2009**, *80*, 87–104. [[CrossRef](#)]
67. Afanasiev, G.V.; Mironov, Y.B.; Pinsky, E.M. East Asian belt of leucogranite-type uranium deposits. *Reg. Geol. Metallog.* **2015**, *61*, 92–100, (In Russian with English Abstract).
68. Mironov, Y.B. *Uranium Metallogeny of Mongolia*; Lap Lambert: Saarbrücken, Germany, 2016; p. 289. (In Russian)
69. Mironov, Y.B.; Shuvalov, Y.M. *Uranium Deposits of Mongolia*; Mongolian University of Science and Technology: Sukhbaatar, Mongolia, 2009; p. 304. (In Russian)
70. Ketris, M.P.; Yudovich, Y.E. Estimations of Clarkes for carbonaceous biolithes: World average for trace element contents in black shales and coals. *Int. J. Coal Geol.* **2009**, *78*, 135–148. [[CrossRef](#)]
71. Taylor, S.R.; McLennan, S.M. *The Continental Crust: Its Composition and Evolution*; U.S. Department of Energy Office of Scientific and Technical Information: Oak Ridge, TN, USA, 1985; p. 312.
72. Kostin, Y.P.; Meytov, E.S. On the genesis of deposits of highly germaniferous coals and criteria for their search. *Proc. USSR Acad. Sci. Geol. Ser.* **1972**, *1*, 112–119. (In Russian)
73. Seredin, V.V. Metalliferous coals: Conditions of formation and prospects of development. In *Russian Coal Base*; Geoinformmark: Moscow, Russia, 2004; Volume 6, pp. 453–519. (In Russian)
74. Sedykh, A.K. *Cenozoic Riftogenic Depressions of Primorye (Geological Structure, Mineralogy, and Geodynamics of Carbon Genesis)*; Dalnauka: Vladivostok, Russia, 2008; p. 248. (In Russian)
75. Chekryzhov, I.Y.; Trach, G.N.; Nechaev, V.P.; Trach, D.A. Occurrences of rare-earth mineralization in South Primorye. *Gorn. Zhurnal* **2018**, *2*, 35–40, (In Russian with English Abstract). [[CrossRef](#)]
76. Arbuzov, S.I.; Spears, D.A.; Ilenok, S.S.; Chekryzhov, I.Y.; Ivanov, V.P. Modes of occurrence of germanium and tungsten in the Spetsugli germanium ore field, Pavlovka brown coal deposit, Russian Far East. *Ore Geol. Rev.* **2021**, *132*, 103986. [[CrossRef](#)]
77. Nechaev, V.P.; Bechtel, A.; Dai, S.; Chekryzhov, I.Y.; Pavlyutkin, B.I.; Vysotskiy, S.V.; Ignatiev, A.V.; Velivetskaya, T.A.; Guo, W.; Tarasenko, I.A.; et al. Bio-geochemical evolution and critical element mineralization in the Cretaceous-Cenozoic coals from the southern Far East Russia and northeastern China. *Appl. Geochem.* **2020**, *117*, 104602. [[CrossRef](#)]
78. Brambilla, D.E. Geología de la zona antracifera de Huayday-Lucma, La Libertad. *Soc. Geol. Perú Bol.* **1957**, *32*, 35–50.
79. Hower, J.C.; Fishel, K.W. Anisotropy of coal reflectance: Example from No. 5 seam (“Bollas”) meta-anthracite, Peru. *Soc. Org. Petrol. Newsl.* **1990**, *7*, 10–11. Available online: <https://www.tsop.org/newsletter.html> (accessed on 20 October 2021).
80. Hower, J.C.; Rathbone, R.F.; Wild, G.D.; Davis, A. Observations on the use of vitrinite maximum reflectance versus vitrinite random reflectance for high volatile bituminous coals. *J. Coal Qual.* **1994**, *13*, 71–76.
81. Flores-Williams, H. Chilean, Argentine, and Bolivian coals. In *Coal Resources of the Americas*; Kottlowski, F.E., Ed.; Geological Society of America: Boulder, CO, USA, 1978; Volume 179, pp. 1–13.
82. Flores, R.M.; Cross, T.A. Cretaceous and Tertiary coals of the Rocky Mountains and Great Plains regions. In *The Geology of North America, V. P-2, Economic Geology*; Gluskoter, H.J., Ed.; Geological Society of America Decade of North American Geology: Boulder, CO, USA, 1991.
83. Burchfiel, B.C.; Davis, G.A. Nature and controls on Cordilleran orogenesis, western United States: Extensions of an earlier synthesis. *Am. J. Sci.* **1975**, *275*, 363–396.
84. Crowley, S.S.; Stanton, R.W.; Ryer, T.A. The effects of volcanic ash on the maceral and chemical composition of the C coal bed, Emery Coal Field, Utah. *Org. Geochem.* **1989**, *14*, 315–331. [[CrossRef](#)]
85. Bragg, L.J.; Oman, J.K.; Tewalt, S.J.; Oman, C.L.; Rega, N.H.; Washington, P.M.; Finkelman, R.B. *U.S. Geological Survey Coal Quality (COALQUAL) Database: Version 2.0. U.S. Geological Survey Open-File Report 97-134, CD-ROM*; U.S. Geological Survey: Reston, VA, USA, 1998.
86. Grimes, D.J.; Marranzino, A.P. *Direct-Current Arc and Alternating-Current Spark Emission Spectrographic Field Methods for the Semiquantitative Analysis of Geologic Materials*; U.S. Geological Survey Circular: Reston, VA, USA, 1968; Volume 591, p. 6.
87. Kaiser, W.R. Coal geology of Texas. In *Keystone Coal Industry Manual*; Primedia: Chicago, IL, USA, 1999; pp. 675–680.
88. Hook, R.W.; Warwick, P.D.; SanFilipo, J.R. Chapter 13: Upper Cretaceous Bituminous Coal Deposits of the Olmos Formation, Maverick County, Texas. In *Geologic Assessment of Coal in the Gulf of Mexico Coastal Plain, USA*; Warwick, P.D., Karlsen, A.K., Merrill, M., Valentine, B.J., Eds.; American Association of Petroleum Geologists: Tulsa, OK, USA, 2011; Volume 62, pp. 277–285.
89. Schmitz, E.J. Geology and mineral resources of the Rio Grande region of Texas and Coahuila. *Trans. Am. Inst. Min. Eng.* **1885**, *13*, 388–405.
90. Tuttle, E.G. The Sabinas coalfield. *Eng. Min. J.* **1894**, *58*, 390–392.
91. Ludlow, E. The coal-fields of Las Esperanzas, Coahuila, Mexico. *Trans. Am. Inst. Min. Eng.* **1902**, *32*, 140–156.
92. Aguilera, J.G. The Carboniferous deposits of northern Coahuila. *Eng. Min. J.* **1909**, *88*, 730–733.
93. Odeja-Rivera, J. Main coal regions of Mexico. In *Coal Resources of the Americas*; Kottlowski, F.E., Ed.; Geological Society of America: Boulder, CO, USA, 1978; Volume 179.
94. Zygarricke, C.J.; Folkedahl, B.C.; Nyberg, C.M.; Feole, I.K.; Kurz, B.A.; Theakar, N.L.; Benson, S.A.; Hower, J.C.; Eble, C.F. Rare-Earth Elements (REES) in U.S. Coal Based Resources: Sampling, Characterization, and Round-Robin Interlaboratory Study.

2019. Available online: <https://edx.netl.doe.gov/dataset/rare-earth-elements-in-u-s-coal-based-resources,rfp-10982-fe0029007-final-report-RRIS-UND.pdf> (accessed on 24 January 2020).
95. Dapples, E.C. Coal metamorphism in the Anthracite-Crested Butte quadrangles, Colorado. *Econ. Geol.* **1939**, *34*, 369–398. [[CrossRef](#)]
 96. Gaskill, D.L.; Colman, S.M.; DeLong, J.E.; Robinson, C.H. Geologic map of the Crested Butte quadrangle, Gunnison County, Colorado. U.S. In *Geological Survey, Geologic Quadrangle Map GQ-1580*; U.S. Geological Survey: Reston, VA, USA, 1986.
 97. Lee, W.T. *The Cerrillos coal field, Santa Fe County, New Mexico. U.S.*; Geological Survey Bulletin: Reston, VA, USA, 1913; Volume 531e, pp. 285–312.
 98. Turnbull, L.A.; Toenges, A.L.; Davis, J.D.; Reynolds, D.A.; Parks, B.C. Miller Gulch and Cook & White coal beds near Cerrillos, Santa Fe County, N. Mex.: Reserves; coking, petrographic, and chemical properties. *U.S. Bur. Mines Rep. Investig.* **1951**, *4814*, 35.
 99. Beumont, E.C. Geology of the Cerrillos coal field, Santa Fe County, New Mexico. In *New Mexico Geological Society Guidebook*; U.S. Geological Survey: Reston, VA, USA, 1979; pp. 269–274.
 100. Hower, J.C.; Hoffman, G.K.; Garrison, T.M. Macrinite and funginite forms in Cretaceous Menefee Formation anthracite, Cerrillos coalfield, New Mexico. *Int. J. Coal Geol.* **2013**, *114*, 54–59. [[CrossRef](#)]
 101. Ryer, T.A.; Phillips, R.E.; Bohor, B.F.; Pollastro, R.M. Use of altered volcanic ash falls in stratigraphic studies of coal-bearing sequences: An example from the Upper Cretaceous Ferron Sandstone Member of the Mancos Shale in central Utah. *Geol. Soc. Am. Bull.* **1980**, *91*, 579–586. [[CrossRef](#)]
 102. Triplehorn, D.M.; Bohor, B.F. Altered volcanic ash partings in the C bed, Ferron Sandstone Member of the Mancos Shale. U.S. In *Geological Survey Open-file Report 81-775*; U.S. Geological Survey: Reston, VA, USA, 1981; p. 43.
 103. Crowley, S.S.; Simon, F.O.; Stanton, R.W. Selected chemical composition of the C bed, Emery coal field, Utah. U.S. In *Geological Survey Open-file Report 60*; U.S. Geological Survey: Reston, VA, USA, 1988; pp. 88–526.
 104. Hower, J.C.; Scott, A.C.; Hutton, A.C.; Parekh, B.K.; Dauley, B. Coal—Availability, mining, and preparation. In *Encyclopedia of Energy Technology and the Environment*; Bisio, A., Boots, S.G., Eds.; John Wiley & Sons, Inc.: Hoboken, NJ, USA, 1995; pp. 603–684.
 105. Rao, P.D.; Smith, J.E. Petrology of Cretaceous coals from Northern Alaska. In *U.S. Department of Energy, DE-FG22080 PC 30237, MIREL Report No. 64*; University of Alaska Mineral Industry Research Laboratory: Fairbanks, AK, USA, 1983; p. 141.
 106. Hoffman, G.K. Geology and quality of Menefee Formation coals, Monero coal field, Rio Arriba County, New Mexico. *New Mexico. Geology* **1991**, *13*, 1–8.
 107. Yudovich, Y.E. Coal inclusions in sedimentary rocks: A geochemical phenomenon. A review. *Int. J. Coal Geol.* **2003**, *56*, 203–222. [[CrossRef](#)]
 108. Dai, S.; Seredin, V.V.; Ward, C.R.; Jiang, J.; Hower, J.C.; Song, X.; Jiang, Y.; Wang, X.; Gornostaeva, T.; Li, X.; et al. Composition and modes of occurrence of minerals and elements in coal combustion products derived from high-Ge coals. *Int. J. Coal Geol.* **2014**, *121*, 79–97. [[CrossRef](#)]
 109. Seredin, V.V. Rare earth elements in germanium-bearing coal seams of the Spetsugli deposit (Primor’e region, Russia). *Geol. Ore Depos.* **2005**, *47*, 238–255.
 110. Arbuzov, S.I.; Chekryzhov, I.Y.; Spears, D.A.; Ilenok, S.S.; Soktoev, B.R.; Popov, N.Y. Geology, geochemistry, mineralogy and genesis of the Spetsugli high-germanium coal deposit in the Pavlovsk coalfield, Russian Far East. *Ore Geol. Rev.* **2021**, *139*, 104537. [[CrossRef](#)]
 111. Dai, S.; Liu, J.; Ward, C.R.; Hower, J.C.; Xie, P.; Jiang, Y.; Hood, M.M.; O’Keefe, J.M.K.; Song, H. Petrological, geochemical, and mineralogical compositions of the low-Ge coals from the Shengli Coalfield, China: A comparative study with Ge-rich coals and a formation model for the Wulantuga Ge ore deposit. *Ore Geol. Rev.* **2015**, *71*, 318–349. [[CrossRef](#)]
 112. Dai, S.; Wang, P.; Ward, C.R.; Tang, Y.; Song, X.; Jiang, J.; Hower, J.C.; Li, T.; Seredin, V.V.; Wagner, N.J.; et al. Elemental and mineralogical anomalies in the coal-hosted Ge ore deposit of Lincang, Yunnan, southwestern China: Key role of N₂–CO₂-mixed hydrothermal solutions. *Int. J. Coal Geol.* **2015**, *152*, 19–46. [[CrossRef](#)]
 113. Reiter, M.; Clarkson, G. Relationships between heat flow, paleotemperatures, coalification, and petroleum maturation in the San Juan Basin, northwest New Mexico and southwest Colorado. *Geothermics* **1983**, *12*, 323–339. [[CrossRef](#)]
 114. Clarkson, G.; Reiter, M. The thermal regime of the San Juan Basin since the Late Cretaceous and its relationship to San Juan Mountains thermal sources. *J. Volcanol. Geotherm. Res.* **1987**, *31*, 217–237. [[CrossRef](#)]
 115. Bustin, R.M.; Moffat, I. Semianthracite, anthracite and meta-anthracite in central Canadian Cordillera: Their geology, characteristics and coalification history. *Int. J. Coal Geol.* **1990**, *16*, 214–216. [[CrossRef](#)]
 116. Kalkreuth, W.; Langenberg, W.; McMechan, M. Regional coalification of lower Cretaceous coal-bearing strata, Rocky Mountain Foothills and Foreland, British Columbia and adjacent parts of Alberta, Canada. *Int. J. Coal Geol.* **1990**, *16*, 219–220. [[CrossRef](#)]
 117. Goodarzi, F.; Grieve, D.A.; Sanei, H.; Gentzis, T.; Goodarzi, N.N. Geochemistry of coals from the Elk Valley coalfield, British Columbia, Canada. *Int. J. Coal Geol.* **2009**, *77*, 246–259. [[CrossRef](#)]
 118. Jones, D.L.; Silberling, N.J.; Hillhouse, J. Wrangellia—A displaced terrane in northwestern North America. *Can. J. Earth Sci.* **1977**, *14*, 2565–2577. [[CrossRef](#)]
 119. Earle, S.; Nelles, D.; Hamilton, T.S. Guide to the geology of central and southern Vancouver Island: Nanaimo to Victoria. In *Proceedings of the 17th Annual Field Conference, Victoria, Pacific Northwest Section of the National Association of Geoscience Teachers, Victoria, BC, Canada, 15–19 June 2015*; pp. 1–39.

120. Van der Flier-Keller, E.; Goodarzi, F. Geological controls on major and trace element characteristics: Cretaceous coal of Vancouver Island, Canada. *Bull. Soc. Geol. De Fr.* **1991**, *162*, 255–265.
121. Van der Flier-Keller, E.; Goodarzi, F. Regional variations in coal quality in the Canadian Cordillera. *Geol. Soc. Am. Spec. Pap.* **1992**, *267*, 165–175.
122. Van der Flier-Keller, E. Rare earth elements in western Canadian coals. *Energy Sources* **1993**, *15*, 623–638. [CrossRef]
123. Haskin, L.A.; Wildeman, T.R.; Haskin, M.A. An accurate procedure for the determination of the rare earths by neutron activation. *J. Radioanal. Chem.* **1968**, *1*, 337–348. [CrossRef]
124. Piper, D.Z. Rare earth elements in the sedimentary cycle: A summary. *Chem. Geol.* **1974**, *14*, 285–304. [CrossRef]
125. Ren, D.; Zhao, F.; Dai, S.; Zhang, J.; Luo, K. *Geochemistry of Trace Elements in Coal*; Science Press: Beijing, China, 2006; pp. 1–556. (In Chinese)
126. Dai, S.; Ren, D.; Chou, C.-L.; Finkelman, R.B.; Seredin, V.V.; Zhou, Y. Geochemistry of trace elements in Chinese coals: A review of abundances, genetic types, impacts on human health, and industrial utilization. *Int. J. Coal Geol.* **2012**, *94*, 3–21. [CrossRef]
127. Dai, S.; Yan, X.; Ward, C.R.; Hower, J.C.; Zhao, L.; Wang, X.; Zhao, L.; Ren, D.; Finkelman, R.B. Valuable elements in Chinese coals: A review. *Int. Geol. Rev.* **2018**, *60*, 590–620. [CrossRef]
128. Cui, X.; Li, J. The Late Mesozoic Stratigraphy and Palaeontology of the Erlian Basin Group in Inner Mongolia. In *Geoscience, the Journal of the Graduate School*; China University of Geosciences: Wuhan, China, 1991; Volume 5, pp. 397–408. (In Chinese)
129. Cui, X.; Li, J. Late Mesozoic basin types and their coal accumulation characteristics of Erlian basins in Inner Mongolia. *Geoscience* **1993**, *7*, 479–484. (In Chinese)
130. Du, G.; Zhuang, X.; Querol, X.; Izquierdo, M.; Alastuey, A.; Moreno, T.; Font, O. Ge distribution in the Wulantuga high-germanium coal deposit in the Shengli coalfield, Inner Mongolia, northeastern China. *Int. J. Coal Geol.* **2009**, *78*, 16–26. [CrossRef]
131. Dai, S.; Wang, X.; Seredin, V.V.; Hower, J.C.; Ward, C.R.; O’Keefe, J.M.K.; Huang, W.; Li, T.; Li, X.; Liu, H.; et al. Petrology, mineralogy, and geochemistry of the Ge-rich coal from the Wulantuga Ge ore deposit, Inner Mongolia, China: New data and genetic implications. *Int. J. Coal Geol.* **2012**, *90–91*, 72–99. [CrossRef]
132. Zhuang, X.; Querol, X.; Alastuey, A.; Juan, R.; Plana, F.; Lopez-Soler, A.; Du, G.; Martynov, V.V. Geochemistry and mineralogy of the Cretaceous Wulantuga high germanium coal deposit in Shengli coal field, Inner Mongolia, Northeastern China. *Int. J. Coal Geol.* **2006**, *66*, 119–136. [CrossRef]
133. Qi, H.; Hu, R.; Zhang, Q. Concentration and distribution of trace elements in lignite from the Shengli Coalfield, Inner Mongolia, China: Implications on origin of the associated Wulantuga Germanium Deposit. *Int. J. Coal Geol.* **2007**, *71*, 129–152. [CrossRef]
134. Wu, W.; Mo, R.; Wang, Z. Occurrence features and geological work of germanium resource in Yimin coal field, Inner Mongolia. *Inn. Mong. Geol.* **2002**, *1*, 27–30. (In Chinese)
135. Li, J.; Zhuang, X.; Querol, X.; Font, O.; Izquierdo, M.; Wang, Z. New data on mineralogy and geochemistry of high-Ge coals in the Yimin coalfield, Inner Mongolia, China. *Int. J. Coal Geol.* **2014**, *125*, 10–21. [CrossRef]
136. Du, G.; Tang, D.Z.; Wu, W.; Sun, P.C.; Bai, Y.L.; Xuan, Y.Q.; Huang, G.J. Preliminary discussion on genetic geochemistry of paragenetic germanium deposit in Shenli Coalfield, Inner Mongolia. *Geoscience* **2003**, *17*, 453–458. (In Chinese)
137. Liu, J.; Xu, Y. Distribution of Ge, Ga, As, S in the coal metamorphized by heat of sub-volcanics. *Coal Geol. Explor.* **1992**, *20*, 27–32, (In Chinese with English Abstract).
138. Brownfield, M.E.; Weaver, J.N. Paleogeography and stratigraphy of Cretaceous coal deposits of North Africa. In *Controls on the Distribution and Quality of Cretaceous Coals*; Peter, J., McCabe, J.T.P., Eds.; The Geological Society of America: Boulder, CO, USA, 1992; pp. 369–384.
139. Hancox, P.J. The Coalfields of South-Central Africa: A current perspective. *Episodes* **2016**, *39*, 407–428. [CrossRef]
140. Olade, M. Evolution of Nigeria’s Benue Trough (aulacogen): A tectonic model. *Geol. Mag.* **1975**, *112*, 575–583. [CrossRef]
141. Hollanda, M.H.B.M.; Archanjo, C.J.; Macedo Filho, A.A.; Fossen, H.; Ernst, R.E.; de Castro, D.L.; Melo, A.C.; Oliveira, A.L. The Mesozoic Equatorial Atlantic Magmatic Province (EQUAMP): A new large igneous province in South America. In *Dyke Swarms of the World: A Modern Perspective*; Srivastava, R.K., Ernst, R.E., Peng, P., Eds.; Springer: Berlin/Heidelberg, Germany, 2019; pp. 87–110.
142. Merrill, M.D.; Tewalt, S.J. GIS representation of coal-bearing areas in Africa: U.S. Geological Survey Open-File Report 2008-1258. 2008. Available online: <https://pubs.usgs.gov/of/2008/1258/> (accessed on 6 September 2022).
143. Akinyemi, S.A.; Hower, J.C.; Madukwe, H.Y.; Nyakuma, B.B.; Nasirudeen, M.B.; Olanipekun, T.A.; Mudzielwana, R.; Gitari, M.W.; Silva, L.F.O. Geochemical, mineralogical, and petrological characteristics of the Cretaceous coal from the middle Benue Trough Basin, Nigeria: Implication for coal depositional environments. *Energy Geosci.* **2022**, *3*, 300–313. [CrossRef]
144. Mangs, A.D.; Wagner, N.J.; Moroeng, O.M.; Lar, U.A. Petrographic composition of coal within the Benue Trough, Nigeria and a consideration of the paleodepositional setting. *Int. J. Coal Sci. Technol.* **2022**, *9*, 35. [CrossRef]
145. Chukwu, M.; Folayan, C.; Pam, G.; Obada, D. Characterization of some Nigerian coals for power generation. *J. Combust.* **2016**, *2016*, 9728278. [CrossRef]
146. Akinyemi, S.A.; Adebayo, O.F.; Nyakuma, B.B.; Adegoke, A.K.; Aturamu, O.A.; OlaOlorun, O.A.; Adetunji, A.; Hower James, C.; Hood Madison, M.; Jauro, A. Petrology, Physicochemical and Thermal Analyses of Selected Cretaceous Coals from the Benue Trough Basin in Nigeria. *Int. J. Coal Sci. Technol.* **2020**, *7*, 26–42. [CrossRef]
147. Obaje, N.G. *Geology and Mineral Resources of Nigeria*; Springer: Berlin/Heidelberg, Germany, 2009; p. 221.

148. Abubakar, M.B. Biostratigraphy, Palaeoenvironments and Organic Geochemistry of the Cretaceous Sequences of the Gongola Basin, Upper Benue Trough. Ph.D. Thesis, Abubakar Tafawa Balewa University Bauchi, Bauchi, Nigeria, 2006; p. 315.
149. Obaje, N.G.; Umar, U.M.; Aweda, A.K.; Ozoji, T.M. Nigerian Cretaceous coal deposits and their petroleum source rock. *Int. J. Pet. Gas Explor. Manag.* **2020**, *4*, 1–14.
150. Obaje, N.G.; Attah, D.O.; Opeloye, S.A.; Moumouni, A. Geochemical evaluation of the hydrocarbon prospects of sedimentary basins in Northern Nigeria. *Geochem. J.* **2006**, *40*, 227–243. [[CrossRef](#)]
151. Ayinla, H.A.; Abdullah, W.H.; Makeen, Y.M.; Abubakar, M.B.; Jauro, A.; Sarki Yandoka, B.M.; Mustapha, K.A.; Zainal Abidin, N.S. Petrographic and geochemical characterisation of the Upper Cretaceous coals and mudstones of Gombe Formation, Gongola sub-basin, northern Benue Trough Nigeria: Implications for organic matter preservation, palaeodepositional environment and tectonic settings. *Int. J. Coal Geol.* **2017**, *180*, 67–82.
152. Yandoka, B.M.S.; Abdullah, W.H.; Abubakar, M.B.; Hakimi, M.H.; Adegoke, A.K. Geochemistry of the Cretaceous coals from Lamja Formation, Yola Sub-basin, Northern Benue Trough, NE Nigeria: Implications for paleoenvironment, paleoclimate and tectonic setting. *J. Afr. Earth Sci.* **2015**, *104*, 56–70. [[CrossRef](#)]
153. Ogala, J.E.; Finkelman, R.B.; Akaegbobi, M.I.; Francis, H. Evaluation of the trace element content of some Nigerian coal samples. *J. Min. Geol.* **2010**, *46*, 151–161.
154. McLennan, S.M. Relationship between trace element composition of sedimentary rocks and upper continental crust. *Geochem. Geophys. Geosyst.* **2001**, *2*, 1–24. [[CrossRef](#)]
155. Zhao, L.; Dai, S.; Nechaev, V.P.; Nechaeva, E.V.; Graham, I.T.; French, D. Enrichment origin of critical elements (Li and rare earth elements) and a Mo-U-Se-Re assemblage in Pennsylvanian anthracite from the Jincheng Coalfield, southeastern Qinshui Basin, northern China. *Ore Geol. Rev.* **2019**, *115*, 103184. [[CrossRef](#)]
156. Zhao, L.; Dai, S.; Nechaev, V.P.; Nechaeva, E.V.; Graham, I.T.; French, D.; Sun, J. Enrichment origin of critical elements (Nb-Ta-Zr-Hf-REE) within coal and host rocks from the Datanhao mine, Daqingshan Coalfield, northern China. *Ore Geol. Rev.* **2019**, *111*, 102951. [[CrossRef](#)]
157. Ahmad, M.; Munson, T.J. *Geology and Mineral Resources of the Northern Territory*; Special Publication No. 5; Northern Territory Geological Survey: Darwin, Australia, 2013.
158. Birch, W.D. *Geology of Victoria*; Geological Society of Australia: Melbourne, Australia, 2003; Volume 23, pp. 1–842.
159. Drexel, J.F.; Preiss, W.V.; Parker, A.J. The Geology of South Australia V.2. The Phanerozoic. In *Geological Survey of South Australia Bulletin*; Department of Mined: Adelaide, Australia, 1995; Volume 54, pp. 1–347.
160. Hutton, A.C. Geological setting of Australasian coal deposits. In *Australasian Coal Mining Practice*; Kininmonth, R., Baafi, E., Eds.; The Australian Institute of Mining and Metallurgy: Victoria, Australia, 2009; pp. 40–84.
161. Jell, P.A. Geology of Queensland. In *Geological Survey of Queensland*; Queensland Government: Brisbane, Australia, 2013; pp. 1–970.
162. Ward, C.R.; Harrington, H.J.; Mallet, C.W.; Beeston, J.W. Geology of Australian coal basins. In *Geological Society of Australia*; Special Publication No.1: Coal Geology Group: Sydney, Australia, 1995; p. 589.
163. Li, Z.; Moore, T.A.; Weaver, S.D.; Finkelman, R.B. Crocoite: An unusual mode of occurrence for lead in coal. *Int. J. Coal Geol.* **2001**, *45*, 289–293. [[CrossRef](#)]
164. Soong, R.; Berrow, M.L. Mineral matter in some New Zealand coals 2. Major and trace elements in some New Zealand coal ashes. *N. Z. J. Sci.* **1979**, *22*, 229–233.
165. Moore, T.A.; Li, Z.; Nelson, C.M.; Finkelman, R.B.; Boyd, R. Concentration of trace elements in coal beds. In *Metal Contaminants in New Zealand*; Moore, T.A., Black, A., Centro, J.A., Harding, J.S., Trumm, D.A., Eds.; Resolutionz Press: Christchurch, New Zealand, 2005; pp. 81–114.
166. Chatterjee, S.; Mastalerz, M.; Drobniak, A.; Karacan, C.Ö. Machine learning and data augmentation approach for identification of rare earth element potential in Indiana Coals, USA. *Int. J. Coal Geol.* **2022**, *259*, 104054. [[CrossRef](#)]
167. Kolker, A.; Scott, C.; Lefticariu, L.; Mastalerz, M.; Drobniak, A.; Scott, A. Trace element partitioning during coal preparation: Insights from U.S. Illinois Basin coals. *Int. J. Coal Geol.* **2021**, *243*, 103781. [[CrossRef](#)]
168. Lefticariu, L.; Klitzing, K.L.; Kolker, A. Rare Earth Elements and Yttrium (REY) in coal mine drainage from the Illinois Basin, USA. *Int. J. Coal Geol.* **2020**, *217*, 103327. [[CrossRef](#)]
169. Li, B.; Zhuang, X.; Querol, X.; Moreno, N.; Córdoba, P.; Shangguan, Y.; Yang, L.; Li, J.; Zhang, F. Geological controls on the distribution of REY-Zr (Hf)-Nb (Ta) enrichment horizons in late Permian coals from the Qiandongbei Coalfield, Guizhou Province, SW China. *Int. J. Coal Geol.* **2020**, *231*, 103604. [[CrossRef](#)]
170. Liu, J.; Song, H.; Dai, S.; Nechaev, V.P.; Graham, I.T.; French, D.; Nechaeva, E.V. Mineralization of REE-Y-Nb-Ta-Zr-Hf in Wuchiapingian coals from the Liupanshui Coalfield, Guizhou, southwestern China: Geochemical evidence for terrigenous input. *Ore Geol. Rev.* **2019**, *115*, 103190. [[CrossRef](#)]
171. Liu, J.; Spiro, B.F.; Dai, S.; French, D.; Graham, I.T.; Wang, X.; Zhao, L.; Zhao, J.; Zeng, R. Strontium isotopes in high- and low-Ge coals from the Shengli Coalfield, Inner Mongolia, northern China: New indicators for Ge source. *Int. J. Coal Geol.* **2021**, *233*, 103642. [[CrossRef](#)]
172. Liu, J.; Yang, Z.; Yan, X.; Ji, D.; Yang, Y.; Hu, L. Modes of occurrence of highly-elevated trace elements in superhigh-organic-sulfur coals. *Fuel* **2015**, *156*, 190–197. [[CrossRef](#)]
173. Mastalerz, M.; Drobniak, A.; Eble, C.; Ames, P.; McLaughlin, P. Rare earth elements and yttrium in Pennsylvanian coals and shales in the eastern part of the Illinois Basin. *Int. J. Coal Geol.* **2020**, *231*, 103620. [[CrossRef](#)]

174. Middleton, A.; Park, D.M.; Jiao, Y.; Hsu-Kim, H. Major element composition controls rare earth element solubility during leaching of coal fly ash and coal by-products. *Int. J. Coal Geol.* **2020**, *227*, 103532. [[CrossRef](#)]
175. Pavlyutkin, B.I.; Petrenko, T.I.; Chekryzhov, I.Y.; Nechaev, V.P.; Moore, T.A. The plant biostratigraphy of the Cenozoic coal-bearing formations in Primorye, Russian Far East. *Int. J. Coal Geol.* **2020**, *220*, 103414. [[CrossRef](#)]
176. Shen, M.; Dai, S.; Graham, I.T.; Nechaev, V.P.; French, D.; Zhao, F.; Shao, L.; Liu, S.; Zuo, J.; Zhao, J.; et al. Mineralogical and geochemical characteristics of altered volcanic ashes (tonsteins and K-bentonites) from the latest Permian coal-bearing strata of western Guizhou Province, southwestern China. *Int. J. Coal Geol.* **2021**, *237*, 103707. [[CrossRef](#)]
177. Strzałkowska, E. Rare earth elements and other critical elements in the magnetic fraction of fly ash from several Polish power plants. *Int. J. Coal Geol.* **2022**, *258*, 104015. [[CrossRef](#)]
178. Sun, B.; Zeng, F.; Moore, T.A.; Rodrigues, S.; Liu, C.; Wang, G. Geochemistry of two high-lithium content coal seams, Shanxi Province, China. *Int. J. Coal Geol.* **2022**, *260*, 104059. [[CrossRef](#)]
179. Wang, X.; Bian, J.; Zeng, F.; Pan, Z.; Chai, P. Aluminum-bearing nano-sized minerals in vitrain band and its implications for modes of occurrence of Al in Carboniferous-Permian coals from the Hedong Coalfield, northern China. *Int. J. Coal Geol.* **2021**, *248*, 103861. [[CrossRef](#)]
180. Moore, T.A.; Dai, S.; Huguet, C.; Pearse, J.; Liu, J.; Esterle, J.S.; Jia, R. Petrographic and geochemical characteristics of selected coal seams from the Late Cretaceous-Paleocene Guaduas Formation, Eastern Cordillera Basin, Colombia. *Int. J. Coal Geol.* **2022**, *259*, 104042. [[CrossRef](#)]
181. Xie, P.; Dai, S.; Hower, J.C.; Nechaev, V.P.; French, D.; Graham, I.T.; Wang, X.; Zhao, L.; Zuo, J. Nitrogen isotopic compositions in NH₄⁺-mineral-bearing coal: Origin and isotope fractionation. *Chem. Geol.* **2021**, *559*, 119946. [[CrossRef](#)]
182. Liu, J.; Dai, S.; Song, H.; Nechaev, V.P.; French, D.; Spiro, B.F.; Graham, I.T.; Hower, J.C.; Shao, L.; Zhao, J. Geological factors controlling variations in the mineralogical and elemental compositions of Late Permian coals from the Zhijin-Nayong Coalfield, western Guizhou, China. *Int. J. Coal Geol.* **2021**, *247*, 103855. [[CrossRef](#)]
183. Wang, J.; Jacobson, A.D.; Sageman, B.B.; Hurtgen, M.T. Stable Ca and Sr isotopes support volcanically triggered biocalcification crisis during Oceanic Anoxic Event 1a. *Geology* **2020**, *49*, 515–519. [[CrossRef](#)]
184. Guo, W.; Nechaev, V.P.; Yan CYang, X.; He, X.; Shan, K.; Nechaeva, E.V. New data on geology and germanium mineralization in the Hunchun Basin, northeastern China. *Ore Geol. Rev.* **2019**, *107*, 381–391. [[CrossRef](#)]
185. Dai, S.; Yang, J.; Ward, C.R.; Hower, J.C.; Liu, H.; Garrison, T.M.; French, D.; O'Keefe, J.M.K. Geochemical and mineralogical evidence for a coal-hosted uranium deposit in the Yili Basin, Xinjiang, northwestern China. *Ore Geol. Rev.* **2015**, *70*, 1–30. [[CrossRef](#)]
186. Tappert, R.; McKellar, R.C.; Wolfe, A.P.; Tappert, M.C.; Ortega-Blanco, J.; Muehlenbachs, K. Stable carbon isotopes of C₃ plant resins and ambers record changes in atmospheric oxygen since the Triassic. *Geochim. Cosmochim. Acta* **2013**, *121*, 240–262. [[CrossRef](#)]